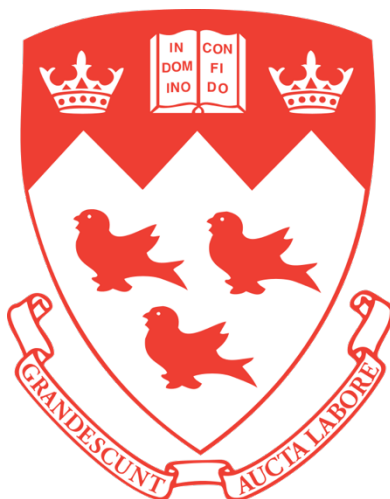


Engineering tough blood clots using bioorthogonal chemistry for temporary embolization



Alexander Nottegar

Department of Mechanical Engineering

McGill University, Montréal

December 2023

A thesis submitted to McGill University in partial fulfillment of the requirements for the degree
of Master of Science

© Alexander Nottegar 2023

Abstract

Endovascular embolization is a minimally invasive medical procedure used to occlude a diseased blood vessel. However, current embolic agents are limited in their use and have been associated with poor biocompatibility and weak mechanical properties. Inspired by autologous blood clots—which were used by early pioneers of embolization—we present *Engineered Blood Clots* (EBCs) as a novel, temporary embolic material designed to leverage the inherent benefits of autologous clots, while providing the robustness and precision of an engineered solution. EBCs are formed using bioorthogonal chemistry, which enables the direct crosslinking of surface-modified red blood cells with biodegradable polymer linkers, integrated within a fibrin matrix derived from the patient's own blood. EBCs are injectable through conventional clinical catheters, forming a highly tough and flexible dual-network hydrogel upon injection. We show this combination of high fracture toughness and low shear modulus results in a highly stable occlusion, resistant to fragmentation or migration. Furthermore, our approach is highly versatile and can be tailored to the desired clinical outcome. EBCs are highly biocompatible, demonstrating regenerative properties, and can be easily removed through natural enzymatic degradation. Preliminary in vivo investigations in rat and porcine models validate the effectiveness of EBCs in providing temporary occlusion, with material degradation observed over a 7-day period. Our results show that EBCs have several advantages over clinically used embolic agents and have the translational potential for temporary embolization applications.

Résumé

L'embolisation endovasculaire est une procédure médicale peu invasive utilisée pour occlure un vaisseau sanguin malade. Cependant, les agents emboliques actuels sont limités dans leur utilisation et ont été associés à une mauvaise biocompatibilité et à de faibles propriétés mécaniques. Inspirés par les caillots sanguins autologues—utilisés par les premiers pionniers de l'embolisation—nous présentons les *Caillots Sanguins Ingénierée (Engineered Blood Clots, EBC)*, comme un nouveau matériau embolique temporaire conçu pour tirer parti des avantages inhérents aux caillots autologues, tout en offrant la robustesse et la précision d'une solution ingénierée. Les EBC sont formés à l'aide de la chimie bioorthogonale, qui permet la réticulation directe de globules rouges dont la surface a été modifiée avec des liants polymères biodégradables, intégrés dans une matrice de fibrine dérivée du propre sang du patient. Les EBC sont injectables par des cathéters cliniques conventionnels et forment un hydrogel à double réseau très résistant et flexible. Nous montrons que cette combinaison d'une grande résistance à la rupture et d'un faible module de cisaillement permet d'obtenir une occlusion très stable, résistante à la fragmentation ou à la migration. En outre, notre approche est très polyvalente et peut être adaptée au résultat clinique souhaité. Les EBC sont hautement biocompatibles, démontrent des propriétés régénératrices et peuvent être facilement retirés par dégradation enzymatique naturelle. Des études préliminaires in vivo sur des modèles rats et porcins valident l'efficacité des EBCs à fournir une occlusion temporaire, avec une dégradation du matériau observée sur une période de 7-jours. Nos résultats montrent que les EBC présentent plusieurs avantages par rapport aux agents emboliques utilisés en clinique et qu'ils ont un potentiel translationnel pour les applications d'embolisation temporaire.

Acknowledgments

Foremost, I would like to express my profound gratitude to Prof. Jianyu Li for his unwavering support, guidance, and mentorship throughout the course of this research. His profound expertise, insightful feedback, and unrelenting patience has played an instrumental role in shaping my time at McGill. His encouragement during challenging times and his faith in my abilities were the anchors that kept me grounded. I am deeply fortunate to have had Prof. Li as my supervisor and I am immensely thankful for the wisdom and perspective he has imparted on me.

Additionally, I owe a heartfelt thanks to all my lab mates, past and present. Each one of you has contributed so much to the enrichment of my research journey. Your camaraderie, constructive critiques, and mutual encouragement were instrumental in fostering both the progress of my work and my growth as a scientist. It has truly been a privilege to work alongside such a dedicated and talented group of individuals.

I would like to extend a special mention to my senior mentor Shuaibing Jiang. His profound knowledge, invaluable advice, and the generosity with which he shared his expertise have been instrumental in navigating the many intricacies of my research journey. I am deeply indebted to him for the countless hours he devoted to helping refine my work and perspective. His mentorship has left an indelible mark on my academic journey, and for that, I am profoundly grateful.

I also extend my sincere appreciation to Dr. Gilles Soulez, Prof. Sophie Lerouge, and the dedicated team at CR-CHUM for their help in conducting the *in vivo* experiments. The professionalism, precision, and commitment they showcased were nothing short of exceptional. I am profoundly thankful for their invaluable contributions and am humbled to have had the opportunity to work with such a distinguished team.

Finally, to my family, words can hardly express the depth of my gratitude for your unwavering support, love, and faith in me. Throughout this journey, your belief in my abilities and your constant encouragement has propelled me forward during the toughest times. Mom and Dad, your sacrifices, teachings, and the values you have instilled in me have shaped who I am. Each of you holds a unique and irreplaceable place in my heart, and I dedicate this achievement to the unwavering love and support you've shown me throughout my life.

Contribution of Authors

This thesis is an original intellectual product of the author, myself, Alex Nottegar. None of the text of the thesis is taken directly from previously published or collaborative articles. I am responsible for the conceptualization, study design, experimentation, data analysis, visualization, and writing of all the chapters in this thesis.

The literature review presented in Chapter 2 was researched and written exclusively by myself. Any insights, interpretations, and conclusions drawn are a direct reflection of my understanding and analysis of the materials consulted.

The experimental methodology presented in Chapter 3 was designed primarily by myself, with inputs from Prof. Jianyu Li and Shuaibing Jiang. In particular, the design and synthesis of Engineered Blood Clots is based on previous, unpublished work led by Shuaibing Jiang. The surgical procedure for the porcine embolization model was designed with inputs from Dr. Gilles Soulez and Prof. Sophie Lerouge.

The experimental work in Chapter 4 is the result of a collaborative effort. Confocal and scanning electron imaging presented in Section 4.1 were performed with the assistance of Xuan Li and Portia Rayner, respectively. Ran Huo assisted with in vitro and ex vivo embolization experiments performed in Section 4.3. The in vitro cytotoxicity studies presented in Section 4.4 were performed with the assistance of Dr. Gaungyu Bao and Shuaibing Jiang. The surgical procedures for the rat abdominal artery embolization model presented in Section 4.5 were performed by Ting Wang. The surgical procedures for the porcine embolization model were performed by Dr. Gilles Soulez with assistance from Prof. Sophie Lerouge, Dr. Malvika Nagrath, Amirali Shahi and the team at the CHUM Research Centre.

The discussion and conclusions detailed in Chapters 5 and 6 are the result of my own intellectual efforts and understandings with inputs and guidance from Prof. Jianyu Li.

Lastly, all the work presented in this thesis benefitted tremendously from the invaluable insights and discussions with my supervisor, Prof. Jianyu Li. The foundational ideas and research design of this thesis were collaboratively conceived by both Prof. Li and myself.

Table of Contents

Abstract	ii
Acknowledgements	iv
Contributions of Authors	v
List of Figures	ix
List of Tables	xi
Abbreviations and Symbols	xii
Chapter 1 Introduction	
1.1 Objectives	1
1.2 Thesis Overview	2
Chapter 2 Background	
2.1 Historical Perspective on Endovascular Embolization.....	3
2.2 Clinical Use of Endovascular Embolization.....	4
2.3 Clinically Used Embolic Agents: Applications and Limitations	5
2.3.1 Coils	6
2.3.2 Gelatin-based Embolic Agents.....	8
2.3.3 Microparticles	9
2.3.4 Liquid/Gel Embolic Agents	10
2.3.5 Emerging Embolic Agents	14
2.3.6 Ideal Embolic Agent	19
2.4 Cellular-based Hydrogels.....	20
2.4.1 Cell Encapsulation	21
2.4.2 Cell Aggregation	22
2.4.3 Cell Crosslinking	23
2.5 Bioorthogonal Chemistry.....	24
2.5.1 Strain Promoted Alkyne-Azide Cycloaddition	24
2.5.2 Tetrazine Ligation	25

2.6	Mechanics of Embolization	26
2.6.1	Overview	26
2.6.2	Elastic Leak Failure Mode	28
2.6.3	Rupture Failure Mode	30

Chapter 3 Materials and Methods

3.1	EBC Preparation and Characterization	32
3.2	Physical Properties Testing	36
3.3	Embolization Modelling	39
3.4	In Vitro Biocompatibility Testing	42
3.5	In Vivo Studies	43

Chapter 4 Results

4.1	Design and Synthesis of Engineered Blood Clots for Embolization	45
4.1.1	Gelation Mechanisms and Kinetics	48
4.1.2	Radiopacity	49
4.1.3	Injectability	50
4.1.4	Tunable Gelation Kinetics	52
4.2	Mechanical Properties of EBCs	53
4.2.1	Enhanced Fracture Toughness	53
4.2.2	Endovascular Adhesion	55
4.2.3	Swelling Properties	55
4.3	Mechanics of Embolization	56
4.3.1	In Vitro Embolization Model	56
4.3.2	Elastic Leak for Reliable Embolization	59
4.4	Biocompatibility and Biodegradation	61
4.4.1	Cytocompatibility and Cell Proliferation	61
4.4.2	In Vitro Biodegradation	62
4.5	In Vivo Embolization	63
4.5.1	Rat Abdominal Artery Embolization	63
4.5.2	Porcine Embolization Model	65

Chapter 5 Discussion

5.1 Design and Optimization of EBCs..... 67
5.2 Mechanics of Embolization 68
5.3 Biocompatibility and Biodegradation..... 70
5.4 In Vivo Embolization..... 71

Chapter 6 Conclusion

6.1 Summary..... 72
6.2 Future Directions 72

Appendix A–Supplementary Information 74

References..... 84

List of Figures

Chapter 2 Background

2.1	Common pathologies treated by endovascular embolization	5
2.2	Various types of clinically used embolic coils	7
2.3	Internal bleeding from postpartum hemorrhage treated by Gelfoam embolization.....	9
2.4	Clinically used liquid embolic agents	11
2.5	Degradation time of various embolic agents	12
2.6	Various approaches of forming cell-based materials	21
2.7	Bioorthogonal click chemistry	26
2.8	Schematic of seal failure modes	27
2.9	Elastic leak of a seal.....	28
2.10	Experimental observations of elastic leak.....	29
2.11	Experimental observations of seal rupture.....	31

Chapter 3 Materials and Methods

3.1	Synthesis of functionalized hyaluronic acid	33
3.2	Fluorescent tagging of azide-modified red blood cells.....	34
3.3	Formation of Engineered Blood Clot by syringe mixing.....	35
3.4	Chemical structure of iodixanol.....	36
3.5	Experimental set-up for injection force measurements	37
3.6	Experimental set-up of mechanical testing	38
3.7	Formation of PDMS vasculature phantom	40
3.8	Experimental set-up of in vitro vasculature flow model.....	41
3.9	Rat abdominal artery embolization.....	43

Chapter 4 Results

4.1	Design principles and characterization of Engineered Blood Clots	47
4.2	Optimization of Engineered Blood Clots as an embolic system.....	49
4.3	Injectability of Engineered Blood Clots through clinical microcatheters.....	51
4.4	Tunable gelation kinetics of the bioorthogonal click clotting system	53

4.5	Mechanical and physical properties of Engineered Blood Clots	54
4.6	In vitro experimental models of embolization	57
4.7	Material properties ensure elastic leak for reliable embolization	60
4.8	Biocompatibility and in vitro degradation of Engineered Blood Clots	62
4.9	In vivo embolization of rat abdominal artery	64
4.10	Preliminary porcine embolization indicates feasibility for temporary applications	66

Appendix A–Supplementary Information

S1	Confocal images of unmodified red blood cells	76
S2	Rheological analysis of Engineered Blood Clots.....	77
S3	Injection of Engineered Blood Clot through 5Fr catheter	78
S4	Percent hemolysis of RBCs after injection	79
S5	Hemocompatibility of Engineered Blood Clots.....	80
S6	Blood clot fibrinolysis spectrophotometric assay	81
S7	Structure of Engineered Blood Clot after cell lysis	82
S8	Porcine embolization model	83

List of Tables

Chapter 2 Background

2.1	Summary of clinically used embolic agents	13
2.2	Summary of emerging liquid/gel embolic agents	19

Abbreviations and Symbols

AU	Absorbance units
AVM	Arteriovenous malformation
Az	Azide
CT	Computed tomography
DBCO	Dibenzocyclooctyne
DMEM	Dulbecco's Modified Eagle Medium
DMSO	Dimethylsulfoxide
DSA	Digital subtraction angiography
EBC	Engineered Blood Clot
EDC	1-Ethyl-3-(3-dimethylaminopropyl)carbodiimide
FBS	Fetal bovine serum
G	Adhesion energy
G'	Storage modulus
G''	Loss modulus
H	Seal diameter
HA	Hyaluronic acid
HU	Hounsfield unit
L	Seal length
MES	2-(N-Morpholino)ethanesulfonic acid
MRI	Magnetic resonance imaging
MW	Molecular weight
MWCO	Molecular weight cut-off
NBC	Native blood clot
n-BCA	n-butyl cyanoacrylate
NHS	N-hydroxysuccinimide
P _c	Elastic leak critical pressure
P _f	Rupture failure pressure
p _i	Leak-initiation pressure
p _s	Steady-state leaking pressure
PBS	Phosphate-buffered saline
PDMS	Polydimethylsiloxane
PRP	Platelet-rich plasma
PVA	Polyvinyl alcohol
RBC	Red blood cell
TCO	Trans-cyclooctene
tPA	Tissue-type plasminogen activator
Tz	Tetrazine
US	Ultrasound
VSR	Volumetric swelling ratio
Γ	Fracture toughness
λ	Dimensionless precompression
μ	Shear modulus

1 Introduction

Endovascular embolization has emerged as a pivotal tool in the modern arsenal of interventional radiology. Temporary embolization, in particular, has proven invaluable in emergent scenarios, such as controlling active bleeding in trauma patients or hemorrhage during childbirth. It provides a life-saving stopgap until a more definitive intervention or natural healing can take place. The current range of embolic agents includes metallic coils, gelatin sponges, and liquid agents such as glues and Onyx. Each with its own strengths and challenges, often mandating a careful selection based on the clinical situation at hand. However, many of these current solutions suffer from poor mechanical properties and biocompatibility issues. Here we present the concept of *Engineered Blood Clots* (EBCs), a promising novel embolic material designed to provide a robust, yet temporary, occlusion. This idea is inspired by early pioneers who attempted to leverage the body's innate response to vascular injury by using natural solutions like autologous blood clots as embolic agents. However, the use of autologous blood clots has fallen out of style, in part due to their poor mechanical properties and unpredictable nature. Thus, the vision of EBCs arises from the desire to merge the natural efficiency of blood clots with the precision and predictability of engineered solutions. EBCs are formed using bioorthogonal chemistry by directly crosslinking surface-modified red blood cells with biodegradable hyaluronic acid, in combination with a fibrin matrix derived from autologous blood. This approach results in a highly biocompatible, artificial clot with enhanced mechanical properties. It ensures a reliable occlusion and introduces the ability to tune the clot's physical and biological properties based on the procedural needs.

1.1 Objectives

The overall goal of this thesis is to design and validate EBCs as a safe and effective material for the purpose of temporary endovascular embolization. We achieve this goal by deconstructing it into three main objectives:

Objective 1: Optimize the EBC material system based on clinical needs using in vitro models that characterize the embolic performance.

Objective 2: Using in vitro and analytical models, understand the mechanics of embolization and relate these findings to material optimization.

Objective 3: Validate these results using in vivo models.

1.2 Thesis Overview

This thesis addresses the objectives outlined above across six chapters, offering a comprehensive overview of the research journey—from the initial problem formulation to the final conclusions and potential applications. Chapter 1 provides a brief introduction to the research, emphasizing its significance, and outlining the research objectives. Chapter 2 provides a general background on the embolization procedure, highlighting the current clinically used and emerging embolic agents, while identifying the major limitations and areas for improvement. In this chapter we will also discuss the chemical techniques used to form EBCs and provide a brief overview of the theory behind the mechanics of embolization. Chapter 3 is dedicated to the methodology, where the experimental and analytical methods used are described in detail. Chapter 4 presents the experimental results, theoretical models representing the mechanics of embolization, and provides a critical analysis. Chapter 5 provides an in-depth discussion of these results, comparing them with the existing literature, offering insights, analyzing the experimental limitations, and provides a discussion on the scientific implications of this work. Finally, Chapter 6 summarizes the key contributions of this research, and introduces potential directions for future research.

2 Background

In modern medicine, there's a growing preference of clinicians for minimally invasive procedures as they aim to reduce trauma to patients. The medical landscape over recent years has seen a shift away from complex open surgeries, towards minimally invasive interventions, which not only pose fewer complications, but often yield superior outcomes at a reduced cost (1). Endovascular embolization stands as a testament to the remarkable advances in the realm of interventional radiology and minimally invasive procedures over the past few decades. Endovascular embolization involves the intentional and controlled occlusion of a targeted blood vessel through the use of an embolic agent, with the aim of stopping blood flow to a particular region (2). Its ability to treat a diverse range of pathologies, from vascular malformations to oncologic applications, such as to occlude the blood vessels supplying a tumour, has ushered in a new era of therapeutic possibilities, diminishing the need for open surgeries, and reducing the associated risks. This chapter seeks to provide a deep dive into the embolization procedure, tracing its historical evolution, evaluating the state-of-the-art treatments, and charting the trajectory of emerging trends and challenges. The spotlight then shifts to the realm of *Engineered Blood Clots*, presenting an analysis of the innovative chemical techniques behind the formation of these highly cellularized gels. Moreover, we explore the intricate mechanics of embolization and the importance of how the mechanical properties of an embolic agent influence the outcomes of this procedure.

2.1 Historical Perspective on Endovascular Embolization

The genesis of endovascular embolization is a testament to both medical innovation and the principle of using the body's own resources for therapeutic purposes. Embolization, as a therapeutic modality, has its roots in the 1960s and 1970s with the first procedures being performed as an adjunct to surgical interventions, offering a less invasive means to manage vascular pathologies (3, 4). In the early stages of the procedure's development, before the advent of synthetic or specialized materials, clinicians often relied on what was naturally available and biocompatible. Autologous blood clots served as one of the earliest embolic agents. By harvesting a patient's own blood and allowing it to clot, physicians would reintroduce the clot into the vascular system to promote targeted vessel occlusion. In the early 1970s, Dr. Charles Dotter performed the

first catheter-directed embolization using autologous blood clots to treat an acutely bleeding artery of the stomach (5). Soon after, autologous blood clots were used to embolize other organs as well. This approach not only minimized the risk of foreign body reactions but also capitalized on the body's innate hemostatic processes. Autologous blood clots are almost entirely biodegradable and cause a minimal inflammatory response, two desirable features in the clinical scenario that not all modern embolic agents can claim (6). However, the use of autologous clots came with challenges, including the body's natural clot lysis—which dramatically limited the length and durability of occlusion. Recanalization can occur within hours, and fragmentation of the clot could lead to distal, non-target embolization (6-8). In parallel to clots, other autologous tissues, such as muscle fragments and fat, were also explored as potential embolic materials (9). These materials offered a natural and biologically compatible means to occlude vessels, especially in larger vascular structures. Yet, as with autologous blood clots, there were limitations concerning their long-term stability, potential of migration, and the degree of precision in delivery.

The clinical need for a precise, radio-opaque embolic agent led to the development of synthetic embolic agents (6). The 1970s marked a significant evolution with the introduction of metallic coils, which offered a more precise delivery and improved clinical outcomes (10). As interventional radiology matured as a specialty, there was a surge in innovation with the development of polymer-based liquid embolic agents (11-13). These decades of evolution not only expanded the indications for embolization but also enhanced its safety profile. However, the use of the aforementioned natural agents, such as autologous blood clots, laid the foundation of endovascular embolization and set the stage for the later introduction of more refined, purpose-engineered embolic materials. Although contemporary embolization techniques have largely moved away from these early agents, understanding their historical role provides valuable context on the evolution and nuances of endovascular treatments.

2.2 Clinical Use of Endovascular Embolization

Since its inception, endovascular embolization has become a versatile tool in a clinician's toolkit, with a broad spectrum of clinical applications (Fig. 2.1). In the neurovascular space, it's an invaluable tool for the treatment of intracranial aneurysms and vascular malformations, such as arteriovenous malformations (AVMs), allowing for targeted occlusion and prevention of catastrophic hemorrhage (14). Embolization also serves as the frontline treatment for uterine

fibroids, offering symptomatic relief while maintaining fertility (15). It has also emerged as an effective technique in oncology, where it is utilized for the pre-operative downsizing of tumours, or as a direct treatment method in procedures like transarterial chemoembolization (TACE) for various types of cancers (16, 17). Additionally, embolization provides a lifesaving means to control and stop active bleeding in cases of traumatic hemorrhage (2). With the continual evolution of technology and techniques, the horizon of endovascular embolization's clinical applications only seems to be expanding, underscoring its integral role in modern medicine.

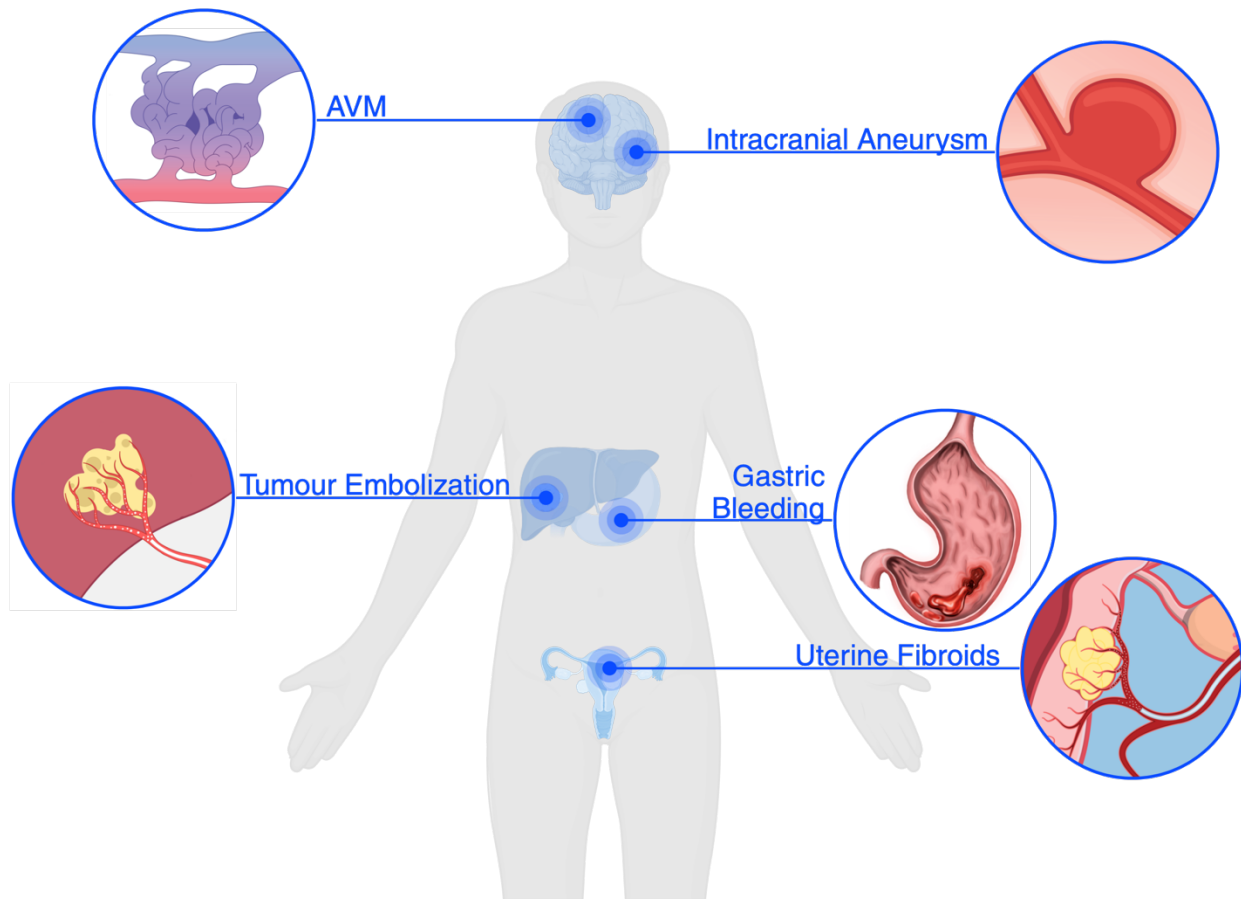


Figure 2.1 Common pathologies treated by endovascular embolization^{i, ii}

2.3 Clinically Used Embolic Agents: Applications and Limitations

Endovascular embolization is an incredibly diverse procedure covering a wide variety of clinical applications, each addressing unique pathophysiological conditions with distinct treatment objectives. As such, it requires a diverse selection of embolic agents. The choice of embolic agent determines the efficacy, precision, and safety of the intervention. No single embolic agent is

universally suited for all purposes, as each material has its advantages and disadvantages. The choice of embolic agent is influenced by a number of factors, such as the experience of the physician, the specific organ or lesion targeted, the intended duration of embolization (whether temporary or permanent), the level of occlusion, and the size and flow conditions of the targeted vessel (18). This section will cover the current clinically used embolic agents, examining their properties, applications, and their limitations in specific clinical situations.

2.3.1 Coils

Among the earliest embolic agents, metallic coils have become foundational in embolization procedures (10). Coils are permanent embolic agents, typically made from bio-inert metals, such as platinum, and are commonly used for the treatment of aneurysms and hemorrhage control (Fig. 2.2a). Coils are designed to promote vessel occlusion through a combination of mechanical obstruction and subsequent thrombogenic reactions by providing a scaffold for thrombus formation. Coil embolization has several advantages; their inertness ensures minimal inflammatory reactions post-procedure. They can also be precisely deployed in a variety of different shapes and sizes of vessel pathologies with a low risk of non-target embolization. Coils, while effective, present certain limitations as embolic agents. Once deployed, they generally remain within the vessel permanently. Metallic coils cause CT artifacts which can obscure embolized segments and impair follow-up evaluations (19). Occlusion from coils is dependent on the coagulation cascade, which limits its effectiveness in patients receiving anticoagulation therapy or those with coagulopathies. Additionally, coils are expensive, and achieving complete occlusion typically requires the use of multiple coils—increasing both the cost and duration of the procedure. Lastly, coils can only be delivered directly at the site of the microcatheter, limiting their use in tortuous or small vessels, or in situations where a distal occlusion is required (20).

Bioactive Coils

Coils promote occlusion through thrombus formation, which is governed by their surface thrombogenicity. Surface modifications to existing bare platinum coils have been made to improve their thrombogenicity. Bioactive coils are coated with materials designed to accelerate the thrombotic process. Early-generation bioactive coils incorporated nylon or silk fibres to promote blood clot formation (21, 22). Fibered coils are generally more thrombogenic than bare platinum coils and further stabilize the thrombus due to fibre dispersion within the clot (22, 23).

Biodegradable polymers, such as poly(lactic-*co*-glycolic acid) (PLGA), have also been used as surface coatings to promote tissue response and thrombus formation (Fig. 2.2b). PLGA-coated coils were reported to accelerate aneurysm healing through enhanced neck neointimal formation and pronounced fibrosis, compared to bare platinum coils (24). However, PLGA-coated coils have faced clinical setbacks due to high recanalization rates (25-28). The premature degradation of PLGA prior to full thrombus formation leads to incomplete volume filling, coil compaction, and eventual recanalization (25, 26). Additionally, increased stiffness and friction against the catheter wall make PLGA-coated coils more difficult to deploy (26-28).

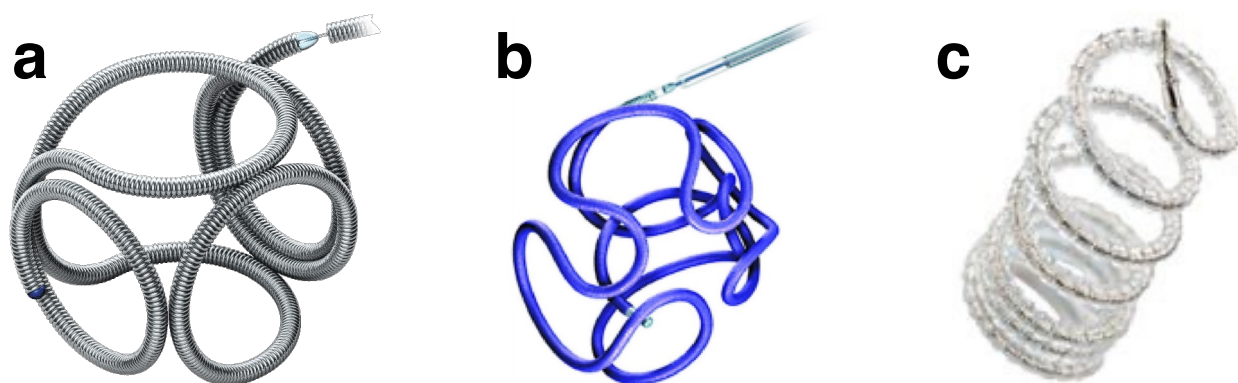


Figure 2.2 Various types of clinically used embolic coils

(a) Bare metal detachable coil (Target 360 Detachable Coil, Stryker Neurovascular), typically made of platinum.ⁱⁱⁱ (b) Matrix bioactive coil (Boston Scientific Neurovascular), coated with PLGA to promote thrombus and neointimal tissue formation. Reproduced with permission from (29). (c) Hydrogel coated coil (AZUR HydroCoil, Terumo). Hydrogel coating expands once in contact with blood to form a mechanical occlusion less reliant on thrombus formation.^{iv}

Hydrogel-coated Coils

Another important parameter in coil embolization is packing density. Typically, recanalization after coil embolization occurs due to coil compaction; a high packing density is required to prevent recanalization (30). Hydrogel-coated coils have been developed to improve the packing density and achieve greater volume occlusion compared to bare platinum coils (Fig. 2.2c). Upon contact with blood, the hydrogel expands to fill the space between the coils. Additionally, hydrogel-coated coils do not rely on thrombus formation, making them useful in situations of reduced coagulation and coagulopathy. Hydrogel-coated coils have been shown to reduce recanalization and recurrence

rates when compared to bare platinum coils (31). However, hydrogel-coated coils must be delivered relatively quickly in order to prevent swelling inside the catheter (1).

2.3.2 Gelatin-based Embolic Agents

Gelatin-based embolic agents—such as gelatin sponge or powders—have been widely used for endovascular embolization since 1964 (32). Derived from purified porcine skin gelatin, gelatin-based embolics are biodegradable agents that offer temporary embolization, making them especially suitable for situations where permanent embolization is not desired. Their primary applications include pre-operative devascularization of tumours (reducing blood loss during surgical resection), in trauma patients presenting with active bleeding, and in non-traumatic hemorrhagic scenarios like gastrointestinal bleeding or post-partum hemorrhage (Fig. 2.3) (33). Gelatin sponge (Gelfoam, Pfizer) rapidly expands once introduced into the vasculature, achieving an occlusion by creating a mechanical barrier while also providing a scaffold for thrombus formation. Gelatin powders lead to a distal embolization of small vessels and are used when a deeper embolization is required. The advantages of gelatin-based embolic agents are that they are readily available, inexpensive, and provide temporary embolization (2). Over time, as the material is absorbed, normal blood flow gradually resumes. This is particularly advantageous in cases like pre-operative tumour embolization, where temporary devascularization can aid surgical resection, but a permanent occlusion is not required. Vessel recanalization after Gelfoam embolization is typically seen within 2–3 weeks but may take up to 4 months (34). However, because of the unpredictable duration of occlusion, Gelfoam embolization may lead to rebleeding or unwanted permanent occlusion. Further, the inflammatory response as a result of the introduction of gelatin-based embolics into the vasculature can cause fibrotic and other changes in the vessel wall that result in a more permanent occlusion, resulting in ischemic complications (35, 36).

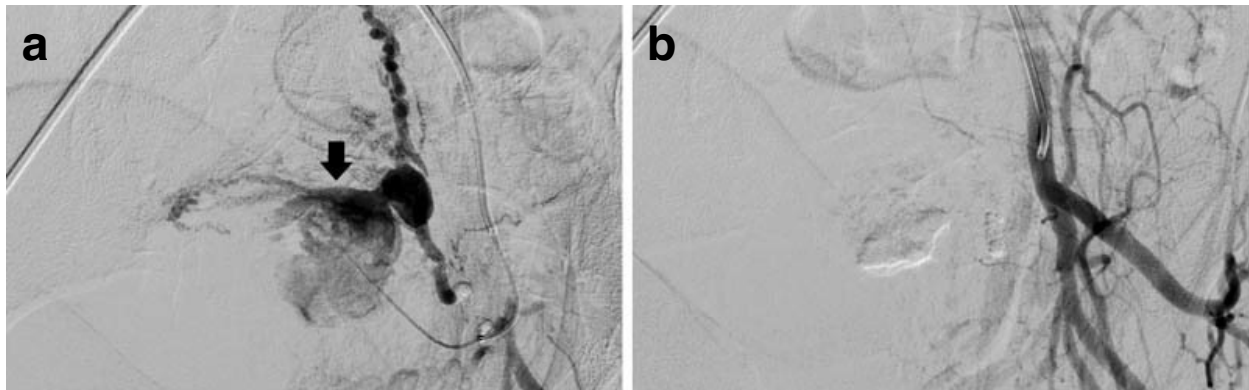


Figure 2.3 Internal bleeding from postpartum hemorrhage treated by Gelfoam embolization

(a) Angiography of the left uterine artery immediately prior to embolization, showing internal bleeding caused by postpartum hemorrhage (black arrow). **(b)** Angiography after embolization with Gelfoam shows successful embolization and lack of bleeding. Reproduced with permission from (37).

2.3.3 Microparticles

Microparticles, often referred to as microspheres or microbeads, represent a pivotal advancement in the field of endovascular embolization. Microparticles can be made from either synthetic or natural polymers, such as polyvinyl alcohol (PVA), trisacryl-gelatin, or polymethyl methacrylate. The precisely calibrated size of these spherical agents offers a predictable level of occlusion. This precision enables clinicians to target specific vascular territories with a high level of accuracy. Once delivered, microparticles travel distally, deep into the microvasculature. The diameter of the vessel where occlusion occurs is heavily dependent on the size of the microsphere, allowing for localized targeted embolization and predictable outcomes (38). Their versatility extends across clinical scenarios, from occluding tumour-feeding vessels in oncologic interventions to treating uterine fibroids and other vascular anomalies (17, 39). For example, in preoperative tumour embolization, achieving a deep, distal embolization is crucial in preventing blood loss (40). To penetrate the vascular bed effectively, relatively smaller microparticles are required. Following distal embolization, more proximal vessels may be embolized with the use of larger particles. This tailored embolization approach results in a more effective treatment (41). For instance, preoperative treatment of meningiomas is most effective with smaller particles (45–300 μm), while for uterine fibroids, larger particles (350–900 μm) are mostly used (42, 43). Some microparticles can be loaded with therapeutic drugs, offering a dual action of embolization and localized drug delivery, a technique particularly useful for TACE procedures of liver cancers (44). However, microspheres are usually restricted to the embolization of small vessels only. Due to their small

size, microparticles can sometimes travel past the intended treatment site and occlude non-target vessels, leading to unintended ischemic complications in adjacent or distal tissues (45, 46). Like all embolic agents, careful patient selection, understanding of the clinical context, and expert technique are essential to minimize potential complications.

2.3.4 Liquid/Gel Embolic Agents

Liquid/gel embolic agents represent a transformative frontier in endovascular embolization techniques. Unlike traditional particulate or coil-based approaches, these agents can be injected to conform precisely to the vasculature's architecture, ensuring a more uniform and robust occlusion. There is a growing interest in their use for peripheral interventions, given their ability to penetrate deep into vascular networks, reaching targets that might be inaccessible or challenging for conventional catheters and coils (1). As such, they offer enhanced precision when embolizing AVMs, tumours, and other vascular diseases—even in the most intricate or tortuous vascular beds. However, as with all embolic agents, their use requires meticulous technique and planning; ensuring that the agent remains confined to the intended territory and minimizing the risk of non-target embolization. Furthermore, liquid/gel agents have been associated with poor biocompatibility due to their use of organic solvents. This can lead to post-embolization pain, vessel wall damage, or even recanalization of the embolized vessel over time (47-50).

n-BCA

N-butyl-2 cyanoacrylate (n-BCA) is a synthetic liquid adhesive which immediately polymerizes when in contact with aqueous fluids, such as blood. Clinically, n-BCA is mainly used for the embolization of high-flow vascular malformations (51). n-BCA forms a stable, permanent occlusion of the vessel, independent of inherent coagulation. It also induces an acute inflammatory reaction in the vessel wall, which progresses to chronic inflammation and necrosis of the intima (52). Fibrosis develops gradually, with the incorporation of the material into the vessel wall and a slow degradation of the material over a couple of years (53). Recanalization can only occur if partial embolization is achieved (7). While its rapid polymerization makes n-BCA effective for permanent vascular embolization, special skills and expertise are required for its use. Its unpredictable polymerization may lead to non-target embolization, especially in high-flow regions (1). Moreover, the polymerization process is exothermic which can be very painful (52). Additionally, due to its adhesive nature, catheters may become entrapped in the occluded vessel;

a potential complication that might occur in the case of reflux, early polymerization, or delayed removal of the microcatheter (36). Therefore, catheters must be withdrawn immediately after n-BCA injection to avoid adhering to vessel walls.

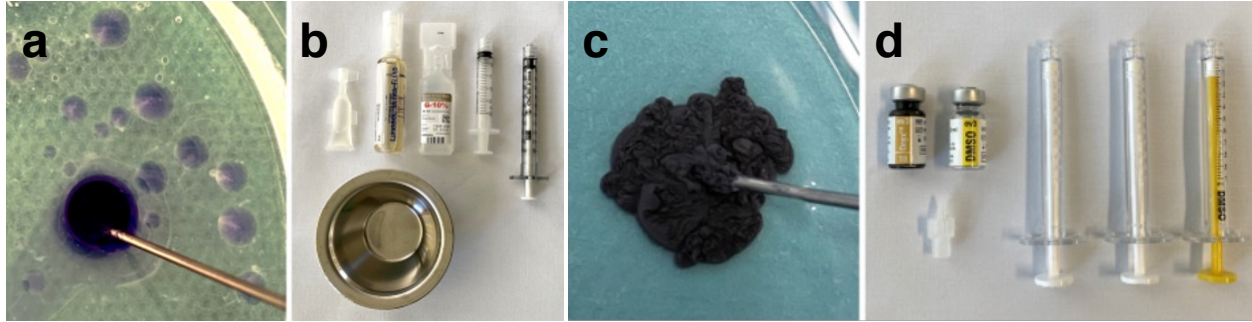


Figure 2.4 Clinically used liquid embolic agents

(a) Appearance of n-BCA after injection into saline (histoacryl shown here for visualization purposes because of its blue colour). (b) Materials required for the injection of n-BCA. (c) Appearance of Onyx after injection into saline. (d) Materials required for the injection of Onyx. Reproduced with permission from (54).

Onyx

Onyx is a non-adhesive liquid embolic agent, consisting of ethylene vinyl alcohol copolymer (EVOH) dissolved in dimethyl sulfoxide (DMSO). Once injected through a microcatheter, DMSO rapidly diffuses into the blood, and EVOH precipitates, forming a solid cast within 5 minutes (11). Onyx results in a permanent occlusion that remains stable for years, independent of a patient's coagulation (55). Onyx is mainly used for the embolization of intracranial AVMs, however, it has also been used in peripheral vascular interventions (56). Distinguished by its prolonged solidification time compared to cyanoacrylates, Onyx allows clinicians better control during deployment, facilitating a more precise embolization of complex vascular malformations. This slow solidification time allows Onyx to penetrate the vasculature forming a deep, distal occlusion. Further, its tunable viscosity, by varying the concentration of EVOH, allows for a tailored approach. Its non-adhesive nature reduces the risk of catheter entrapment, however, there is still a risk of embedding the catheter if Onyx refluxes around the catheter tip (7). The main limitation of Onyx is associated with the use of DMSO, which is associated with both cardiovascular- and neuro-toxicity (47, 48). Rapid injection of Onyx may cause vasospasm and necrosis due to the high concentrations of DMSO at the catheter tip (57). Therefore, a slow injection rate is required.

In addition, DMSO can dissolve plastics. Therefore, specialized and costly DMSO-compatible catheters are required (1).

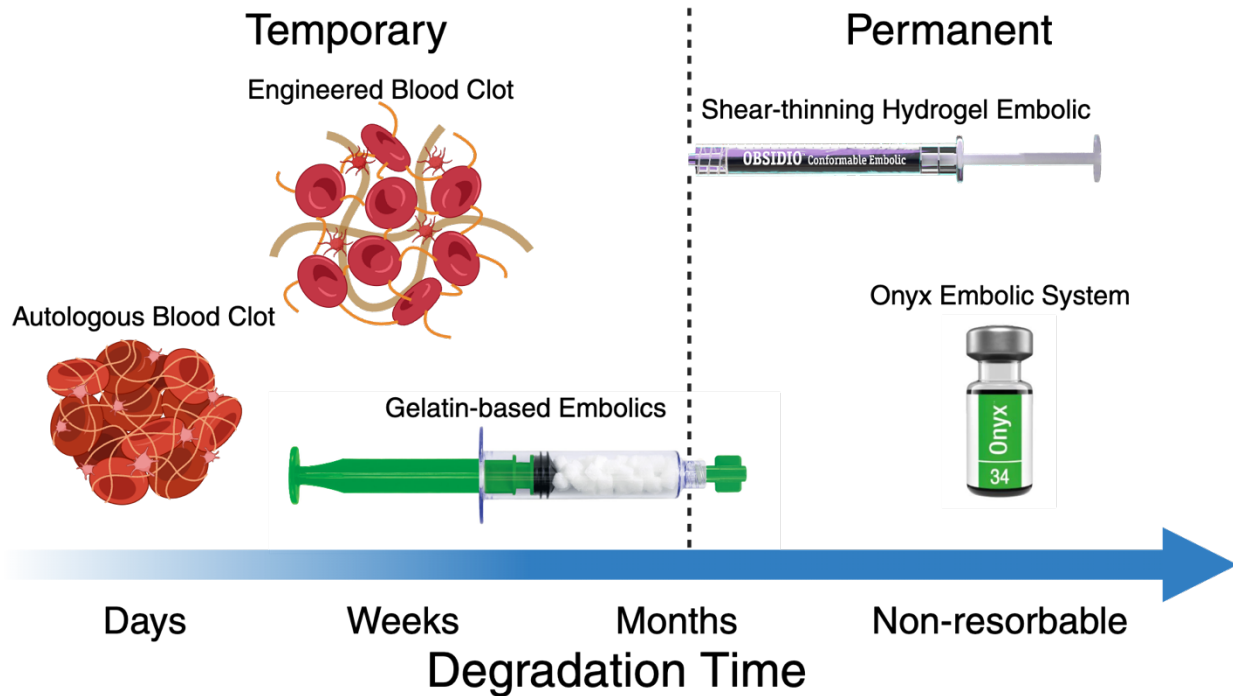


Figure 2.5 Degradation time of various embolic agents^{1, v}

Schematic showing the degradation times of various embolic agents compared to EBCs. Gelatin-based embolics degrade within weeks to months. Shear-thinning hydrogel embolic agent (Obsidio Conformable Embolic, Boston Scientific) takes months to fully degrade, but is considered a permanent embolic agent. Months-long degradation times generally results in a permanent occlusion. Onyx is non-resorbable and is considered a permanent embolic agent.

Sclerosing Agents

Sclerosing agents are a unique class of embolic agents typically used for the treatment of organ ablation, such as tumours, AVMs and varicosities (36). Unlike traditional embolic materials that act primarily by mechanical occlusion, sclerosing agents work by inducing chemical damage to the endothelial lining of vessels, promoting thrombosis and subsequent fibrosis, thereby leading to permanent vessel occlusion. Commonly used sclerosants include sodium tetradecyl sulfate, polidocanol, and ethanol. Ethanol is one of the most commonly used sclerosing agents. It incites a strong inflammatory response that destroys the blood vessel walls, causing an immediate precipitation of endothelial cells and proteins, leading to rapid vessel thrombosis and occlusion (36). While these agents can be highly effective, their use requires significant expertise and

caution. They can be associated with complications such as skin necrosis, tissue damage, and systemic reactions if not administered with care. Severe complications such as cardiac arrest and pulmonary embolism have been reported (58).

Table 2.1 Summary of clinically used embolic agents

Embolic Agent	Description	Typical Applications	Occlusion Duration	Toxicity/Vascular Reaction
Coils				
Bare metal coil	Thin metallic coils that interrupt blood flow and provide a scaffold for thrombus formation.	Aneurysms, hemorrhage control	Permanent	None
Bioactive coil	Metallic coils coated with a bioactive material to promote healing or thrombus formation.	Aneurysms, hemorrhage control	Permanent	Inflammatory response (depending on surface coating)
Hydrogel-coated coil	Metallic coils coated with a hydrogel which swells once in contact with blood.	Aneurysms	Permanent	None
Particulates				
Autologous clot	Blood clot formed from patient's own blood.	Hemorrhage control	Temporary	None
Gelatin	Slurry of gelatin sponge or powder derived from purified porcine skin.	Hemorrhage control	Temporary	Moderate inflammatory response
Microspheres	Calibrated microparticles made from synthetic or natural polymers	Tumour embolization, uterine fibroids	Permanent or Temporary	None
Liquid/gels				
n-BCA	Cyanoacrylate-based glue which polymerizes upon injection.	AVM embolization	Permanent	Necrosis of endothelium and tissue damage
Onyx	EVOH dissolved in DMSO which precipitates and forms a solid cast upon injection.	AVM embolization	Permanent	System toxicity, vasospasm, and tissue necrosis
Sclerosing agents	Sclerosing agent, such as ethanol, induces a severe inflammatory response leading to rapid vessel thrombosis.	AVM embolization	Permanent	Severe inflammatory response, tissue necrosis, and systemic toxicity

2.3.5 Emerging Embolic Agents

The limitations of current embolic agents have motivated the development of hydrogel-based agents as an emerging frontier for embolization interventions. These hydrogels are designed to be injectable in a liquid state and solidify in situ within the vascular network. The allure of hydrogel agents lies in their biocompatibility, tunable physical properties, and potential for drug delivery. Hydrogels can be tailored to exhibit controlled degradation over time, allowing for temporary vessel occlusion or even the gradual release of therapeutic agents. They are also appealing for the potential use in regenerative medicine; envisioning scenarios where the embolic agent might not only occlude a vessel but also promote tissue healing or regeneration. Although undoubtedly promising, hydrogel-based agents are still in the nascent stages of clinical adoption, with ongoing research focused on optimizing their properties, understanding their long-term effects, and expanding their clinical applications.

Ionically Crosslinked Systems

Calcium-crosslinked alginate hydrogels have been used as an embolic agent due to their high mechanical strength in their post-crosslinked solid form, low viscosity in their initial liquid form, high biocompatibility, and excellent shear-thinning behaviour (59). The embolic agent is a two-component system, consisting of an alginate polymer solution and calcium chloride (CaCl_2). Once injected, Ca^{2+} ions bind the guluronic acid sites of the alginate strands to form a stable gel (59). Alginate hydrogels have been studied extensively for various uses in bioengineering, such as polymer films, cell encapsulation, wound dressings, and surgical sponges (60-63).

The biocompatibility and embolic properties of the calcium-alginate system was tested in rat kidney capsules and rabbit kidneys (59). The short- and long-term tissue reactivity was tested by injecting calcium alginate into the fat capsule surrounding the kidney of a rat. Histological sections of the implant after 1-week showed little to no change in tissue density or cell distribution, corresponding to a highly biocompatible material. Furthermore, the alginate and calcium chloride solutions were injected from the renal vessels into the vasculature of a rabbit kidney to determine the extent of endovascular occlusion. The solutions solidified in situ, via ionic crosslinking with the calcium ions, forming a stable vascular plug that stopped all flow out of the kidney and maintained vascular occlusion during the one-week study.

A long-term study using a porcine aneurysm model was performed to study the long-term embolic properties of the calcium-alginate gel (64). Alginate and calcium chloride solutions were injected simultaneously through a concentric dual-lumen catheter into the aneurysm, with temporary balloon protection across the aneurysm neck. Within 5 minutes, complete and stable aneurysm filling was achieved. At one month after embolization, fibrous tissue growth was observed across the aneurysm neck—occluding the aneurysm from the parent vessel. Aneurysms were completely healed within 90 days, with no tissue necrosis or neointimal growth into the parent vessel. Additionally, no migration or dislodgment of the hydrogel was observed during the 90-day period after embolization.

Photo-crosslinking Systems

In situ photo-crosslinking of hydrogels has emerged as alternative strategy to provide control over the gelation process during the embolization procedure. This approach allows for low-viscosity precursor solutions to reach distal locations before gelation via UV-crosslinking (65). Through a UV-integrated microcatheter, hydrogel precursors with low-viscosity and shear-thinning properties are delivered. These precursors are UV-activated and formulated from poly(ethylene glycol diacrylate) (PEGDA), silicate nanoplatelets, and the photoinitiator lithium phenyl-2,4,6-trimethylbenzoylphosphinate (LAP). At the tip of the microcatheter a 100 mW, 405 nm fibre-coupled laser source was used to enable controlled UV-gelation of the hydrogel (66). This hydrogel system was tested in vivo with a porcine aneurysm model (67). Using balloon-assisted embolization and UV-activation, aneurysms were filled completely with no recanalization or complications. These findings were confirmed at a four-week follow-up angiography. Histological results revealed cross-linked hydrogel and thrombosis within the aneurysm after four weeks and endothelialization over the neck of the aneurysm.

Temperature-Sensitive Gelling Systems

Chitosan has been extensively explored for biomedical applications. Chitosan, dissolves in acidic solutions and precipitates once the pH exceeds 6.2 (68). When combined with a weak base such as β -glycerophosphate (β -GP), chitosan solutions remain in solution at room temperature and physiological pH, but will undergo a sol–gel transition upon heating to physiological temperatures (69). This property of thermogelation, in addition to its high biocompatibility, makes chitosan/ β -GP solutions an interesting candidate as an embolic agent.

Preliminary in vivo tests involving chitosan/ β -GP solutions indicate successful embolization of the splenic and gastric artery in swine, with occlusion lasting for at least 2 hours after injection (the time frame of this study) (70). The chitosan/ β -GP system also demonstrated successful embolization in long-term in vivo studies. One study, showed the embolization and complete occlusion of rabbit renal arteries with no recanalization during an eight-week observation period (71). The occlusion led to the infarction of the embolized kidney, with no indication of inflammation in the target renal artery or kidney. The colour of the embolized kidney was pale and it was considerably smaller than the control kidney, indicating a successful occlusion. The chitosan/ β -GP system was also used for embolization in a porcine cerebral AVM model (72). Histological and angiographic analysis 6 weeks after the embolization confirmed that the AVM model remained completely embolized. The hydrogel filled the vascular cavity, and the tunica intima and smooth muscle layer remained intact and visible; no signs of vessel wall inflammation or necrosis were observed.

pH-Sensitive Gelling Systems

pH-sensitive hydrogels have been proposed as embolic agents since they can be delivered in liquid form and solidify at the targeted site in response to pH shifts (73-75). pH-sensitive materials undergo a sol–gel transition due to the pH change between the hydrogel precursor solution and the injection conditions. Sulfamethazine (SM) has been used for this application because it can transition from an ionized state at high pH to a deionized state at a physiological pH, due to its weakly anionic nature (75). SM-based hydrogels possess a low viscosity at high pH levels, facilitating easy injection through microcatheters, and exhibit a sol–gel transition at physiological pH levels resulting in a solid hydrogel at the injection site (73).

Preliminary embolization tests using a rabbit renal artery model and a rabbit liver model demonstrated the feasibility of using a pH-sensitive, SM-based hydrogel system as an embolic agent (75). The hydrogel was examined by follow-up angiography, histological analysis, and comparison of the embolization efficacy of treated organs at various time points. Instant vascular occlusion after the injection of the pH-sensitive material was confirmed by angiography. The injection was carried out smoothly without blockage of the catheter. Angiography at 5-, 9-, and 32-days post-treatment showed no signs of recanalization; histological sections obtained three days post-embolization revealed the presence of the hydrogel in both the central and peripheral areas of

the kidney. Furthermore, kidney damage was observed in the target kidney after embolization, indicating an ischemic change caused by the occlusion. At 32 days post-treatment the kidney was less than half of the original size with a completely damaged interior, confirming the long-term embolization efficacy of the embolic material. Similar results were also observed for the liver embolization model.

Shear-thinning Hydrogels

There has been a growing interest in the use of shear-thinning hydrogels for embolization procedures. Shear-thinning hydrogels are physically crosslinked hydrogel systems that exhibit reduced viscosity at high shear rates. As opposed to in situ gelling hydrogel systems, shear-thinning hydrogels remain in a gel state and are injectable due to their shear-thinning properties. Once injected shear-thinning hydrogels form an impenetrable occlusive cast that is not reliant on the inherent coagulation process (76). A hydrogel system consisting of gelatin and synthetic silicate nanoplatelets (Laponite XLG) has been proposed as an embolic agent for peripheral vasculature interventions (76). When dissolved in water, a shear-thinning hydrogel is formed due to strong electrostatic interactions between the negative electrostatic charges on the two sides of the nanoplatelets and the positive charges on the gelatin polymer chains. Due to the anisotropic distribution of surface charges on the nanoplatelets—positive along the edge and negative on the top and bottom surfaces—they form self-assembled structures which dynamically break and reform, upon external stimuli, resulting in shear-thinning behaviour (77).

Shear-thinning hydrogels have been tested in both small and large animal in vivo models (76). Hydrogels were injected into mouse femoral arteries to assess for non-target embolization in vivo. Laser Doppler imaging showed sustained and complete occlusion of the vessel, resulting in an interruption of hindlimb perfusion. MicroCT imaging showed no signs of recanalization and no detectable non-target distal migration, indicating a stable occlusion without fragmentation. A porcine model was used to assess the feasibility of the shear-thinning hydrogel in large animals. Injection into the left external iliac artery resulted in an immediate occlusion with no evidence of displacement or fragmentation. Next, the hydrogel was used to embolize the forelimb venous vasculature. CT imaging performed 24 days after the procedure revealed no evidence of pulmonary embolism. Histological analysis showed no signs of recanalization after 24 days. Further, it was revealed that macrophages surrounded the hydrogel, indicating ongoing degradation of the

material inside of the embolized vessel. Connective tissue deposition at the occlusion sites further indicates the unlikelihood of recanalization.

In Situ Chemically Crosslinked Systems

In situ chemically cross-linking hydrogel systems undergo a chemical reaction before injection and then gel in situ in a time-dependent manner. These material systems can be potentially used for embolization procedures if the material can be injected before gelation occurs. One such material system, the PPODA-QT system, consists of liquid monomers poly(propylene glycol) diacrylate (PPODA) and pentaerythritol tetrakis(3-mercaptopropionate) (QT). After mixing of the monomers a basic solution is introduced to initiate the reaction. Thiol groups on QT undergo deprotonation in basic aqueous solutions and react with the acrylate group on PPODA via a Michael-type addition (78). This reaction forms a chemically crosslinked hydrogel network.

This material system has been examined in vivo, in a porcine aneurysm embolization model (79). Experimental aneurysms were embolized with the injection of PPODA-QT under balloon protection across the neck. Angiography showed total occlusion and complete filling of the aneurysms with PPODA-QT. Histological analysis revealed neointimal tissue growth across the neck of the aneurysms. However, complications occurred due to overfilling of the aneurysms with PPODA-QT, resulting in stretching of the aneurysm. To overcome this, partial aneurysm filling was used, which resulted in complete aneurysm occlusion after 1 month, with complete neointimal tissue growth over the aneurysm neck. Further, this partial filling approach resulted in no cases of aneurysm overfilling or stretching. A 6-month pilot study was carried out in a canine lateral wall aneurysm model (80). Again, aneurysms were occluded with the injection of PPODA-QT under temporary balloon protection. Angiography revealed complete aneurysm occlusion 6 months after PPODA-QT embolization. Histology images of the aneurysm showed robust neointimal tissue growth and endothelialization at the PPODA-QT interface. However, one major concern with the PPODA-QT system is the usage of highly toxic monomers, PEGDA and QT. Unreacted monomers may leach from the gel causing serious complications (81).

Table 2.2 Summary of emerging liquid/gel embolic agents

Embolic Agent	Gelation Mechanism	Ref.
Calcium alginate	Ionic crosslinking	(59)
PEGDA/LAP	Photo-crosslinking	(65)
PEGDMA/PEG-BAPO	Photo-crosslinking	(82)
Chitosan/ β -glycerophosphate	Temperature induced sol-gel transition	(83)
PAAm-based hydrogels	Temperature induced sol-gel transition	(84)
FHSgel	Temperature induced sol-gel transition	(85)
mPEG-PLA	Temperature induced sol-gel transition	(86)
Silk-elastin like protein polymer hydrogel	Temperature induced sol-gel transition	(87)
SM-based hydrogels	pH induced sol-gel transition	(73)
Gelatin/laponite nanoplatelets	Shear thinning	(76)
GO-enhanced polymer hydrogel	Shear thinning	(88)
PPODA-QT	In situ chemical crosslinking	(78)
Alg-MA/CMC-MA DCN hydrogel	In situ chemical crosslinking	(89)
PEG acrylate/redox initiators	In situ chemical crosslinking	(90)
GPX	Coacervation	(91)
Salmine sulfate/IP6	Coacervation	(92)
PLTTG/DMSO	Precipitation	(93)
Poly(cation-adj- π) blood glue	Electrostatic interactions with blood contents	(94)

2.3.6 Ideal Embolic Agent

Endovascular embolization is a highly diverse procedure with a variety of clinical applications and desired outcomes. As we have outlined, there is a large and highly diverse selection of embolic agents, each used for a specific application. While there is no all-encompassing embolic agent, the *ideal* embolic material should possess these general properties:

- 1) **Radiopaque**—The ideal embolic material should be radiopaque so that it is visible on the common imaging modalities such as angiography, computed tomography (CT) imaging, magnetic resonance imaging (MRI), and ultrasound (US) imaging. Further, the material should not cause imaging artifacts or distortions.

- 2) **Injectable**—The ideal material should be easily injectable through clinically used microcatheters and should be non-adhesive to the catheter material to prevent trapping of the catheter within the vasculature.
- 3) **Mechanically Robust**—The ideal material should have adequate mechanical properties so that it is able to form a stable occlusion which is resistant to fragmentation and migration. Further, these properties should be tunable to allow for use in various applications.
- 4) **Biocompatible**—The ideal material should be highly biocompatible so to prevent potential adverse complications. The material should allow for cell proliferation and promote the healing of the diseased vessel.
- 5) **Biodegradable**— Finally, the material should be biodegradable. This property will depend on the desired outcomes—whether a temporary or permanent embolization is preferred—but the material should generally be biodegradable to allow for new tissue formation. For the purpose of this work, we will focus on applications requiring a temporary embolization.

2.4 Cellular-based Hydrogels

Cell-based therapy is a fast-evolving field in the medical sciences which involves the introduction or use of cellular materials to promote healing, tissue regeneration, or even targeted drug delivery. The use of cellular therapies in the realm of endovascular embolization has been seldom explored. The potential to combine cellular therapies with other materials—like hydrogels—to create composite embolic agents that can offer intrinsic biocompatibility, controlled degradation, localized drug release, and tissue regeneration, is of great interest. Beyond mere occlusion, cells may be harnessed to promote vascular wall repair or reduce inflammation post-embolization, mitigating some of the adverse reactions seen with conventional agents. This was seen in the early days of endovascular embolization where clinicians used natural cell-based materials, such as autologous blood clots or muscle fragments, due to their intrinsic biocompatibility. While the concept is rich in potential, it is also replete with challenges, from ensuring cellular viability and functionality post-delivery to managing potential immune reactions. Consequently, the ability to engineer cell membranes to impart non-native properties to cells has emerged as a powerful method to form cell-based materials. By mimicking the innate hierarchical assembly properties found in natural cellular structures, this approach amplifies the therapeutic potential of cell-based materials (95). Nevertheless, as the boundaries of interventional medicine continue to expand, so

do the boundaries of material science and cell-based therapies. Cellular therapies may redefine the paradigms of endovascular embolization in the years to come. In this section we will cover cell-based hydrogels and their potential for use as embolic agents in minimally invasive interventions.

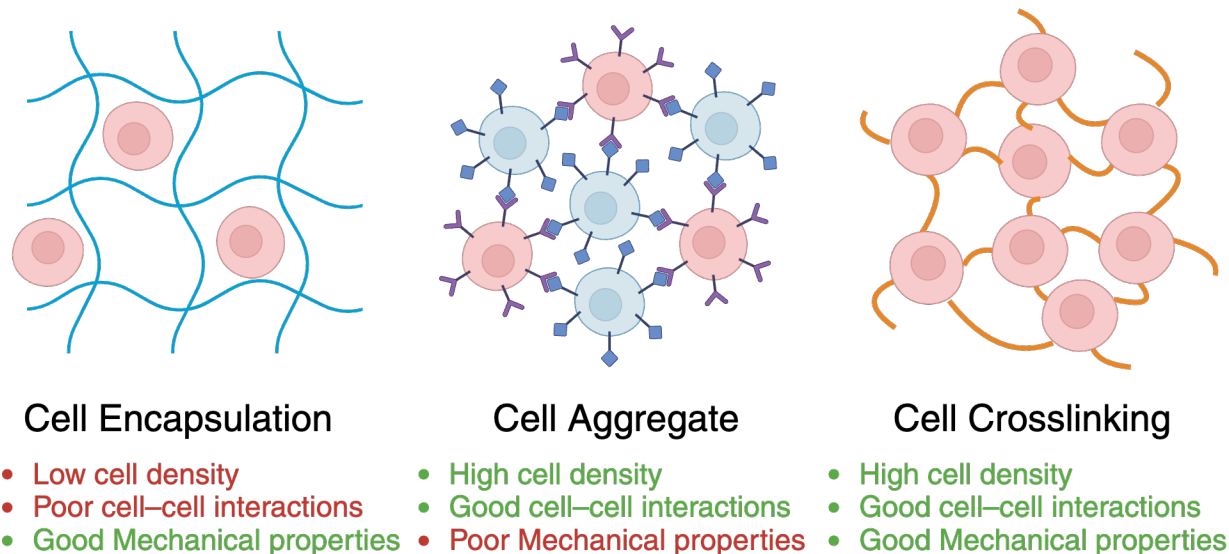


Figure 2.6 Various approaches of forming cell-based materialsⁱ

Schematic showing the various approaches of forming cell-based materials with the advantages and disadvantages of each method.

2.4.1 Cell Encapsulation

Cell-encapsulating hydrogels are perhaps the simplest approach to forming cell-based hydrogels. Hydrogels, with their high water content and biocompatible nature, have emerged as a prime candidate for cell encapsulation in tissue engineering and regenerative medicine. Cell-encapsulating hydrogels act as three-dimensional scaffolds that can house and nurture cells—providing a conducive microenvironment that mimics the native extracellular matrices. Such hydrogels can be tailored to meet specific requirements, such as mechanical strength, porosity, and degradation rate, ensuring that the encapsulated cells thrive and function optimally. Various methods of cell encapsulation in hydrogels have been described (61, 96-99). At its core, this procedure involves suspending cells within a hydrogel precursor solution, which is then subjected to conditions that induce gelation. Cells can also be encapsulated in injectable hydrogels to deliver cells to a particular site of interest for in situ regeneration of a tissue (98). Both natural biopolymers, including collagen, hyaluronic acid (HA), alginate, and chitosan, as well as synthetic polymers like polyethylene glycol (PEG) and poly(vinyl alcohol) (PVA), have been explored as

hydrogel network precursors (98). Natural biopolymers possess inherent bio-active components, such as cell-binding ligands, that are vital for cellular activity. However, they often face issues like batch-to-batch inconsistency and limited tunability in material properties (98). On the other hand, synthetic polymers offer precise control over various material properties, but are bioinert, meaning they are biocompatible but do not inherently support or enhance cell behaviour (98).

While cell-encapsulating hydrogels have shown great promise in regenerative medicine and various therapeutic applications, they are not without their limitations. Due to the nanoporosity of the hydrogel network—which is significantly smaller than the micrometre size of a cell—encapsulation of cells within a hydrogel imposes a physical constraint around the cell (99). As a result, diffusion limitations, especially of oxygen, decrease cell viability in the center of the material and impose size restrictions (99). Therefore, cell-encapsulated hydrogels have limited cell densities, especially for large hydrogel constructs (100). Furthermore, hydrogel encapsulation can limit cell activity such as cell interactions, proliferation, and matrix deposition (101).

2.4.2 Cell Aggregation

Cell aggregate structures overcome some of the limitations seen with cell-encapsulated hydrogels. Cell aggregation describes the clustering and adhesion of initially separate cells to form an aggregate material. Cell aggregate-based materials, due to their high cell densities and lack of matrix immobilization, exhibit better cell–cell interactions than cell-encapsulating hydrogels. Cell aggregates more closely resemble the native tissue structure, preserve cell function, and enhance survival (101). These materials can be either formed by conventional spontaneous aggregation or by advanced cell surface engineering to induce cell aggregation and fuse into larger cohesive constructs (102). Cell surface engineering offers a nuanced approach to guiding the formation of cell aggregate structures by directly modifying the cellular interface. This is achieved through the introduction of functional molecules, ligands, or polymers to the cell membrane—enabling tailored cell–cell interactions and self-assembly. One popular method is the use of bioorthogonal click chemistry, where modified cells are equipped with reactive groups that readily bind to complementary groups on adjacent cells, promoting aggregate formation. In one example tetrazine (Tz) and trans-cyclooctene (TCO) functional groups were conjugated to the cell surface leading to covalently bound cell aggregate structures (103). The binding of synthetic DNA fragments to cell surfaces has also been explored to promote selective cell–cell interactions driven by the high-

affinity hybridization of two complementary strands (104). It has been demonstrated that the decoration of cell surfaces with complementary DNA structures enables the programming of cell–cell adhesion and the formation of cell aggregate structures in a well-defined manner. Lipid-based modifications, such as the incorporation of liposomes loaded with adhesive peptides or functional groups, offers another avenue for controlling cell surface properties and consequent aggregation behaviours (105, 106). Additionally, the use of magnetic nanoparticles tethered to the cell membranes can be leveraged to manipulate and cluster cells under the influence of external magnetic fields (107).

While cell aggregate structures have shown significant potential in tissue engineering applications, they are not without inherent limitations—especially as it relates to their potential use in endovascular embolization applications. The main limitation of cell aggregate–based materials as it relates to embolization applications is the long immobilization time required to obtain a cohesive structure (100). Furthermore, these constructs have demonstrated inferior mechanical properties, which may prevent the formation of a stable vascular occlusion (108). Controlling the size and uniformity of cell aggregates can also be challenging, as well as the scalability of producing large numbers of uniform aggregates, while maintaining their functional properties (109). In the context of embolization, where precise control over vessel occlusion is paramount, these variabilities would tend to be problematic.

2.4.3 Cell Crosslinking

Cell-crosslinked gels combine properties of both cell-encapsulating hydrogels and cell aggregates, making a unique class of materials. These gels utilize cells as crosslinkers where they interact with biopolymers through multiple adhesive connections to form highly cellularized, hydrogel-like materials, termed *cytogels*¹. As opposed to conventional cell-laden hydrogels, where mechanical properties are governed by the polymeric network, cytogels utilize cells as the active structural element within the polymer matrix, where each polymer chain is attached simultaneously to multiple ligands of the surface of adjacent cells creating a 3D hierarchical structure (95). This approach is highly appealing as it can achieve a high cell density, as well as minimize the need for excessive biomaterial, as only a small polymer concentration is required to achieve superior

¹ Hydrogels that incorporate cells not just for their biological function but also as a part of the material's architecture or structural framework.

mechanical properties (95). One important consideration in forming cytogels is the method of crosslinking. Several strategies have been employed, including receptor-ligand recognition, electrostatic interactions, and hydrophobic insertions (94, 110-114). In regards to embolization, the crosslinking method must demonstrate rapid reaction kinetics, cytocompatibility, and should not generate any cytotoxic byproducts. One class of chemical reactions, *bioorthogonal click chemistry*, is of particular interest due to it possessing these characteristics.

2.5 Bioorthogonal Chemistry

Bioorthogonal chemistry refers to a class of click chemical reactions² that occur under physiological conditions; whose components react rapidly and without interfering with, or being affected by, any surrounding biological processes (115). The term was first introduced by Dr. Carolyn Bertozzi, for which she was awarded the Nobel Prize in 2022 (116). Bioorthogonal reactions have emerged as a compelling tool in the development of embolic agents. Their inherent speed and selectivity allows for fast in situ gelation of the embolic material within the vasculature, without affecting the surrounding biological system (Fig. 2.7a). Furthermore, the modularity of click reactions means that various functional groups or bioactive molecules can be incorporated with ease, enabling the creation of embolic agents tailored to specific clinical scenarios or patient needs. The biocompatibility of bioorthogonal reactions is especially crucial in the sensitive and dynamic environment of the vasculature, where adverse reactions or toxic byproducts are detrimental. Leveraging the attributes of bioorthogonal click chemistry can provide both the precision and adaptability required in the design and application of next-generation embolic agents.

2.5.1 Strain Promoted Alkyne-Azide Cycloaddition

The classic click chemistry reaction, the azide-alkyne cycloaddition (AAC), involves a 1,3-dipolar cycloaddition between an azide and an alkyne to form a stable triazole—originally described by Huisgen (117). Since then, azides have proven to be a particularly powerful functional group for bioorthogonal reactions (115). Azides are completely absent from biological systems and possess bioorthogonal reactivity to most biological functional groups (118). Additionally, their small size allows them to be easily incorporated onto biomolecules with minimal perturbation (115).

² Click chemistry refers to a class of modular chemical reactions that are fast, efficient, and high-yielding, akin to "clicking" pieces together. Bioorthogonal chemistry is a class of such reactions.

However, the AAC reaction has limited applicability in biological systems due to its requirement of high temperatures, or pressures, to achieve a reasonable reaction rate (119). Sharpless and Meldal independently reported the dramatic improvement of this reaction using a copper(I) catalyst, resulting in a highly selective reaction with fast kinetics at physiological conditions (120, 121). However, copper-catalyzed azide-alkyne cycloaddition (CuAAC) relies on the use of a copper catalyst which is highly cytotoxic, thus precluding any applications where cells must remain viable. In 2004, Bertozzi introduced strain promoted alkyne-azide cycloaddition (SPAAC), also termed the Cu-free click reaction, a bioorthogonal reaction in which the alkyne is incorporated within a strained cyclooctyne system—which increases its reactivity and circumvents the requirement for a copper catalyst (Fig. 2.7b) (119). Among the many cyclooctynes, dibenzocyclooctyne (DBCO) exhibits fast kinetics with azides and good stability in aqueous buffers (122, 123). Additionally, under physiological conditions, DBCO exhibits excellent bioorthogonality and will not react with the many function groups that are naturally present in biological systems (124).

2.5.2 Tetrazine Ligation

Following the emergence of bioorthogonal chemistry a variety of alternative reactions have been developed and applied for use in biological systems. Among these, the tetrazine–transcyclooctene (TCO) ligation stands out due to its extremely fast kinetics. This ligation chemistry is based on an inverse electron-demand Diels-Alder (IEDDA) reaction between tetrazine (Tz) and TCO to form a stable dihydropyrazine product (Fig. 2.7c) (125). This reaction is highly selective, with ultrafast kinetics unmatched by any other bioorthogonal reaction. Due to its fast kinetics, this reaction can be performed under highly dilute conditions, which is often required in biological systems (125). However, tetrazines have varying stabilities in aqueous solutions, with the most reactive tetrazines also being the least stable. Disubstituted tetrazines, such as monomethyl tetrazines, have shown improved stabilities without significantly reducing their reactivities (126).

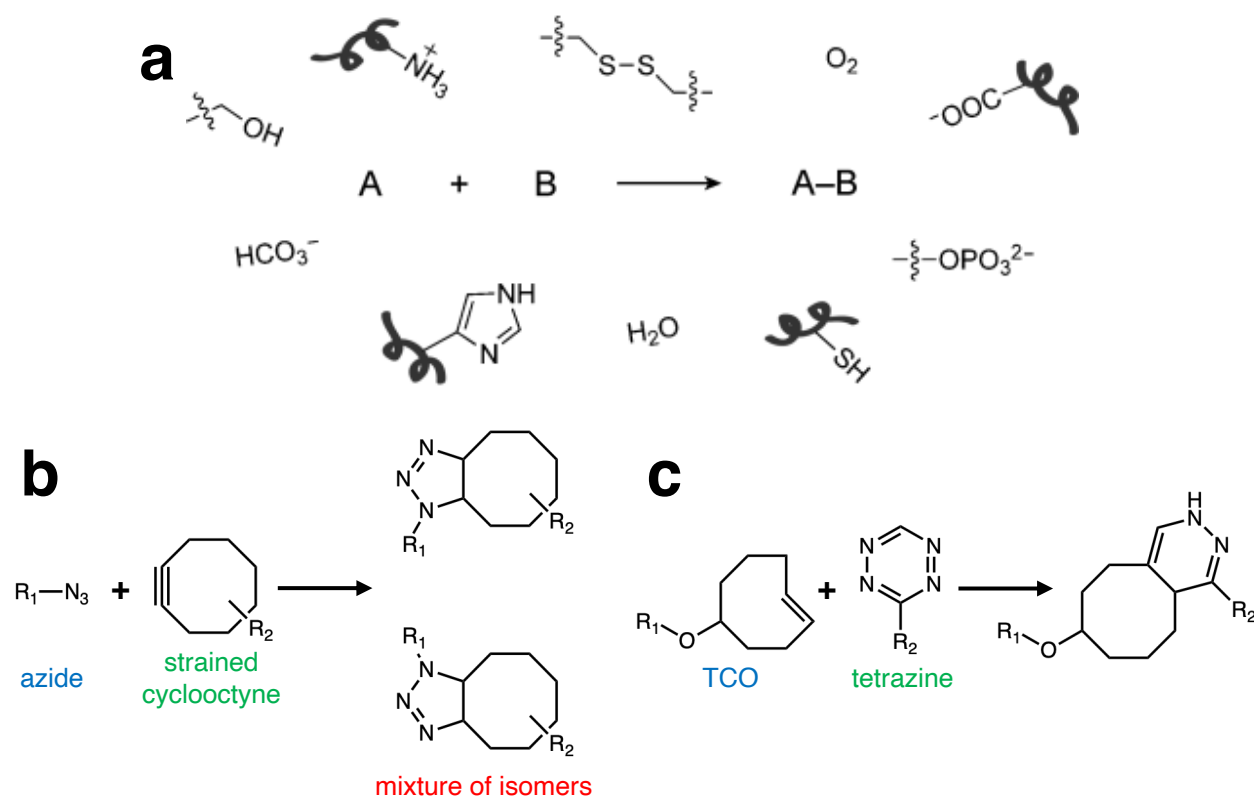


Figure 2.7 Bioorthogonal click chemistry

(a) Schematic illustrating a bioorthogonal reaction. Compounds A and B must selectively react with one another while in the presence of the various functionalities found within biological systems, some examples of which are indicated. Reproduced with permission from (115). (b) Bioorthogonal SPAAC reaction between an azide and a strained cyclooctyne. (c) Bioorthogonal IEDDA reaction between TCO and Tz.

2.6 Mechanics of Embolization

The review will now shift back to the realm of embolization to cover a topic, which previously has seldom been discussed. That is of the mechanics of embolization and how this relates to the choice of an embolic material. In this section we will cover elastomer sealing theory, drawing interesting parallels to the mechanics of embolization, specifically regarding the failure modes seen in the context of embolization, such as the fragmentation of an embolic material.

2.6.1 Overview

Few studies have investigated the mechanics of embolization. The studies that have researched this topic have focused on the mechanics related to the fracture of blood clots which cause an embolism (127-130). The major difference between these studies and the case of embolization

procedures, is that the former focuses on a partially occluded vessel and not the case of a fully occlusive seal—which is the case for embolization when using a particulate or gel embolic agent.

The mechanics of embolization can be better understood when examined through the lens of elastomer sealing theory, which delves into the principles governing the closure or blockage of channels. Elastomer seals—often made from materials like rubber, silicone, or other flexible polymers—are used in a wide variety of applications across different industries and are ubiquitous in our daily lives. They also play a role in the context of embolization. At its core, embolization seeks to provide an effective seal within the vasculature, preventing the flow of blood through the targeted vessel. In this context, embolic agents can be regarded as elastomer seals, blocking blood flow within a vessel. A thorough understanding of elastomer sealing theory can thus guide the optimization of embolic agents, ensuring a robust occlusion is formed, that is resistant to fragmentation or migration of the embolic material.

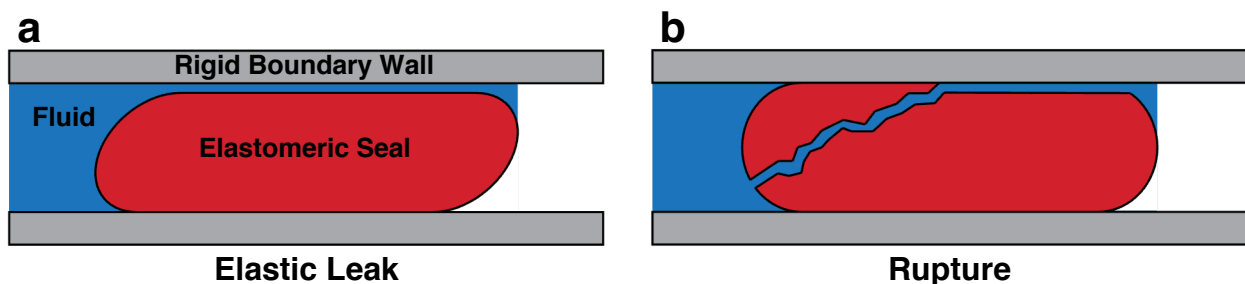


Figure 2.8 Schematic of seal failure modes

(a) Elastic leak failure mode. No material damage occurs; failure is due to elastic deformation. **(b)** Rupture failure mode. Failure is due to fracture of seal material.

Elastomeric seals function by forming a contact stress with the surrounding rigid boundary. The fluid sealed in this system has a different pressure compared to the ambient condition. Subject to a pressure gradient, a seal may leak by elastic deformation or by rupture (Fig. 2.8). Zhigang Suo and his group have developed a theoretical model to predict the leaking pressure of elastomeric seals (131-133). This model was originally developed to describe the failure modes of elastomeric seals used as packers in oilfields. However, through our work we develop the insights and experimental links that connect this theoretical model to embolization applications. According to this model, the seal leaks by elastic deformation when the fluid pressure exceeds the contact pressure between the seal and the rigid wall (131). The seal leaks by rupture when the energy release rate of a crack exceeds the fracture toughness of the elastomer (132).

2.6.2 Elastic Leak Failure Mode

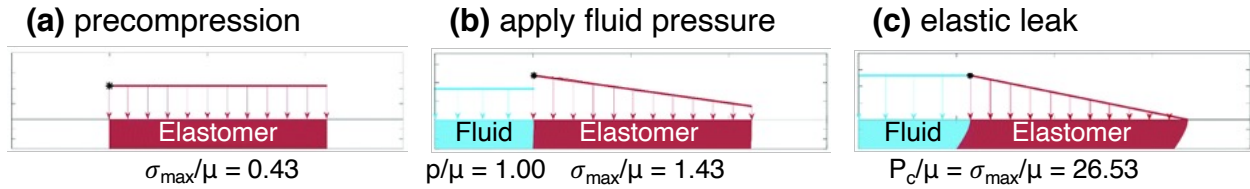


Figure 2.9 Elastic leak of a seal

(a) Before fluid pressure is applied, the precompression of the elastomer causes a homogeneous contact stress (σ) on the boundary wall. **(b)** Fluid pressure (p) is applied. When the fluid pressure is lower than the maximum contact pressure—which occurs at the upstream corner of the seal—the seal does not leak. **(c)** When the fluid pressure reaches a critical point (P_c) where it is equal to the maximum contact pressure, elastic leak occurs. No material damage occurs, the seal leaks due to elastic deformation. Adapted from (133).

When a seal fails by elastic deformation this is known as an *elastic leak*. An initial contact pressure (σ) is formed by precompression of the elastomer against the rigid walls (Fig. 2.9a). The ratio λ is a dimensionless measure of precompression, $\lambda = H/H_0 = L_0/L$ —where H and H_0 are the elastomer heights in compressed and uncompressed states, respectively, and L and L_0 are the elastomer lengths. The pressure differential across the seal causes elastic deformation of the seal. As the seal is deformed, the contact pressure between the wall and the seal drops linearly along its length (Fig. 2.9b); the maximum contact pressure occurs at the upstream corner of the seal. When the fluid pressure is low the maximum contact pressure is larger than the fluid pressure, preventing the fluid from leaking. When the fluid pressure reaches a critical pressure, P_c , it surpasses the maximum contact pressure in some part of the contact region; the seal and the boundary wall lose contact in this region (Fig. 2.9c). The contact pressure still drops linearly along the length of the seal, therefore as the fluid penetrates the contact it is pulled by the lower and lower contact stress ahead, forming a leaking path. This mode of failure is entirely due to elastic deformation, meaning the seal leaks without any material damage. The critical condition for leak by elastic deformation takes the form—where μ is the shear modulus of the seal material (133):

$$P_c = \mu \frac{L}{H} \sqrt{6(1 - \lambda^4)} \quad (2.1)$$

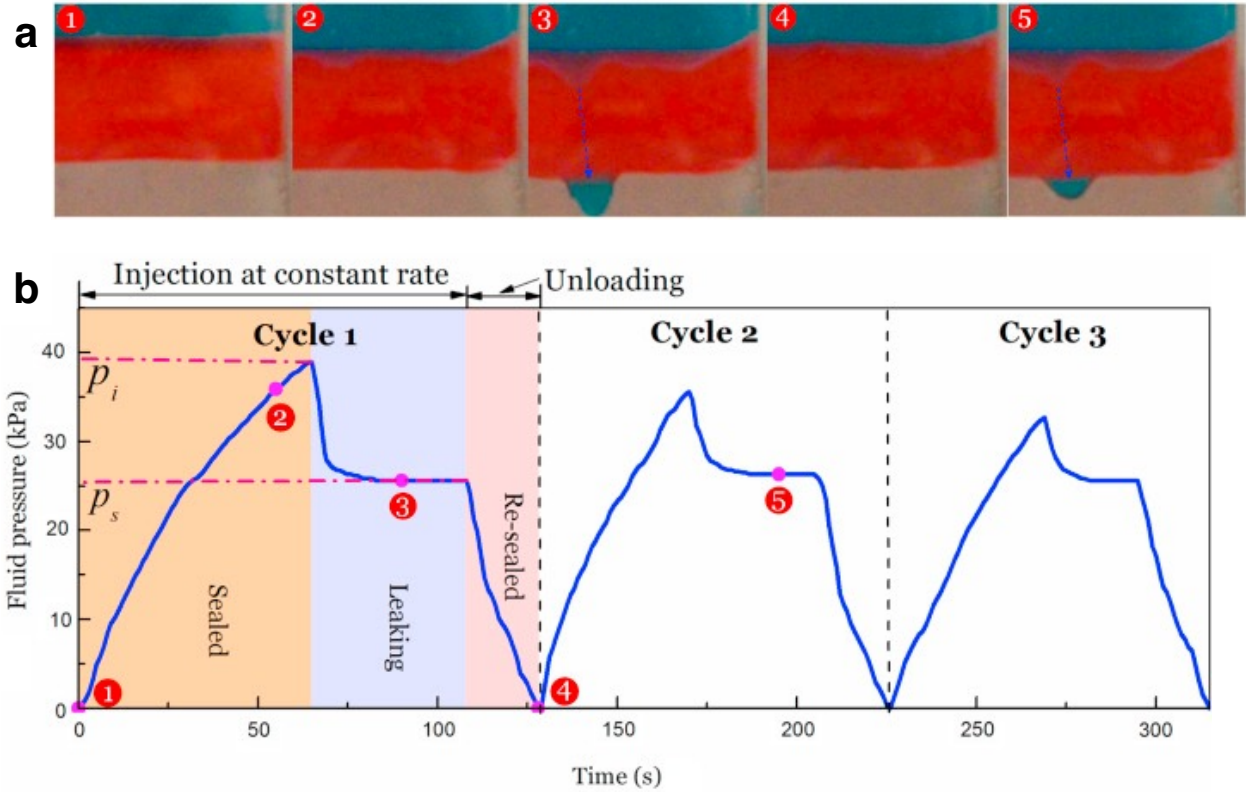


Figure 2.10 Experimental observations of elastic leak

(a) Five snapshots showing the states of a hydrogel seal failing by elastic leak, corresponding to points on the pressure-time curve in (b). Steady-state leaking occurs in images 3 and 5, blue arrows point to the leaking fluid. (b) The characteristic pressure-time curve for the elastic leak failure mode. After steady-state leaking is achieved the fluid pressure is removed and the seal is allowed to reform. Three loading-unloading cycles are plotted. The leak-initiation pressure (p_i) decreases after the first cycle, however, the steady-state leaking pressure (p_s) remains relatively constant. Reproduced with permission from (131).

Experimental studies by Liu et. al. demonstrate failure by elastic leak (131). The experimental results show a seal failing by elastic (recoverable) deformation (Fig. 2.10). Initially, as the fluid pressure rises, the hydrogel seal deforms but does not leak. Upon reaching a peak pressure value, the fluid pressure drops, and a leaking path forms at the interface between the hydrogel and rigid wall. The fluid pressure then settles at a plateau and the seal leaks in a steady-state (p_s). Because no material damage occurs in the failure mode, the seal can be reformed by removing the fluid pressure and allowing for the hydrogel to recover its initial configuration. The behavior of the seal is repeatable from cycle-to-cycle, with nearly identical steady-state leaking pressures, while the leak-initiation pressure reduces as the experiment is repeated. Equation 2.1 predicts the steady-state leaking pressure ($p_s = P_c$), it ignores the influence of friction and adhesion between the seal

and wall. The leak-initiation pressure (p_i) is larger as additional fluid pressure is required to overcome friction and adhesion. However, when the leak reaches a steady-state the hydrogel stops deforming, and the additional fluid pressure to overcome friction is no longer necessary. Thus, a lower fluid pressure is required to sustain the steady leak. After the initial cycle, friction and adhesion are reduced, as fluid is trapped at the interface. Therefore, subsequent cycles require a lower leak-initiation pressure.

2.6.3 Rupture Failure Mode

The other failure mode observed in seals is leak by rupture, in which a crack propagates from one end of the seal to the other. The critical pressure for the onset of the propagation will depend on the initial crack. The model assumes a crack length of L_c which is much smaller than the total length of the seal ($L_c \ll L$). The energy release rate, G , is defined as the reduction in elastic energy divided by the area of crack growth. The energy release rate can be calculated as (132):

$$G = \frac{p^2 H^3}{6\mu L^2 \lambda^3} \quad (2.2)$$

When the energy release rate, G , reaches the material fracture toughness³, Γ , the crack begins to propagate. Inserting the condition of rupture ($G = \Gamma$) into equation 2.2, we obtain the critical fluid pressure for rupture of the seal:

$$P_f = \frac{L}{H} \sqrt{6 \frac{\Gamma \mu \lambda^3}{H}} \quad (2.3)$$

Wang et. al. performed experimental studies demonstrating the rupture failure mode of a hydrogel seal (132). The experimental results show that the crack initiation within the hydrogel corresponds to a rapid drop in pressure (Fig. 2.11). As opposed to what is observed in the elastic leak failure mode—in which the pressure plateaus at a steady-state leaking pressure—the pressure for the rupture failure mode drops to zero, corresponding to catastrophic failure of the seal.

³ Fracture toughness is defined as the energy required to extend a unit area of a crack. It is a material property that quantifies a material's resistance to crack propagation. It measures the ability of a material to absorb energy and prevent fracture, especially in the presence of a pre-existing flaw or crack. The term “fracture toughness” is often used interchangeably with the term “fracture energy”.

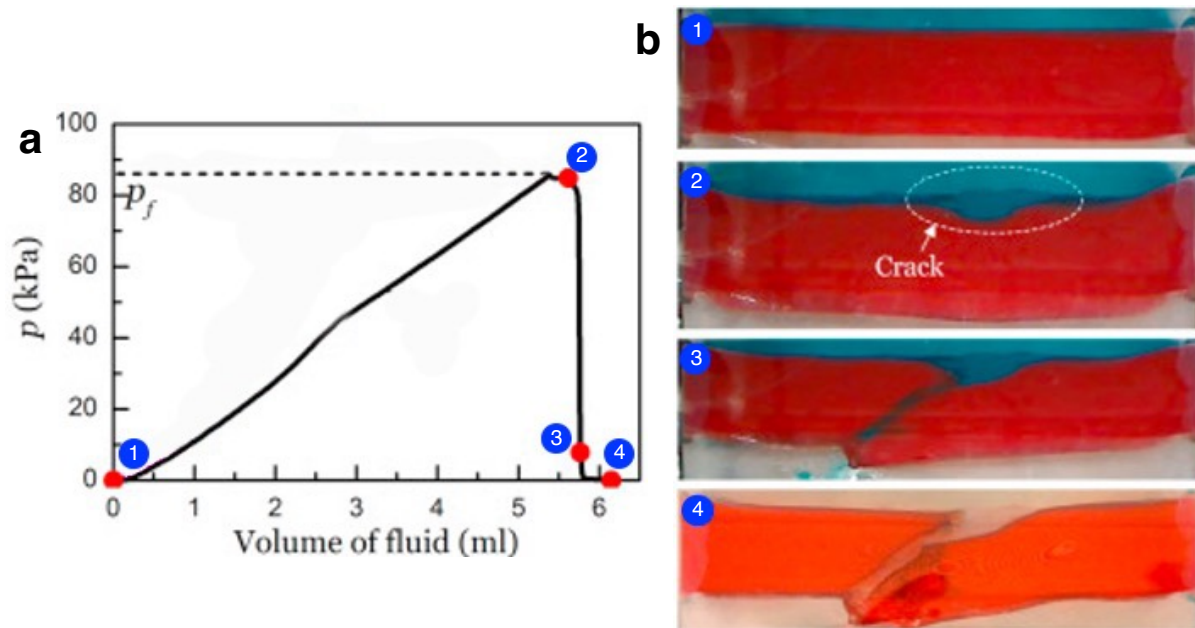


Figure 2.11 Experimental observations of seal rupture

(a) Characteristic pressure–volume injected (P–Q) graph for the rupture failure mode of a seal. (b) Four snapshots showing the states of a hydrogel seal failing by rupture, corresponding to points on the P–Q curve in (a). Crack initiation occurs in image 2, followed by a rapid drop in pressure as the crack quickly propagates from the front of the seal to the back. Adapted from (132).

It is an important question to ask how a material will fail. For instance, if a seal undergoes elastic leak before the material is damaged, the sealing capacity can still be recovered if the fluid pressure is lowered below the steady-state leaking pressure. Conversely, if a seal leaks by rupture, the loss of sealing capacity is irreversible. In the context of embolization, failure by rupture can cause fragmentation and distal migration of the embolic material, while failure by elastic leak represents a more robust occlusion, resistant to these complications. Using this theoretical model of elastomer seal failure, we can draw significant conclusions about the performance of embolic materials—which is instrumental in predicting their efficacy and safety in clinical applications. However, this model presents some limitations when its applicability is extended to the mechanics of embolization. For the case of embolization, the seal is enclosed in a cylindrical vessel, whereas this model describes a seal enclosed between two rigid walls. Additionally, the model overlooks the influence of adhesion, which could potentially lead to a higher sealing pressure, thereby affecting the embolic performance and the subsequent outcomes. These unaddressed factors underscore the necessity for future investigations to take these limitations into account, ensuring a more accurate and comprehensive understanding of embolic materials within the clinical setting.

3 Materials and Methods

Chapter 3 presents an overview of the materials and methods used to conduct the experiments and analysis for this thesis. These experiments were designed to determine the optimal formulation of EBCs for embolization applications. The narrative of this chapter unfolds the vast array of materials, biochemical techniques, mechanical testing apparatuses, and analytical tools employed to achieve this goal. The chapter starts with an overview of EBC synthesis, providing an outline of the polymer linkers, biochemical reagents, and the bioorthogonal chemistry toolkit that serve as the building blocks of EBCs. The chapter then shifts to a summary of the tests designed to provide an overview of the physical properties of EBCs. We will then focus specifically on the *in vitro* embolization models, detailing the experimental tests and theoretical models used to uncover the mechanics of embolization. The next section covers biocompatibility and elaborates on the experimental design tailored to scrutinize the interaction between EBCs and the biological environment. Lastly, we describe the rat and porcine models which evaluate the embolic capabilities of EBCs *in vivo*.

3.1 EBC Preparation and Characterization

Functionalized Hyaluronic Acid Synthesis

Hyaluronic acid (HA, MW ~ 2000 kDa) used for EBC formation was purchased from Lyphar Biotech. Carboxyl groups on HA were modified with a click chemistry functional group—either dibenzocyclooctyne (DBCO) or tetrazine (Tz)—using EDC/NHS carbodiimide chemistry following previously established protocols (Fig. 3.1) (134). First, sodium hyaluronate was dissolved at a concentration of 0.5% wt/v in a 100 mM MES buffer solution (0.3 M NaCl, pH 6.0). EDC and NHS (Sigma-Aldrich, 03450 and 130672, respectively) were added at 2.5-times molar excess of the carboxyl groups of HA, followed by either sulfo DBCO-amine or methyltetrazine amine (Click Chemistry Tools, 1227 and 1011, respectively) at 0.75 mmol per gram of HA. The reaction was stirred at room temperature for 24 hours and subsequently transferred to 14 kDa MWCO dialysis tubing (Sigma-Aldrich, D9527) and dialyzed for 5 days against a decreasing salt gradient—from 150 mM to 0 mM NaCl (150 mM, 100 mM, 50 mM, 0 mM, 0 mM, for 24 hours per solution). To obtain sterilized HA, the solution was subsequently dialyzed in a 50% v/v ethanol

solution for 24 hours followed by DI water for 2 days (changing the solution every 24 hours). After dialysis, the solution was frozen at -80°C overnight and lyophilized (Labconco Freezone 4.5L - 84C) for 48 hours.

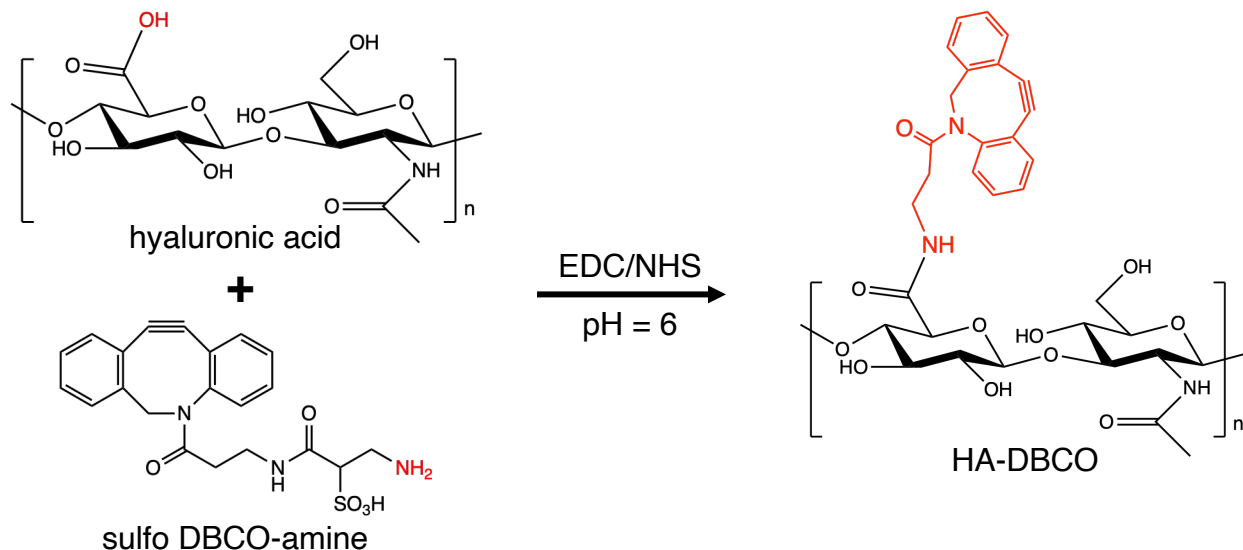


Figure 3.1 Synthesis of functionalized hyaluronic acid

Synthesis of HA-DBCO via carbodiimide chemistry. Through the use of EDC and NHS, the amine group of sulfo DBCO-amine is conjugated to the carboxyl group of HA, forming HA-DBCO. A similar reaction is used to synthesize HA-Tz, except methyltetrazine-amine is used instead of sulfo DBCO-amine.

Functionalized Hyaluronic Acid ^1H NMR Characterization

The resulting functionalized polymers were characterized using ^1H nuclear magnetic resonance spectrometry (^1H NMR, 400 MHz Varian Mercury). Deuterium oxide (D_2O) was used as the solvent and the results were analyzed to obtain the degree of substitution (DS%) of the DBCO or Tz functional group to carboxyl groups on HA. Chemical shift values were reported in parts per million (ppm). The degree of substitution (DS%) was calculated by the following equation:

$$DS\% = \frac{I_C \cdot N_{HA}}{I_{HA} \cdot N_C} \cdot 100\%$$

where I_C and N_C are the integral value and number of protons for the click moieties ($\delta=7.27\text{--}7.51$ ppm for DBCO, and $\delta=7.47\text{--}7.57$ ppm or $\delta=8.40\text{--}8.30$ ppm for Tz). I_{HA} and N_{HA} are those for the N-acetyl methyl groups on HA ($\delta=1.9\text{--}2.0$ ppm) (135-137).

Red Blood Cell Surface Modification

Red blood cells (RBCs) used for cell surface modification were obtained from bovine whole blood in CPD anticoagulant (Lampire Biological Laboratories, 7200804). RBC surfaces were modified with the complementary click chemistry motif through a reaction between primary amines located on the cell surface and NHS esters containing the click moiety—either Az for HA-DBCO or TCO for HA-Tz. First, citrated whole blood was centrifuged (1000g, 5 min) to separate the RBCs from the plasma. The separated RBCs were then thoroughly washed three times with cold PBS (9:1 PBS to RBC ratio) and centrifuged to remove the supernatant. Following washing, RBCs were resuspended in PBS at a 9:1 PBS to RBC ratio followed by the addition of a stock solution (25 mg/mL dissolved in DMSO) of either Azido-PEG4-NHS Ester or TCO-PEG4-NHS Ester (Click Chemistry Tools, AZ103 and A137 respectively) to achieve a final concentration of 1 mg/mL. The solution was then incubated at 37°C for 45 minutes to allow the reaction to complete. Following incubation, the solution was centrifuged, and the supernatant was gradually replaced with fresh PBS as to slowly remove the DMSO to prevent hemolysis from occurring, followed by another three complete PBS washes and the complete removal of the supernatant.

Modified Red Blood Cell Confocal Imaging

RBC surface modification was observed using confocal imaging. Az-modified RBCs were suspended in PBS at a 9:1 PBS to RBC ratio and incubated with a Cy5 DBCO fluorescent probe (Click Chemistry Tools, A130) at a concentration of 10 $\mu\text{g/mL}$ for 1 hour at 37°C (Fig. 3.2). Following incubation, the modified cells were thoroughly washed with PBS three times to remove the unreacted fluorescent probe. The fluorescently labelled RBCs were then diluted in PBS at a 100:1 PBS to RBC ratio and imaged using a confocal laser scanning microscope (Zeiss, LSM710).

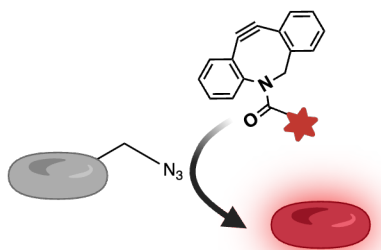


Figure 3.2 Fluorescent tagging of azide-modified red blood cellsⁱ

RBC-Az are tagged with a DBCO conjugated Cy5 fluorescent probe. DBCO reacts with the Az groups on the cell surface to confirm their presence through confocal imaging.

Preparation of EBCs

EBCs used for embolization were prepared by forming a crosslinked cellular network of RBCs, integrated with the native fibrin network and other blood components. Functionalized HA was dissolved overnight in Visipaque 320 (GE HealthCare, V-560) at various concentrations ranging from 1% to 4% (wt/v). Modified whole blood was obtained by substituting native RBCs with modified RBCs suspended in an equal volume of platelet-rich plasma (PRP)—obtained by centrifuging whole blood at 300g for 15 minutes. To initiate the native and click clotting simultaneously, modified blood was recalcified using a calcium chloride (CaCl_2) solution at a final concentration of 30mM. Equal volumes of modified blood and the HA solution were then quickly mixed in syringes until fully homogeneous (Fig. 3.3). For example, an initial 2% wt/v HA-DBCO solution mixed with an equal volume of modified blood results in a final polymer concentration of 1% wt/v and a 25% v/v cell ratio.

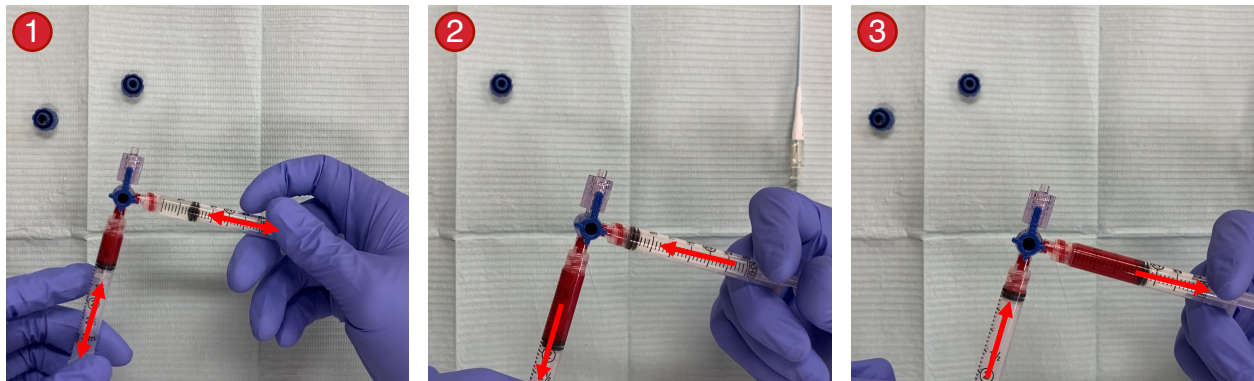


Figure 3.3 Formation of Engineered Blood Clot by syringe mixing

Images showing syringe mixing of EBC using two 3-mL syringes and a 3-way stopcock. Syringes containing functionalized HA solution and modified blood are connected to a 3-way stopcock and mixed until homogeneous. After mixing, the 3-way stopcock can be connected to a microcatheter for embolization. The user should pay close attention to detail to remove all bubbles before syringe mixing.

Scanning Electron Microscopy

The morphology of EBC was observed using a field emission scanning electron microscope (FE450, FEI) with an accelerating voltage of 10 kV under various magnifications. EBC samples were fixed with 4% paraformaldehyde and subsequently dehydrated using an increasing ethanol gradient from 30% to 100% (v/v). The dried samples were then coated under 4 nm of platinum, using a high-resolution sputter coater (ACE600, Leica), to increase surface conductivity.

Native Blood Clot Formation

Native blood clots (NBCs) were formed following a previously established protocol (138). To initiate the native clotting cascade bovine whole blood was recalcified using a CaCl_2 solution at a final concentration of 30 mM. Following recalcification, the blood clot was incubated at 37°C for 1 hour and sealed to maintain humidity during the coagulation process.

3.2 Physical Properties Testing

Rheological Analysis

All rheological measurements were made using the Discovery HR-2 rheometer (TA Instruments) with a 20-mm steel parallel plate and 1-mm gap at a temperature of 37°C , to mimic physiological temperatures. Mineral oil was applied around the circumference of the plate to prevent material dehydration during testing. The Storage modulus (G'), loss modulus (G''), and gelation kinetics were measured using a time sweep over 3600s at 0.1% shear strain and 1Hz. The time to full gelation was defined as the time it takes for the storage modulus to reach 95% of the plateau value. A frequency sweep was performed at frequencies from 0.001 to 100 Hz at 0.5% shear strain.

EBC Radiopacity

CT imaging of EBC samples was performed using a Bruker Skyscan 1172 microCT system. Samples containing 0, 10, 20, or 30 (% wt/v) of iodixanol (Fig. 3.4) were loaded into 1-mL syringes and loaded into the microCT scanner. Syringes containing Visipaque 320 were tested for comparison. The acquisition was realized using the following parameters: 75 kV and 420 mA. The radiopacity of the different EBC compositions was evaluated using NRECON 3D reconstruction software (Bruker) by calculating the mean X-ray attenuation in Hounsfield units (HU).

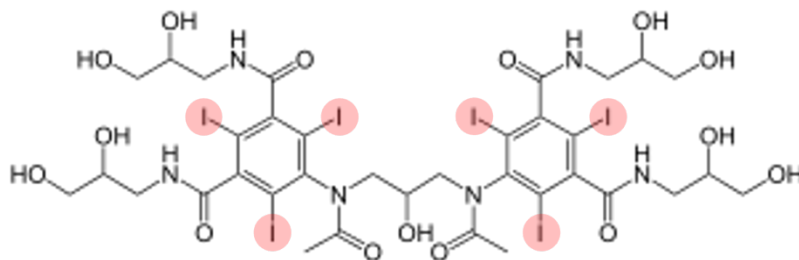


Figure 3.4 Chemical structure of iodixanol

Chemical structure of the radiocontrast agent iodixanol, sold under the brand name Visipaque. Bound iodine (highlighted in red) makes the molecule radiopaque.

Injection Force Measurement

An injection force test was performed to measure the injectability of EBCs through clinically used microcatheters. A 3-mL syringe (BD Luer-Lock tip, 309657) containing 1 mL of material was fixed to the lower gripper of a mechanical tester (Instron model 5965) (Fig. 3.5). The syringe plunger was depressed by a compression plate connected to a 1-kN load cell at a constant flow rate of 1 mL/min. The samples were injected through 150cm 2.4Fr SuperCross™ microcatheters (Teleflex, 5305) into a PBS solution. The injection force, which was defined as the plateau force, and the cohesion of the material after injection were both analyzed. Injection of Onyx 34 (Medtronic) and Visipaque 320 were used as references.

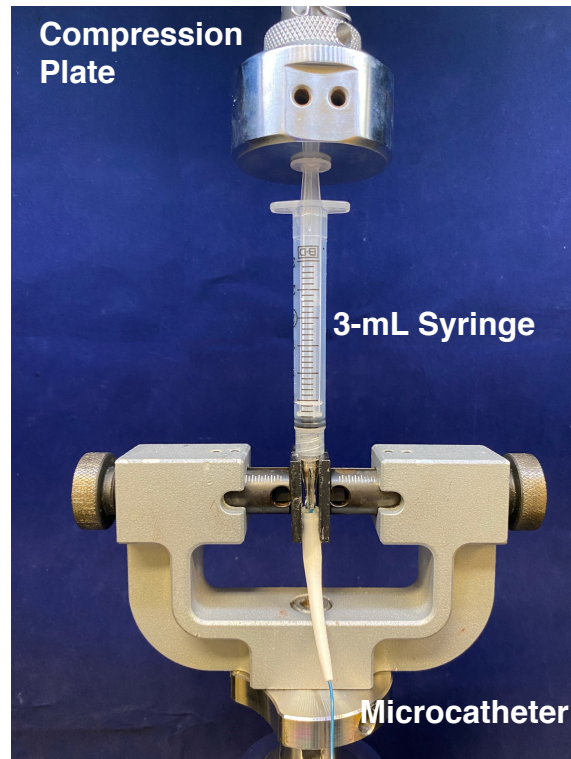


Figure 3.5 Experimental set-up for injection force measurements

3-mL syringe is fixed to an Instron mechanical tester. The compression plate pushes on the syringe plunger which injects the material through a microcatheter connected to the syringe.

Fracture Toughness Measurement

A modified lap shear test was performed to measure the fracture toughness of EBCs following an established protocol (138). Samples were injected into a $20 \times 15 \times 1.5 \text{ mm}^3$ PTFE mould and covered with a PTFE sheet. EBC and NBC samples were sealed and incubated at 37°C for 1 hour to allow

for full gelation. After gelation, samples were removed from the moulds and glued to two thin polyethylene terephthalate (PET) films on each side as rigid backings. An initial edge crack of 5mm was introduced in the middle of each sample. The specimens were loaded vertically onto an Instron machine equipped with a 10-N load cell with a displacement rate set at 2 mm/min (Fig. 3.6a). The fracture toughness (Γ) was calculated as the total work (W_t)—the area under the force-displacement curve—divided by the fracture surface area (A):

$$\Gamma = \frac{W_t}{A}$$

The fracture surface area (A) is the product of the sample width and the total crack length. The total crack length is defined as the sample length minus the initial crack length. The fracture surfaces were examined post-testing to confirm cohesive failure. The fracture toughness of NBCs and Onyx 34 were measured for comparison.

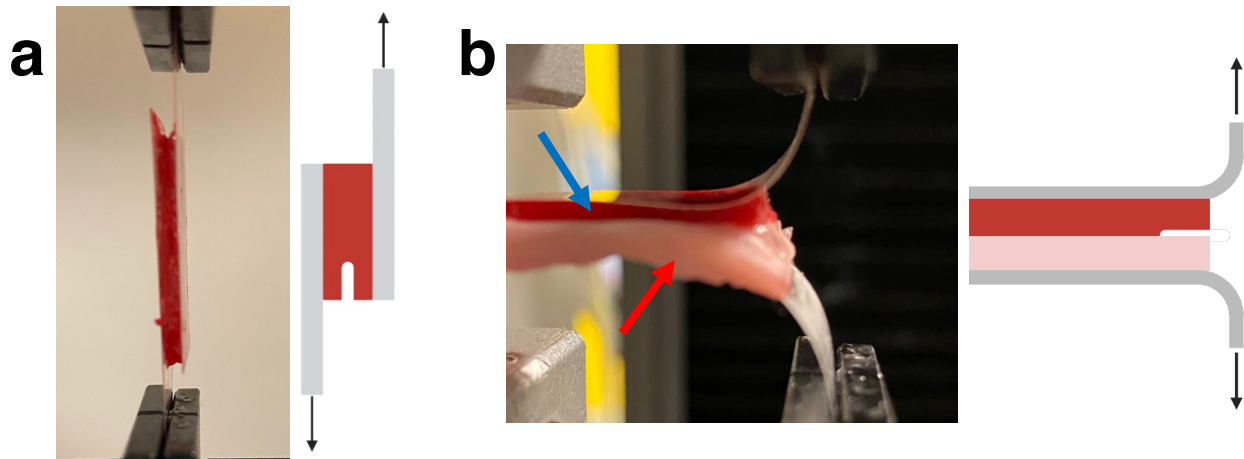


Figure 3.6 Experimental set-up of mechanical testing

(a) Image and schematic showing the modified lap-shear test used to measure material fracture toughness. EBC is adhered between two PET films which are fixed to an Instron mechanical tester. (b) Image and schematic showing the 180-degree peeling test used to measure adhesion energy. EBC (blue arrow) is adhered to the inside of a bovine artery (red arrow).

Adhesion Measurement

A 180-degree peeling test was performed to measure the adhesion energy between EBCs and various materials. Fresh bovine arteries (Montpak International, Terrebonne, Canada) were cut along the length of the vessel to create a flat surface. Samples were injected into a $30 \times 10 \times 1.5 \text{ mm}^3$ elastomer mould which was applied to the inner lumen of the arteries. For adhesion tests on the

subendothelial layer, the endothelium was delicately removed through gentle rubbing with a cotton thread. Samples were sealed and incubated at 37°C for 1 hour to allow for full gelation. No compression was applied to the specimens. After gelation, the elastomer moulds were carefully removed, and thin PET films were glued to the EBC and backside of the vessel as rigid backings. An initial crack of 5 mm was introduced between the EBC and the blood vessel. The specimens were attached to an Instron machine equipped with a 10-N load cell with a displacement rate set at 100 mm/min (Fig. 3.6b). The test was repeated to measure the adhesion between EBCs and a thin nylon film (McMaster-Carr, 8539K192). The adhesion energy (G) was calculated as two-times the plateau force ($F_{plateau}$) divided by the width of the specimen (w):

$$G = \frac{2F_{plateau}}{w}$$

Volumetric Swelling Measurement

Material samples were prepared into disk shapes 5 mm in diameter and 1.5 mm in height, immersed in PBS in a sealed Petri dish, and incubated at 37°C. After 24 hours the swollen diameters and heights were measured using a digital caliper. Swelling was quantified using the volumetric swelling ratio, which was calculated as the volume of the swollen state (V_s) divided by the initial sample volume (V_i):

$$\text{Volumetric Swelling Ratio (VSR)} = \frac{V_s}{V_i}$$

3.3 Embolization Modelling

In Vitro Vasculature Flow Model

In vitro vasculature phantoms were fabricated by casting PDMS (Sylgard 184, Dow Corning) around sacrificial PVA moulds. This method was adapted from a previous protocol (139). Specifically, sacrificial moulds were 3D-printed (Ender-3 V2, Creality) from water-soluble PVA filaments (PVA 3D Printer Filament, Monoprice). After printing, the moulds were briefly immersed in warm water to smooth the surface. PDMS (10:1 base to crosslinker ratio) was then degassed in a vacuum chamber before being poured over the 3D-printed moulds. After casting, the assembly was placed in an oven at 60°C for 3 hours to allow for full curing of the PDMS (Fig.

3.7a). After curing, the assembly was placed in an ultrasonic water bath at 50°C until the PVA was fully dissolved (Fig. 3.7b).

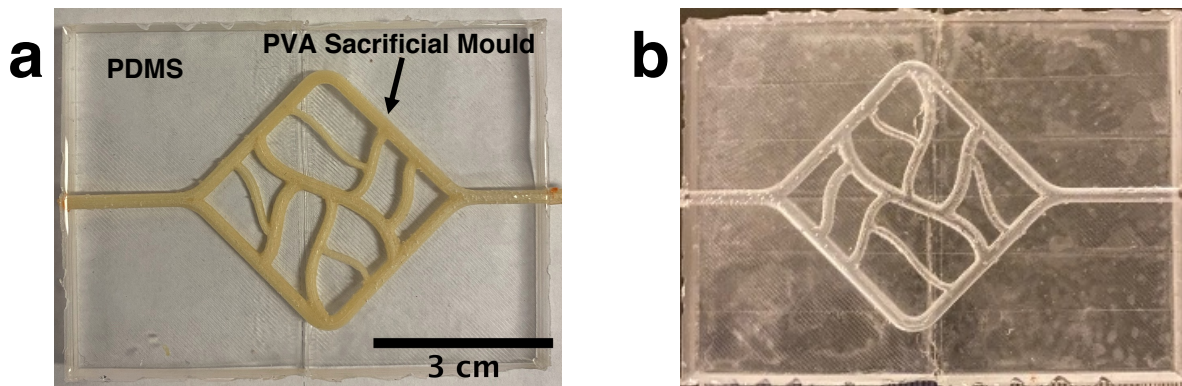


Figure 3.7 Formation of PDMS vasculature phantom

(a) Image of PVA sacrificial mould cast in PDMS before dissolution. (b) Image of PDMS vasculature phantom after the dissolution of the sacrificial PVA mould in an ultrasonic water bath.

The vasculature phantoms were connected to a biomimetic pulsatile pump (TrandoMed, EDU-P120) which simulates the activity of the human heart. The phantoms were connected to the pump via silicone tubes, 3 mm in diameter, representing a feeding artery and a draining vein. A third silicone tube was also connected proximal to the vasculature phantoms via a Y-connector, to allow for pressure release after embolization (Fig. 3.8). The vasculature phantom was specifically designed to model an AVM, where the deep penetration of the embolic material into the nidus is required; the size of the phantom was modeled to be physiologically relevant (140, 141). The vasculature phantom had vessels of various diameters, from 1 mm to 3 mm, with a total volume of 2652 mm³. The system was perfused with a water-glycerol solution (3:2 ratio of water to glycerol) with the temperature set to 37°C. To mimic physiological conditions, we set the pulsatile pump parameters as follows: pulsation frequency—60 bpm; pressure at pulsation output end—90 mmHg (142); flow at pulsation output end—220 mL/min (143). A 2.4Fr microcatheter (SuperCross™ 5305, Teleflex) was inserted into the system via a hemostatic Y-adapter proximal to the phantom. EBC was injected into the system to embolize the phantom vasculature until the material reached the draining vein or reflux occurred into the feeding artery. Following embolization, the depth of penetration of the embolic material into the vasculature phantom was analyzed.

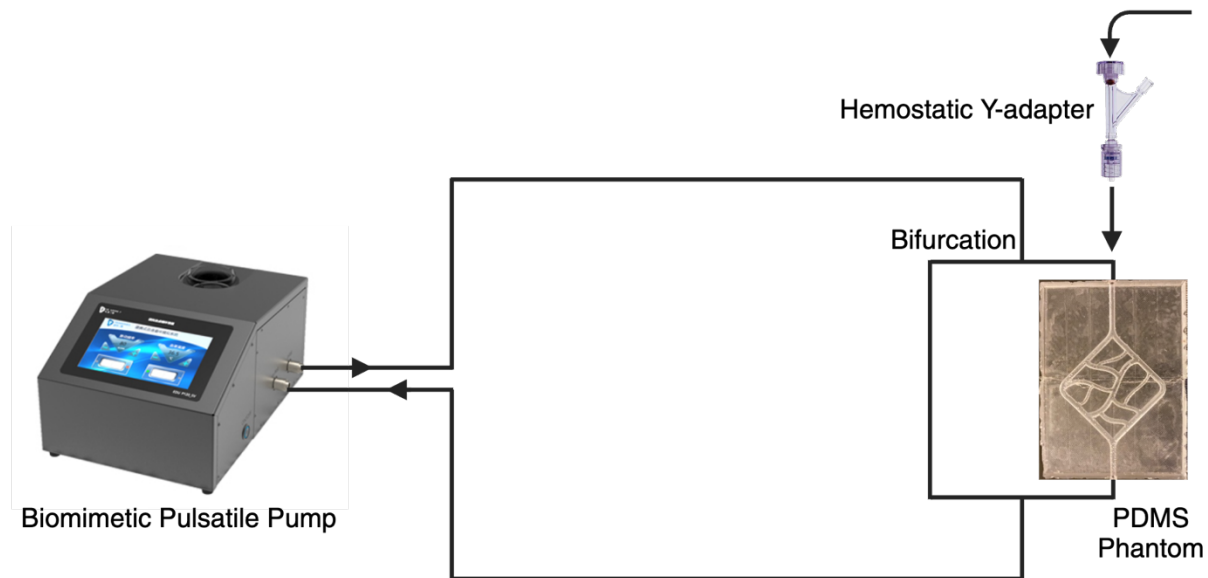


Figure 3.8 Experimental set-up of in vitro vasculature flow model

Schematic of the in vitro set-up to model the penetration depth of embolic materials. A biomimetic pulsatile pump was set to mimic physiological conditions. A 2.4Fr microcatheter was introduced via a hemostatic Y-adapter to inject the embolic material into the vascular phantom. A bifurcation was added to allow for pressure release after embolization.

In Vitro Occlusion Model

An in vitro occlusion test was performed to evaluate the embolic properties of EBCs. PDMS tubes (3 mm inside diameter and 1.5 mm thickness) were used as blood vessel phantoms. The diameter of the PDMS phantom was chosen to match that of a small artery which would be typically targeted for embolization (144). A water-glycerol solution, consisting of a 60:40 (% v/v) ratio of water to glycerol, was used as a blood-mimicking fluid due to its similar viscosity to blood. The water-glycerol solution was flowed through the tubes with the use of a syringe pump. A 5Fr catheter (Cook Medical, G13794) was fed into the tubing to inject the EBC directly into the PDMS vessel phantom. The catheter was removed, and the flow rate of the syringe pump was set to 10 mL/min. The pressure was monitored upstream with a pressure gauge. The pressure-time curves, including the maximum embolization pressure, were recorded. The tests were repeated with NBCs and Onyx 34 as comparisons. The test was also repeated using bovine arteries (average diameter: $4.23 \text{ mm} \pm 0.44 \text{ mm}$), Montpak International, Terrebonne, Canada) as the occlusion vessel. The arteries were connected to the syringe pump with the use of zip-ties. Anticoagulated bovine whole blood was flowed through the system and the pressure was monitored upstream.

3.4 In Vitro Biocompatibility Testing

Cytotoxicity

Cytotoxicity tests were performed using immortalized human vocal fold fibroblasts following ISO 10993-5 standards (145). Extracts were prepared by incubating EBC in cell culture medium for 24 hours, while 20 000 cells per well were seeded in a 96-well plate. For every 200 mg of EBC, 1 mL of Dulbecco's Modified Eagle's medium (DMEM) was added. Following incubation, extracts were supplemented with 1% penicillin-streptomycin and either with or without 10% fetal bovine serum (FBS). The culture medium within the 96-well plate was then replaced with the supplemented extracts. Completed pristine DMEM was used as a positive control and extract of Onyx 34 was used as a comparison. The cells were cultured for 24 hours inside an incubator, in an environment at 37 °C, 95% relative humidity, and 5% CO₂ atmosphere. Cell viability was assessed using a Live/Dead viability kit (Invitrogen, L3224), following the protocol of the manufacturer. Confocal laser scanning microscopy (Zeiss, LSM710) was used for investigation. Live cells were visualized in green and dead cells in red. The images were analyzed using ImageJ software (National Institutes of Health). Cell viability was defined as the percentage of live cells in the sample, while the cell density of a sample was used to measure cell proliferation.

In Vitro Degradation

In vitro degradation assays were performed to measure the fibrinolysis and enzymatic degradation of EBCs. To measure the effect of fibrinolysis, EBCs and NBCs were incubated in plasma supplemented with tissue plasminogen activator (tPA). All samples were first washed thoroughly in PBS to remove excess Ca²⁺ ions. After, samples were prepared of the same size and weighed using an analytical balance at time 0. Plasma was obtained by centrifugation of bovine whole blood at 1000g for 5 minutes. 10 µg/mL of tPA (Sigma-Aldrich, T0831) was added to the plasma (146). The samples were sealed and incubated in the supplemented plasma at 37°C under gentle agitation (100 rpm). At pre-determined time points, the plasma was removed, and the remaining material was weighed. At each time point the plasma was replaced with fresh supplemented plasma.

EBCs were incubated in PBS containing hyaluronidase to measure the enzymatic degradation. The degradation of Onyx 34 was measured for comparison. 60 ng/mL of hyaluronidase (bovine testicular hyaluronidase, Sigma-Aldrich, H3506) and 0.01% wt/v sodium azide (NaN³, Sigma-Aldrich, S2002) were added to PBS (147). The samples were incubated in the supplemented PBS,

sealed, and placed at 37°C under gentle agitation (100 rpm). At pre-determined time points, the PBS was removed, and the remaining material was weighed. At each time point the PBS was removed and replaced with fresh supplemented PBS.

3.5 In Vivo Studies

Rat Abdominal Artery Embolization

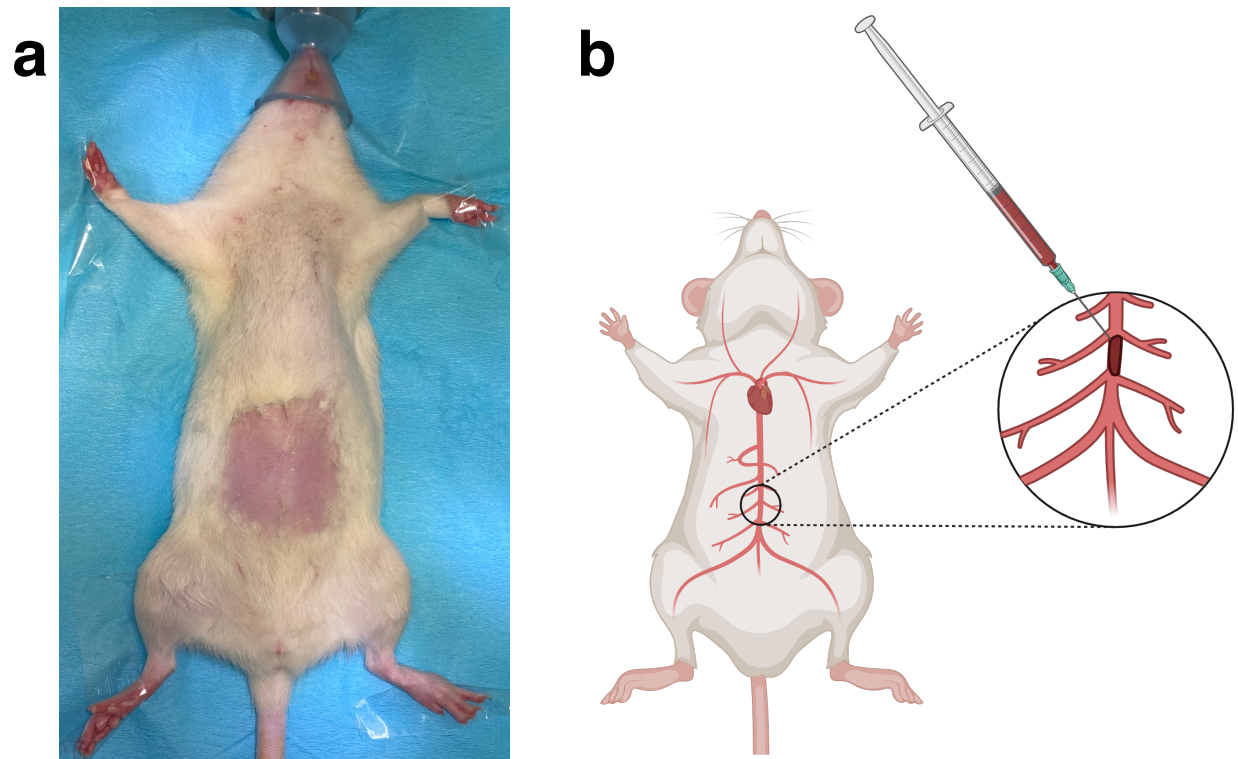


Figure 3.9 Rat abdominal artery embolization

(a) Image of rat laying in a supine position before the surgery showing the surgical area. (b) Schematic illustrating the embolization of the rat's abdominal artery using a 30G needle.ⁱ

In vivo rat embolization procedures were approved by the McGill University Animal Care Committee (Protocol # 2019-8098) and performed according to the guidelines of the Canadian Council on Animal Care. Female Sprague Dawley rats (250a–300g, n = 4) were purchased from Charles River Laboratories (Wilmington, USA). Initially, rats were anesthetized using isoflurane (4% isoflurane in oxygen) in an induction chamber. Anesthesia was maintained at 2% isoflurane using a nose cone during the surgery. After anesthesia, the rats were placed in a supine position for the duration of the surgery (Fig. 3.9a). Initially, before the surgery, the hindlimb skin color was observed and recorded. Abdominal hair was removed, and the area was cleaned with an antiseptic

solution. A 1 cm incision was made longitudinally along the abdomen of the rat and the abdominal artery was exposed. 100 μ L of EBC was injected distally into the artery using a 30G needle (Fig. 3.9b). After injection, the incision was closed with a 5-0 polypropylene suture. Throughout the surgery, the hindlimb skin color was observed. Post-surgery, rats were euthanized and subjected to microCT scanning imaging (Mediso nanoScan PET/CT) to confirm embolization. All images were recorded and analyzed using ImageJ software to produce three-dimensional (3D) images.

Porcine Embolization Model

In vivo porcine embolization procedures were conducted according to the guidelines of the Canadian Council on Animal Care and approved by the Institutional Animal Protection Committee at the University of Montreal Hospital Research Centre (CRCHUM). Pigs ($n = 2$) were acclimatized for seven days prior to the experiment. Two days before the procedure, blood was harvested from the animals to allow for preparation of the embolic agent. Pigs were fasted (food only) the day before the experiment. For the procedure, all animals received xylazine (2 mg/kg) and ketamine (25 mg/kg, intramuscularly) as preanesthetic medication. Anesthesia was induced using propofol (1.66 mg/kg, intravenously) and maintained throughout the procedure by isoflurane inhalation. After the induction of anesthesia, femoral access was obtained through US guidance. A 5Fr sheath was positioned, followed by the catheterization of the hepatic artery using a 4Fr Cobra catheter. A supraselective catheterization of a segmental artery was performed using a 2.8Fr microcatheter. Digital subtraction angiography (DSA) of the segmental artery was performed to opacify the vessels under fluoroscopic guidance. Then, each segmental artery was embolized using EBCs. Following embolization, a DSA was performed to assess arterial occlusion. The splenic artery; one segmental artery of each renal artery (lower pole); a segmental gastric artery; and a left and right segmental hepatic artery were all embolized following the same methodology. Following the procedure, animals were recovered from anesthesia and survived for 7 days before euthanasia. Prior to euthanasia, animals were reanesthetized for angiography and terminal imaging.

Statistical Analysis

A sample size of $n \geq 3$ was used for all experiments. Data are shown as mean \pm SD. Statistical analysis was performed using one-way ANOVA and post hoc Tukey tests for multiple comparisons or Student's t-tests for comparison between two groups. P values < 0.05 were considered statistically significant.

4 Results

Chapter 4 presents the experimental results of this work, wherein the previously conceived ideas and subsequent laboratory investigations are analyzed, leading us to draw conclusions and scientific implications of the work. The chapter begins with a detailed analysis of the design principles regarding EBCs for embolization, chronicling the journey from conceptualization to realization, and further, optimization of the material system for the specific purpose of embolization. The focus then shifts to the mechanical properties of EBCs, clearly illustrating how the engineered constructs fare in mimicking the functionality of native blood clots while bearing the advantages of enhancement through engineering design. This section will lead us into a discussion on the mechanics of embolization, where the behaviour of embolic materials under physiological mechanical conditions is scrutinized. The importance of material properties is dissected to understand the mechanics underlying successful embolization. Next, we delve into the biocompatibility tests which provide an exploration into the biological performance of EBCs and ensures the safety and efficacy of this novel technique. Here we will see how the combination of autologous and biocompatible components through bioorthogonal chemistry, contributes to a highly biocompatible material system. The chapter culminates with the in vivo experiments, where the rubber meets the road. The trials conducted and the resultant data gathered here provide a glimpse into the real-world potential and the hurdles that lie ahead.

4.1 Design and Synthesis of Engineered Blood Clots for Embolization

The design of EBCs is inspired by native blood clots (NBCs), which serve as natural hemostatic agents to halt excessive bleeding during injuries. NBCs possess many advantages that are not seen in today's clinically used embolic materials. Clots form a temporary barrier, sealing the vessel from bleeding and allowing the tissue repair process to begin. They also create a framework for new tissue to grow into, forming a scaffold for wound healing. However, while NBCs have many advantages when it comes to embolization, they also have many drawbacks which has limited their use in clinical interventional radiology (6, 7). Here we further engineer NBCs, forming *Engineered Blood Clots* (EBCs), which possess the intrinsic advantages of NBCs but are designed to be easily used in an interventional radiology clinical setting. To form EBCs that can be effectively used for

embolization our design combines the native clotting process with bioorthogonal crosslinking of red blood cells and biodegradable polymer linkers (Fig. 4.1a). This results in a dual-network, cellular-based hydrogel that demonstrates excellent mechanical properties and biocompatibility. The choice of bioorthogonal crosslinking is an important one because it ensures high biocompatibility and will not disrupt the biological system. This contrasts with the current clinically used treatments, such as Onyx or n-BCA, which require harsh chemicals or solvents for gelation. Further, the dual-network structure of EBCs and the high deformability of RBCs contribute to their superior mechanical properties. Resulting in a robust embolic material which can form a stable occlusive seal that is mechanically resistant to fragmentation.

Hyaluronic acid (HA) was chosen as the polymer linker due to its high biocompatibility, degradation *in vivo*, and long hydrodynamic size which allows for effective linking of the cells. Carboxyl groups present on HA were modified with click chemistry functional groups (either DBCO or Tz) using EDC/NHS chemistry. ¹H NMR was employed to confirm the successful modification of the resulting polymers and quantify the degree of substitution of the click moiety (Fig. 4.1c and d). Proton peaks between 7.27–7.51 ppm account for the 8 hydrogens on the aromatic rings of the DBCO moiety, which are labelled **i** on the HA-DBCO chemical structure (Fig. 4.1c). The peak at 1.9–2.0 ppm corresponds to the 3 hydrogens of the N-acetyl methyl (–CH₃) groups on HA, labelled **ii** on both the HA-DBCO and HA-Tz structure (Fig. 4.1c and d). The peaks between 7.47–7.57 ppm and 8.40–8.30 ppm correspond to 2 hydrogens each on the phenyl ring of the Tz moiety, labelled **i** and **iii** on the HA-Tz chemical structure (Fig. 4.1d). The degree of substitution was calculated to be 8–14% for both HA-DBCO and HA-Tz.

RBC membranes were modified with the complementary click motif through carbodiimide chemistry—either Az for HA-DBCO or TCO for HA-Tz. Pegylated labelling reagents containing the click motif are linked to an NHS ester moiety which covalently binds to primary amines located on RBC surface membrane proteins (Fig. 4.1e). Confocal imaging was used to confirm the presence and even distribution of these click motifs on the surface of RBC-Az modified cells (Fig. 4.1f), whereas negligible fluorescent signal was detected on unmodified RBCs (Fig. S1).

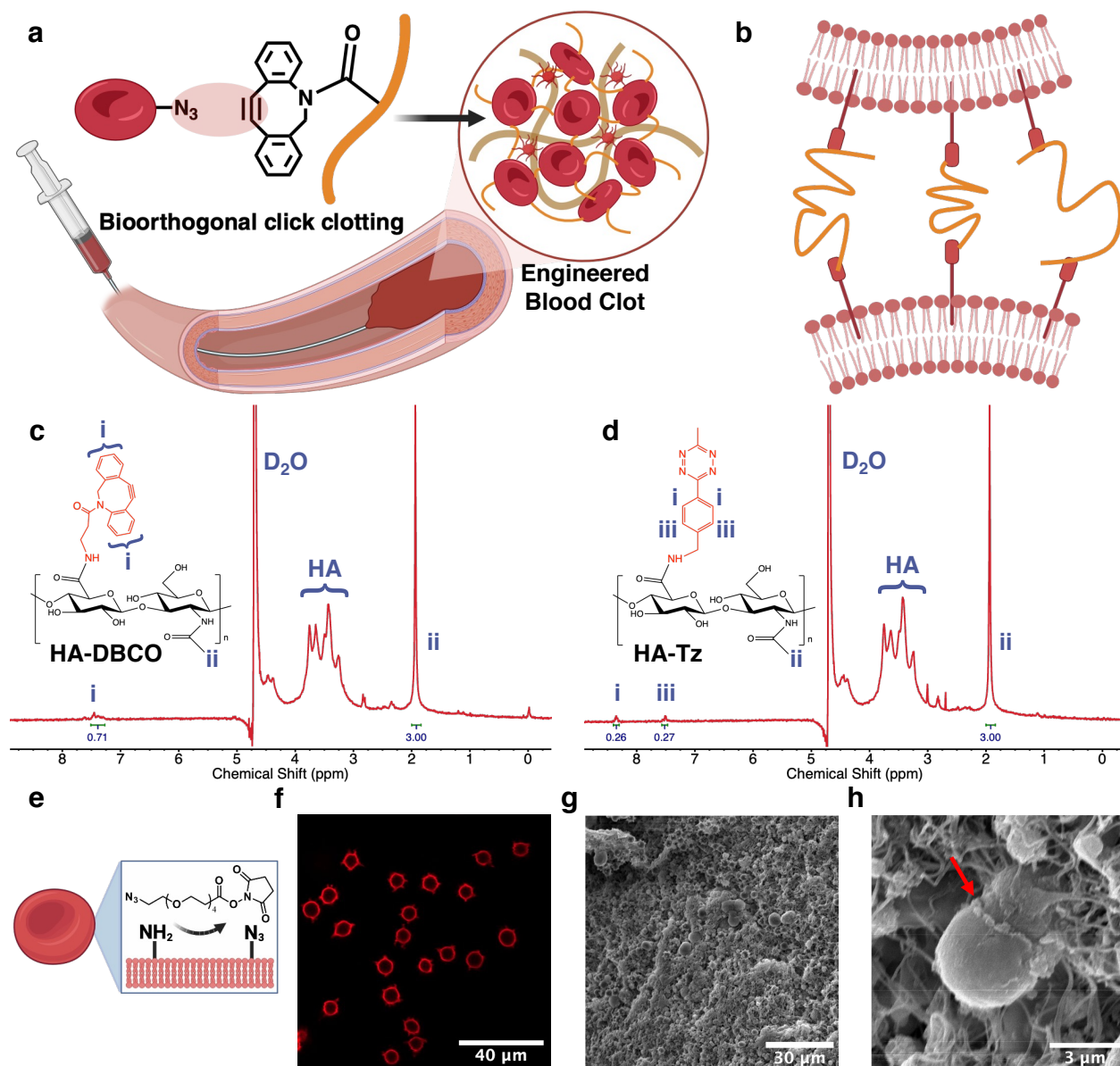


Figure 4.1 Design principles and characterization of Engineered Blood Clots

(a) Schematic of EBC as an embolic agent, showing cell-crosslinking strategy and embolization of a blood vessel via injection of EBC.¹ (b) HA polymer linkers form multiple connections to RBC membrane proteins, gluing together cell membranes.¹ (c, d) ¹H NMR spectrum of HA-DBCO/HA-Tz with protons attributed to DBCO/Tz and HA N-acetyl methyl groups, labelled as i/iii and ii, respectively. (e) Schematic showing RBC surface modification with azide groups, through a reaction between Az-NHS esters and amine groups on the RBC surface.¹ (f) Confocal image showing successful modification of RBCs with Az groups on the cell surface via the use of a DBCO-linked red fluorescent probe. (g) SEM image showing the structure of EBCs. (h) SEM image showing RBCs are linked together within EBC.

4.1.1 Gelation Mechanisms and Kinetics

Mixing of functionalized polymer linkers and modified RBCs results in the instant formation of a cellular crosslinked cytogel. Both bioorthogonal reactions explored—HA-DBCO + RBC-Az and HA-Tz + RBC-TCO—resulted in an initial storage modulus (G'_{0}) which was larger than the initial loss modulus (G''_{0}) (Fig. 2a); while mixing unmodified RBCs and HA results in a G' which is similar to G'' , behaving as a viscous solution (Fig. S2a). The structure was examined by SEM showing the cellular-based nature of the material (Fig. 4.1g). Due to the large size difference between RBCs (8 μm : diameter) and the HA polymer linkers (150 nm: effective diameter), HA acts as a cellular glue, which covalently binds the cells together (Fig. 4.1h). Click-modified cell surface proteins can bind and crosslink with multiple HA linkers (Fig. 4.1b), resulting in an interconnected RBC network in conjunction with the native fibrin network.

To understand the gelation kinetics of the click clotting process we uncoupled the bioorthogonal and native clotting processes. A rheological time sweep was performed on EBCs without the addition of Ca^{2+} ions, to prevent the fibrin network formation (Fig. 4.2a). These results demonstrate the gelation occurring solely from the bioorthogonal reaction between the HA polymer linkers and the modified RBCs. Here, we demonstrate two separate bioorthogonal reactions with distinct reaction kinetics. The IEDDA reaction involving HA-Tz and RBC-TCO exhibits extremely fast kinetics, resulting in a nearly instantaneous gelation of EBC_{Tz} . In contrast, the SPAAC reaction between HA-DBCO and RBC-Az demonstrates much slower kinetics. Specifically, EBC_{DBCO} undergoes a more gradual gelation process, showing a gradual increase of G' before reaching a plateau value.

Further, we conducted rheological tests of varying cell-polymer mixtures to probe the effect of cell-polymer interactions on EBC formation. Because the functionalized HA is acting as a cellular crosslinking agent, varying the density of cell-polymer crosslinks will dramatically influence the rheological properties. By increasing the HA-DBCO concentration in EBC_{DBCO} we observe an increase in G' (Fig. 4.2b), while G'' remained generally constant. It follows that increasing the polymer concentration results in a stiffer, more elastic gel. Interestingly, we found a critical polymer concentration of 0.5% wt/v which resulted in a sufficient number of linkages to form a stable gel. Polymer concentrations of less than 0.5% w/v resulted in poor rheological properties. Varying the RBC density results in a similar influence on the rheological properties (Fig. 4.2c).

Here we find the elastic properties plateau at cell densities of 25% v/v. Further increases in cell densities may result in over-crowding of RBCs and poor mixing with HA. A cell density of 25% v/v corresponds to mixing equal volumes of functionalized HA with modified blood—since blood contains around 50% hematocrit. Further, we found that cell densities of less than 5% v/v resulted in poor rheological properties, as cells are too sparse to form an interconnected network.

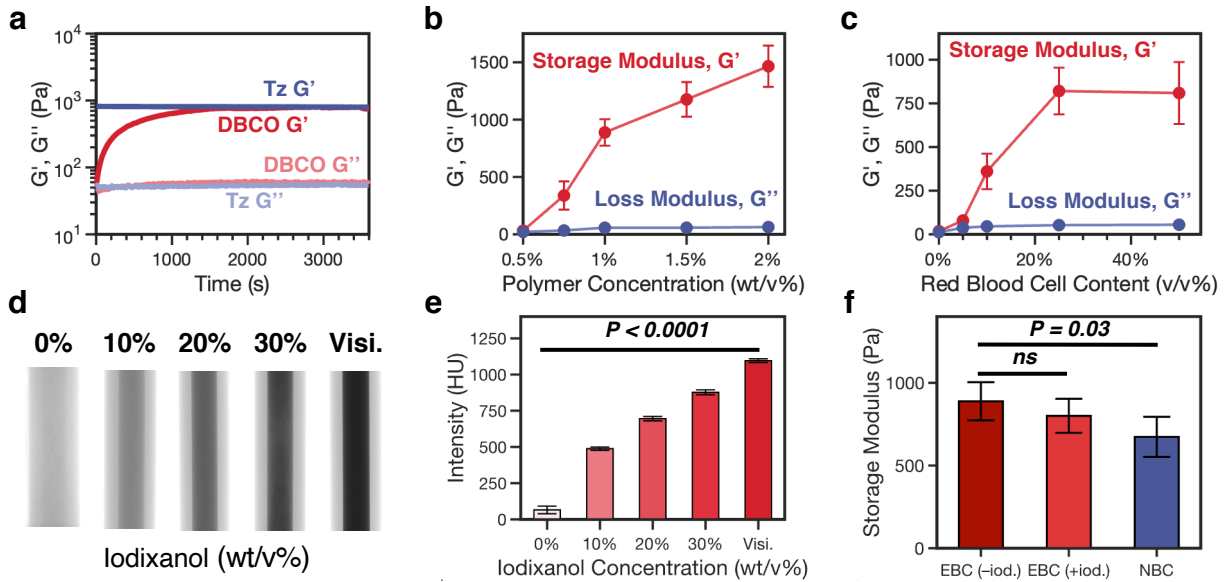


Figure 4.2 Optimization of Engineered Blood Clots as an embolic system

(a) Time sweep of EBCs using various bioorthogonal reactions showing characteristic click clotting profiles. (b) The effect of polymer concentration on EBC rheological properties. EBC_{DBCO} containing 25% v/v RBC-Az and various HA-DBCO concentrations is used as a model system. (c) The effect of modified RBC content on EBC rheological properties. EBC_{DBCO} containing 1% wt/v HA-DBCO and various RBC-Az concentrations is used as a model system. (d) In vitro μ CT images of 1-mL syringes containing EBC as a function of iodixanol concentration. Syringes filled with Visipaque 320 (Visi.) were tested for comparison. (e) Influence of iodixanol concentration on signal intensity in HU of EBCs. (f) Influence of the incorporation of 30% wt/v iodixanol (iod.) on the rheological properties of EBCs. Values in (b), (c), (e) and (f), represent the mean \pm SD (n = 3). P values were determined by one-way analysis of variance (ANOVA) with Tukey post hoc comparisons—not significant (ns), P > 0.05.

4.1.2 Radiopacity

One critical design parameter when developing an embolic material is its radiopacity. A material must be radiopaque to allow for visibility of the material by the interventionalist during the procedure. To do so, we incorporated the radiopaque agent iodixanol (Visipaque 320, 652 mg/mL

of iodixanol) into EBCs. Iodixanol is an iodine-based, non-ionic, isosmotic radiocontrast agent that is visible on the common imaging modalities, such as angiography, CT imaging, and MRI (148). Further, iodixanol does not cause imaging artifacts, which are associated with tantalum powders or metallic coils, and impair the evaluation of the diseased area on follow-up imaging. The use of iodixanol as a radiopaque agent in hydrogel results in non-permanent visibility due to a rapid release of the contrast agent after injection (70). Non-permanent visibility is suitable for clinical applications as radiopacity is only required during the embolization procedure, while long-term radiopacity could affect follow-up imaging (68). The radiopacity of EBCs with varying concentrations of iodixanol was evaluated *in vitro*, using microCT imaging (Fig. 4.2d). Concentrations exceeding 30% wt/v iodixanol led to notable declines in EBC mechanical properties. However, the incorporation of 30% wt/v iodixanol provided sufficient signal intensity for satisfactory visibility and did not significantly impact EBC mechanical properties (Fig. 4.2e), which were marginally stiffer compared to those of NBCs (Fig. 4.2f, S2b). EBCs with a 30% wt/v iodixanol composition were used for subsequent tests.

4.1.3 Injectability

Another critical parameter in the design of an embolic material is the injectability. An embolic material must be injectable through long microcatheters but undergo fast gelation to form a stable, robust occlusion upon injection. The rheological properties of a material will dictate its injectability. In particular, a material's shear-thinning properties are a critical aspect of designing injectable materials. EBCs exhibit shear-thinning behaviour; the complex viscosity decreases as the frequency increases (Fig. 4.3c). To understand how the shear-thinning properties change over time, we performed a frequency sweep on EBCs immediately after mixing and after 1 hour—allowed to fully gel. Both EBCs—initial and after full gelation—exhibited shear-thinning behaviours. This is crucial to ensure continuous delivery throughout the injection window. To test the injectability of EBCs we measured the force required to inject the material through a 2.4Fr microcatheter (Fig. 4.3a). The applied force increases until it reaches a plateau force, defined as the injection force (Fig. 4.3d and f). At this point, the material would begin to extrude from the catheter. EBCs formed a continuous, cohesive stream upon injection from 2.4Fr and 5Fr catheters (Fig. 4.3b and S3). Rupture of RBCs after injection through a 2.4Fr microcatheter was negligible—< 10% hemolysis and < 5% for polymer concentrations under 2% wt/v (Fig. S4). The injection force was measured for both EBC_{DBCO} and EBC_{Tz}, and compared to that of clinically used

materials Onyx 34 and Visipaque 320 (Fig. 4.3e). EBC_{Tz} can be considered to represent the fully gelled state. While EBCs have a larger injection force than that of Onyx and Visipaque it is still considered to be injectable (149). Even the fully gelled form, EBC_{Tz}, is still injectable, but with some difficulties. Decreasing the polymer concentration makes EBC easier to inject (Fig. 4.3g), however, it also results in reduced mechanical properties. 1% wt/v HA-DBCO was chosen as the ideal compromise between injectability and sufficient mechanical properties. However, the polymer concentration can be varied depending on the application or desired outcomes.

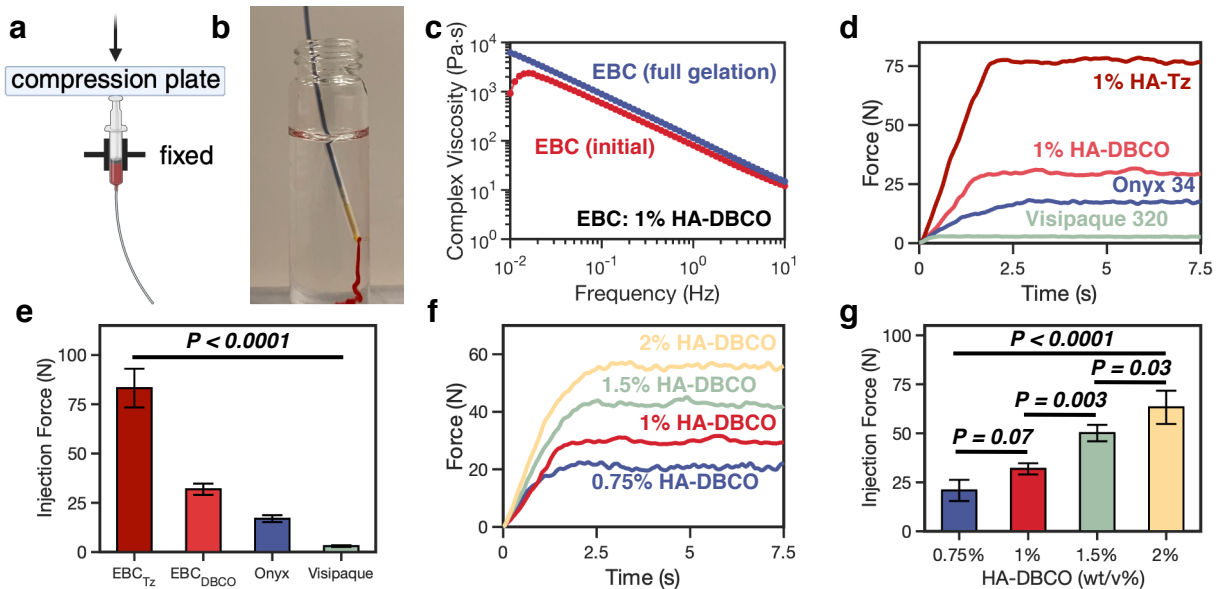


Figure 4.3 Injectability of Engineered Blood Clots through clinical microcatheters

(a) Schematic showing injection force experimental set-up using an Instron mechanical tester. **(b)** Continuous, cohesive stream of EBC being injected through a 2.4Fr microcatheter into PBS. **(c)** Frequency sweep showing shear-thinning properties EBC_{DBCO} containing 1% wt/v HA-DBCO. A frequency sweep was performed immediately after mixing (initial) and 1 hour after mixing (full gelation). **(d)** Characteristic injection force curves of various materials in 3-mL syringes injected through a 2.4Fr microcatheter at a rate of 1 mL/min. The average value of the plateau is used to quantify the injection force. **(e)** Injection force for different materials. EBC_{Tz} is used to represent the fully gelled state. **(f)** Characteristic injection force curves of EBC_{DBCO} with various concentrations of HA-DBCO. **(g)** Injection force for EBC_{DBCO} of various HA-DBCO concentrations. Values in (e) and (g), represent the mean \pm SD ($n = 3$). P values were determined by one-way analysis of variance (ANOVA) with Tukey post hoc comparisons.

4.1.4 Tunable Gelation Kinetics

The varied considerations of the embolization procedure underscore the need for a versatile, tunable material system. Among the factors clinicians consider when selecting an embolic material for a particular application is its penetration depth. Certain applications call for deep penetration into the vasculature, while others require a material to be more mechanically robust immediately upon injection. For instance, in preoperative procedures for liver resections, where temporary embolization is used to induce hypertrophy of the future liver remnant, precise penetration into specific liver vasculature is crucial (150). Here we demonstrate the tunability of EBCs' gelation kinetics using a range of bioorthogonal and natural reactions (Fig. 4.4a). The bioorthogonality of the RBC crosslinking process allows us combine this with the native clotting cascade. When combining EBC_{Tz} with PRP and Ca²⁺ ions, we observed instantaneous gelation via RBC Tz–TCO crosslinking, followed by a gradual stiffening due to the fibrin network formation (Fig. 4.4b). By substituting the ultrafast Tz-TCO reaction with the slower DBCO-Az crosslinking (EBC_{DBCO}) we can slow the gelation kinetics (Fig. 4.4b). Further, as both reactions are highly selective, they are mutually orthogonal. As such, utilizing these two reactions in combination provides further control over the gelation kinetics. Combining equal volumes of HA-Tz and HA-DBCO, and by extension equal volumes of RBC-TCO and RBC-Az, results in gelation kinetics falling between the extremes of EBC_{Tz} and EBC_{DBCO}. For all tested conditions, the initial storage modulus (G'_0) exceeds the initial loss modulus (G''_0), indicating instant gelation. In this case, we quantify the gelation kinetics by the time to full gelation—defined as the time it takes for G' to reach 95% of its plateau value. The time to full gelation ranges from around 5 minutes for EBC_{Tz} to around 18 minutes for EBC_{DBCO} (Fig. 4.4c).

The gelation time is expected to influence the penetration depth. The depth of penetration of different EBC formulations was demonstrated using an in vitro vasculature model, where PDMS phantoms were connected to a pulsatile pump set to emulate physiological conditions. EBCs were injected through 2.4Fr microcatheters proximal to the phantom models and the depth of penetration was observed. After injection, slow-gelling EBC_{DBCO} can flow deep into the vasculature, completely occluding the vasculature (Fig. 4.4d). Conversely, fast-gelling EBC_{Tz} was deposited directly at the catheter tip and did not flow due to the instantaneous click clotting (Fig. 4.4e). After injection EBC_{Tz} would reflux around the catheter, forming a proximal plug in the feeding artery.

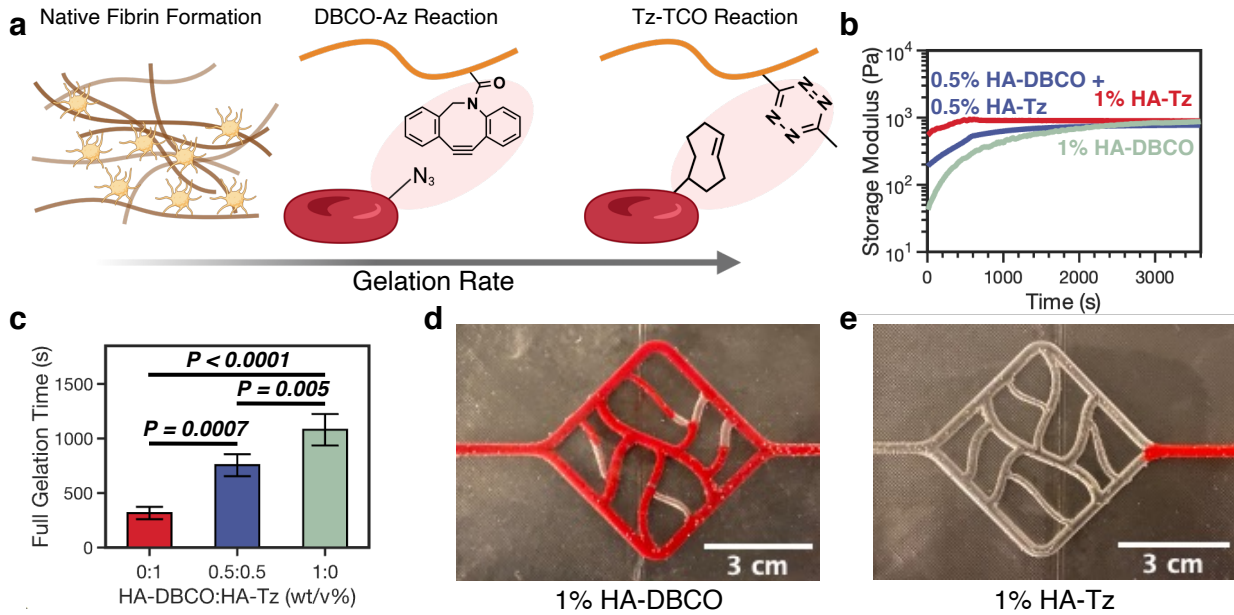


Figure 4.4 Tunable gelation kinetics of the bioorthogonal click clotting system

(a) Schematic showing the various gelation rates of the different clotting systems used in EBCs.ⁱ (b) Time sweep of G' on EBCs containing various ratios of bioorthogonal ligation pairs. Gelation kinetics can be tuned for different applications by modifying this ratio. (c) Time to full gelation (defined as the time it takes for G' to reach 95% of its plateau value) of EBCs containing various ratios of bioorthogonal ligation pairs. (d) Image of PDMS vasculature phantom after injection of EBC_{DBCO} containing 1% wt/v HA-DBCO showing depth of penetration. EBC_{DBCO} is able to fully penetrate the vasculature, reaching the draining vein. (e) Image of PDMS vasculature phantom after injection of EBC_{Tz} containing 1% wt/v HA-Tz showing the depth of penetration. EBC_{Tz} does not penetrate the vasculature, forming a proximal plug in the feeding artery. Values in (c), represent the mean \pm SD ($n = 3$). P values were determined by one-way analysis of variance (ANOVA) with Tukey post hoc comparisons.

4.2 Mechanical Properties of EBCs

4.2.1 Enhanced Fracture Toughness

A requirement of the ideal embolic material is the ability to form a robust, stable occlusion, resistant to fragmentation or migration. Current clinically used liquid embolic agents, such as Onyx or n-BCA, are extremely fragile which can result in fracture of the material after injection (151, 152). Other materials, such as Gelfoam or autologous blood clots, are injected as fragments which result in a distal embolization. However, uneven distribution of particle sizes limits the reproducibility and predictability of the embolization (6). EBCs are injected as a cohesive mass, relying on a combination of native fibrin formation and strong covalent crosslinking to form tough,

dual-network cytogel in situ. This structure of EBCs promises high resistance against fracture. To test this point, we measured the fracture toughness of EBCs using a modified lap-shear test (Fig. 4.5a). Fracture toughness of EBCs (55.94 J/m^2) were enhanced around 8-fold compared to that of NBCs (6.06 J/m^2) and Onyx (6.91 J/m^2) (Fig. 4.5b). The enhanced fracture toughness of EBCs can be attributed to its unique structure. The two interpenetrating networks work symbiotically, highly elastic, crosslinked RBCs dissipate energy, while structural integrity is maintained through the fibrin network.

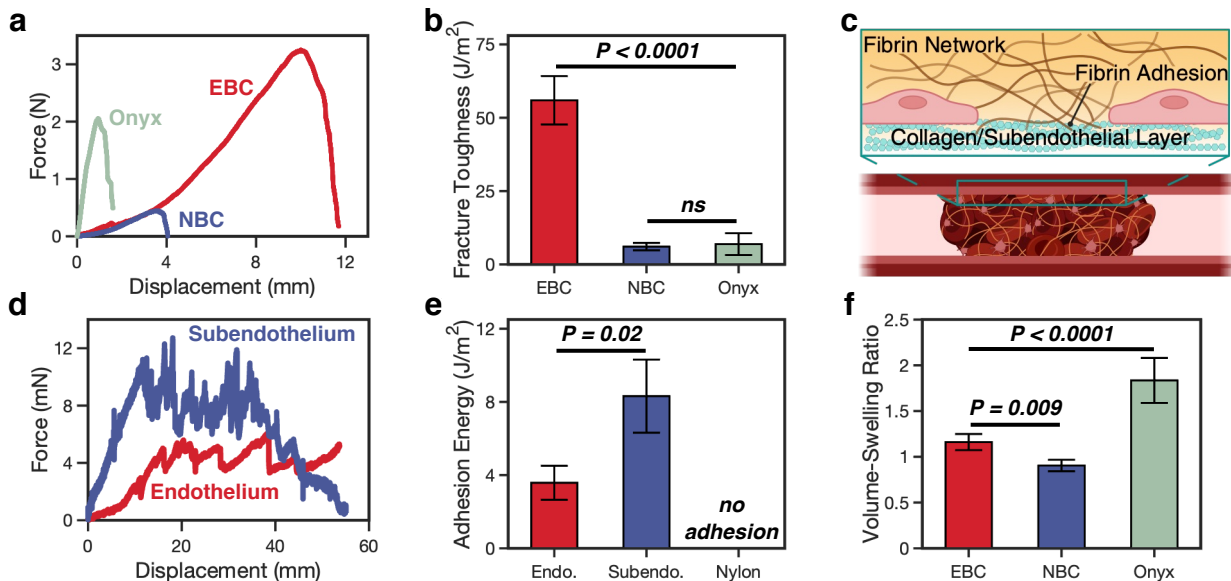


Figure 4.5 Mechanical and physical properties of Engineered Blood Clots

(a) Characteristic force-displacement curves obtained from modified lap-shear tests, comparing EBCs, NBCs, and Onyx 34. **(b)** Fracture toughness of EBCs, NBCs, and Onyx 34. **(c)** Schematic showing adhesion of EBCs to vasculature after injection. Fibrin, a component of EBCs, is able to form covalent bonds with collagen present in the endothelial and subendothelial layers.ⁱ **(d)** Characteristic force-displacement curves obtained from 180-degree peeling tests, comparing adhesion of EBCs to bovine artery endothelium and subendothelium. **(e)** Adhesion energy of EBCs to endothelium and subendothelium layers. **(f)** Volumetric swelling ratios of EBCs, NBCs, and Onyx 34 after incubation in PBS for 24 hours. $\text{VSR} < 1$ indicates volumetric contraction; $\text{VSR} > 1$ indicates volumetric expansion. Values in (b), (e) and (f), represent the mean \pm SD. $n = 3$ for (b) and (e); $n = 5$ for (f). P values were determined by one-way analysis of variance (ANOVA) with Tukey post hoc comparisons for (b) and (f), and by two-sided Student's t test for (e).

4.2.2 Endovascular Adhesion

Another important mechanical property to consider for embolization procedures is the adhesiveness of a material. This pertains to the ability of the embolic agent to adhere to both the endovascular surface and the delivery device during the operation. Onyx is advertised as a non-adhesive embolic agent because it does not adhere to the catheter, thereby reducing the risk of catheter entrapment within the vessel (153). In contrast, the highly adhesive n-BCA embolic agents can reflux around the catheter and trap it within the vasculature, leading to serious complications (152). Ideal embolic agents should strongly adhere to the vasculature to reinforce occlusion and reduce migration, but not to the catheter. This criterion could be met with EBCs, wherein fibrin and platelets enable the selective adhesion to the vasculature. Specifically, fibrin can form covalent bonds with collagen (154), the main component of the subendothelial layer, that is exposed during vascular injury (155) (Fig. 4.5c). Platelets have also shown to adhere to the endothelium which can then bind with fibrin/fibrinogen (156).

We tested the adhesion of EBCs to various substrates using a 180-degree peeling test (Fig. 4.5d). EBCs were able to form an interfacial bond with the endothelial layer of a bovine artery (Fig. 4.5e). However, this resulted in relatively small adhesion energies (3.58 J/m^2). The adhesion energy was enhanced around 2-fold (8.31 J/m^2) when we tested the adhesion between EBCs and the subendothelial layer (Fig. 4.5e). The adhesion of between EBCs and the subendothelial layer was measured to model a situation where embolization would occur on an inflamed or damaged vessel, such as in the case of hemorrhage control. While EBCs demonstrated adhesion towards the vasculature they were non-adhesive towards catheters. The adhesion between EBCs and nylon, a commonly used material in the fabrication of microcatheters, was measured to test potential catheter adhesion. However, EBC adhesion with nylon could not withstand the force of gravity, so the exact adhesion energy was below the detection limit of this method (Fig. 4.5e).

4.2.3 Swelling Properties

Material swelling is another important aspect of embolization, as it ensures a tight occlusive seal of the artery. The volumetric swelling ratio (VSR) was measured to understand the swelling mechanics of EBCs (Fig. 4.5f). Samples were formed in pre-determined sizes and incubated in PBS for 24 hours before measuring the VSR. NBCs have a $\text{VSR} < 1$ due to the clot contraction, driven by activated platelets and causing compaction of the fibrin network along with compression

of the embedded RBCs (157). However, EBCs do not demonstrate clot contraction even though they contain both platelets and a fibrin network. Unlike NBCs, the fibrin network does not solely dictate the structure of EBCs—as activated platelets are unable to contract the interconnected RBC-polymer network. EBCs demonstrate slight swelling ($VSR = 1.16$) in PBS. Onyx swells much more than both NBCs and EBCs ($VSR = 1.83$). This is important because Onyx is non-adhesive so expansion of the material after injection—due to EVOH precipitation—is what ensures an occlusive seal.

4.3 Mechanics of Embolization

4.3.1 In Vitro Embolization Model

We designed an in vitro embolization model to test whether EBCs could form a stable occlusion, resistant to physiological blood pressures without fragmentation or displacement. The model consisted of PDMS tubes (diameter: 3 mm) as vessel phantoms (Fig. 4.6a) and a water-glycerol solution with a viscosity matching that of blood (dynamic viscosity: 5 cP) (70). A syringe pump was used to flow the water-glycerol solution through the PDMS vessel phantom, while a pressure gauge monitored the pressure of occlusion. Both EBCs and Onyx were able to successfully embolize the vessel phantoms at superphysiological pressures ($p > 120$ mmHg)—demonstrating their ability to effectively form an occlusive seal, blocking blood flow (Fig. 4.6f). EBCs with 1% wt/v HA-DBCO were able to form a stable occlusion at pressures over 3-times the systolic blood pressure (403.26 mmHg). Importantly, the failure modes for these materials are drastically different, which could be attributed to their different mechanical properties (Fig. 4.6g) (133). EBCs are soft and tough and fail by elastic leak—this is when the seal fails entirely by elastic deformation, meaning the seal leaks without any material damage. This is demonstrated by the embolization pressure-time curve (Fig. 4.6b), where EBCs initially fail at a maximum leak-initiation pressure (p_i), and then plateau at a steady-state leaking pressure (p_s). The embolic material undergoes no fragmentation or migration within the PDMS tube, therefore, the seal can reform if the pressure is lowered to below that of p_s . This is demonstrated in figure 4.6b, where the pressure is completely removed, and the seal is allowed to reform. We see p_s is highly repeatable cycle-to-cycle, while p_i is reduced after the first cycle—this is due to fluid trapped at the interface between gel and PDMS reducing the friction (131). The elastic deformation leading to the elastic leak failure can be seen through cusping of the EBC at the upstream face of the

material; we can also observe the initial leak path and the steady-state leaking, where the EBC remains stable within the PDMS phantom (Fig. 4.6c). The material was removed from the PDMS phantom after testing to reveal it remains completely intact, with no observable material damage (Fig. 4.6h). Our observations are in complete quantitative agreement with those from Liu et. al. (131)—where they describe the elastic leak failure mode of a hydrogel seal.

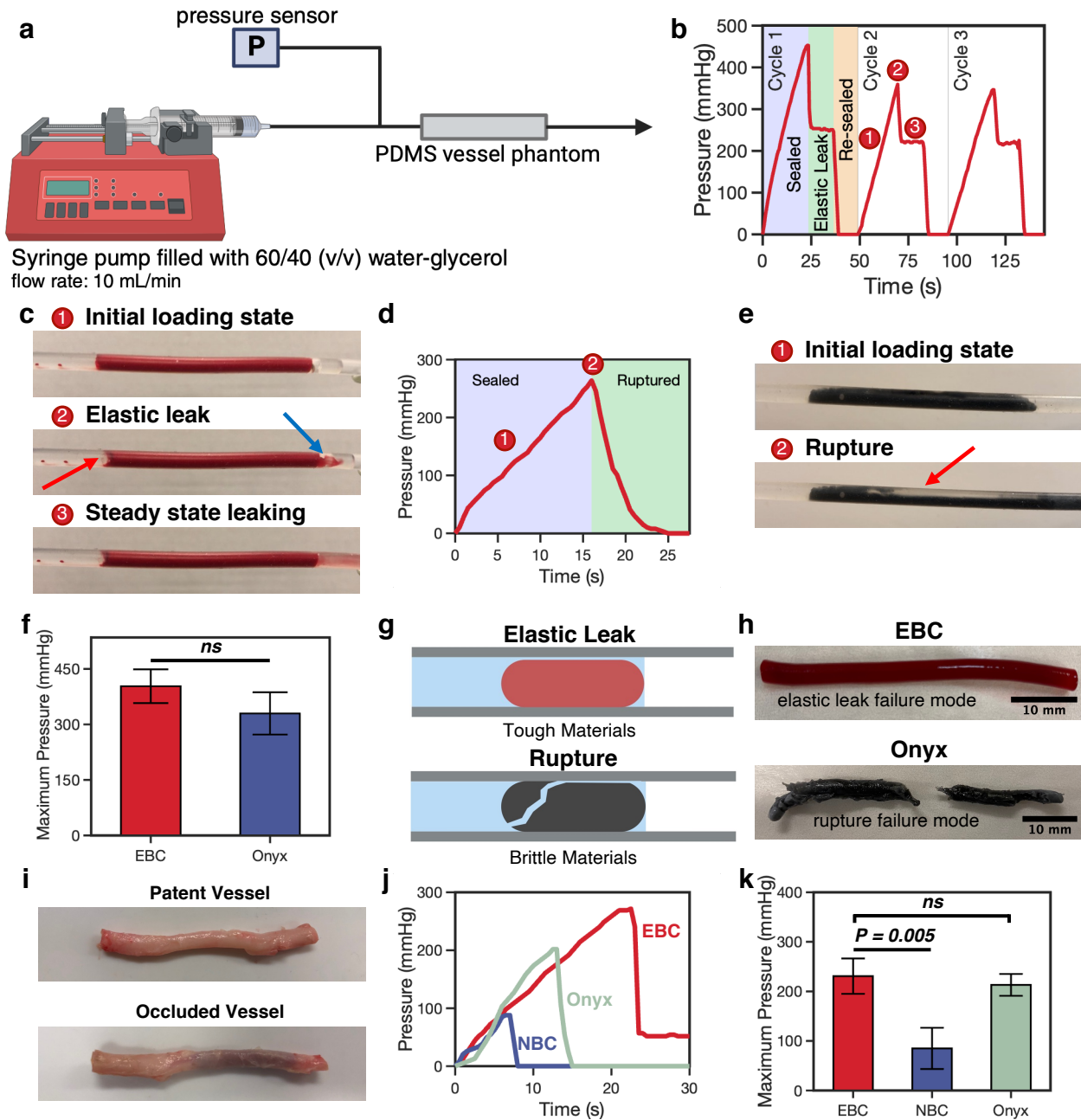


Figure 4.6 In vitro experimental models of embolization

(a) Schematic showing the experimental set-up of the in vitro occlusion model using a syringe pump, PDMS phantoms, and a pressure sensor to measure the embolization pressure.ⁱ **(b)** Characteristic embolization pressure-time curve for EBCs showing the elastic leak failure mode. After a steady-state leaking pressure is reached, the force applied on the syringe pump is removed and the seal is allowed to reform. Three loading-unloading cycles are plotted. **(c)** Three snapshots of EBC occlusion correspond to states marked in the pressure-time curve in *(b)*. The red arrow in image 2 is indicating cusping (elastic deformation) occurring before elastic leak. The blue arrow in image 2 is indicating the initial fluid leakage. **(d)** Characteristic embolization pressure-time curve for Onyx showing the rupture failure mode. **(e)** Two snapshots of Onyx occlusion correspond to states marked in the pressure-time curve in *(d)*. The red arrow in image 2 is indicating the catastrophic fracture of the material. **(f)** Maximum embolization pressure obtained by EBC and Onyx from the in vitro PDMS model. **(g)** Schematic showing the two failure modes observed. Material properties, such as fracture toughness, determine how material fails during embolization. **(h)** Images showing the two failure modes. Materials were retrieved after testing by cutting of the PDMS phantoms. **(i)** Images of patent and occluded bovine arteries, embolized with EBC. **(j)** Characteristic ex vivo embolization pressure-time curves of EBC, NBC, and Onyx. **(k)** Maximum ex vivo embolization pressures. Values in *(f)* and *(k)*, represent the mean \pm SD. $n = 5$ for *(f)*; $n = 3$ for *(k)*. P values were determined by two-sided Student's t test for *(f)*, and by one-way analysis of variance (ANOVA) with Tukey post hoc comparisons for *(k)*—not significant (ns), $P > 0.05$.

Conversely, Onyx is stiff and brittle, and fails by rupture—which results in permanent damage and potential fragmentation of the material. While the maximum embolization pressure of Onyx is similar to that for EBCs (Fig. 4.6f), the failure mode is drastically different. After the failure of Onyx, there is no steady-state leaking pressure that occurs—the pressure drops rapidly to zero (Fig. 4.6d). This indicates no elastic leak occurs and the failure is entirely due to irreversible material damage (132). In this case, the seal cannot be reformed, and fracture of the material occurs. This can be observed through images showing the fragmentation of the material during testing (Fig. 4.6e), and after the material was removed from the PDMS phantom (Fig. 4.6h).

Comparable results were observed from ex vivo occlusion studies with explanted bovine arteries (Fig. 4.6i). It is worth noting a larger drop in pressure from p_i to p_s , for the EBC occlusion, than what is observed in the in vitro, PDMS model (Fig. 4.6j). This is potentially due to greater adhesion and friction between the EBC and bovine endovascular layer, as well as the elastic deformation of the artery due to pressure build-up. In this case, EBCs were able to form a stable occlusion at superphysiological pressures greater than that of NBCs, but comparable to Onyx (Fig. 4.6k).

4.3.2 Elastic Leak for Reliable Embolization

The failure behaviour of an embolic material is a crucial consideration as it relates to the design of an embolic agent. Failure of an embolic material by elastic leak provides a more reliable occlusion as it acts as a safety valve of sorts, allowing for pressure release without irreversible material damage—which can cause fragmentation of the embolic agent and possible off-target complications. A seal fails by elastic leak when the critical pressure for elastic leak is larger than the rupture failure pressure ($P_c > P_f$). The critical pressure for elastic leak (P_c) and the rupture failure pressure (P_f) are theoretically derived from equations 2.1 and 2.3 (132, 133). From equations 2.1 and 2.3, we can define the criteria for failure by elastic leak as:

$$\frac{\Gamma}{\mu} > H(\lambda^{-2} - 1)$$

where Γ is the fracture toughness, μ is the shear modulus, H is the seal diameter, and λ is a dimensionless measure of precompression. Figure 4.7a shows a phase diagram of the failure modes for embolization. At a fixed precompression λ and given a set of geometric parameters, the mechanical properties of a seal will determine the failure mode—by elastic leak or by rupture. H/L represents the non-dimensionalized geometric parameter (L is the seal length) while $\Gamma/\mu L$ represents the non-dimensionalized material parameter.

The term P_f/P_c represents the failure mode of embolization. When $P_f/P_c < 1$, the seal fails by elastic leak. Conversely, when $P_f/P_c > 1$ the seal will fail by rupture (Fig. 4.7b). For a given precompression and vessel diameter, there exists a critical Γ/μ ratio—termed $(\Gamma/\mu)_c$ —below which the embolic material will fail by rupture rather than elastic leak. It follows that the Γ/μ ratio should be optimized for an embolic material if resistance to fragmentation is desired. Figure 4.7c shows an Γ - μ Ashby plot of the embolic materials tested in this study. The shear modulus was determined from the material's storage modulus (a measure of elastic response) which is analogous to the shear modulus in purely elastic materials. EBCs exhibit a Γ/μ ratio greater than both NBCs and Onyx, giving them the ability to provide a more reliable embolization, resistant to fragmentation, setting them apart from stiff and brittle materials.

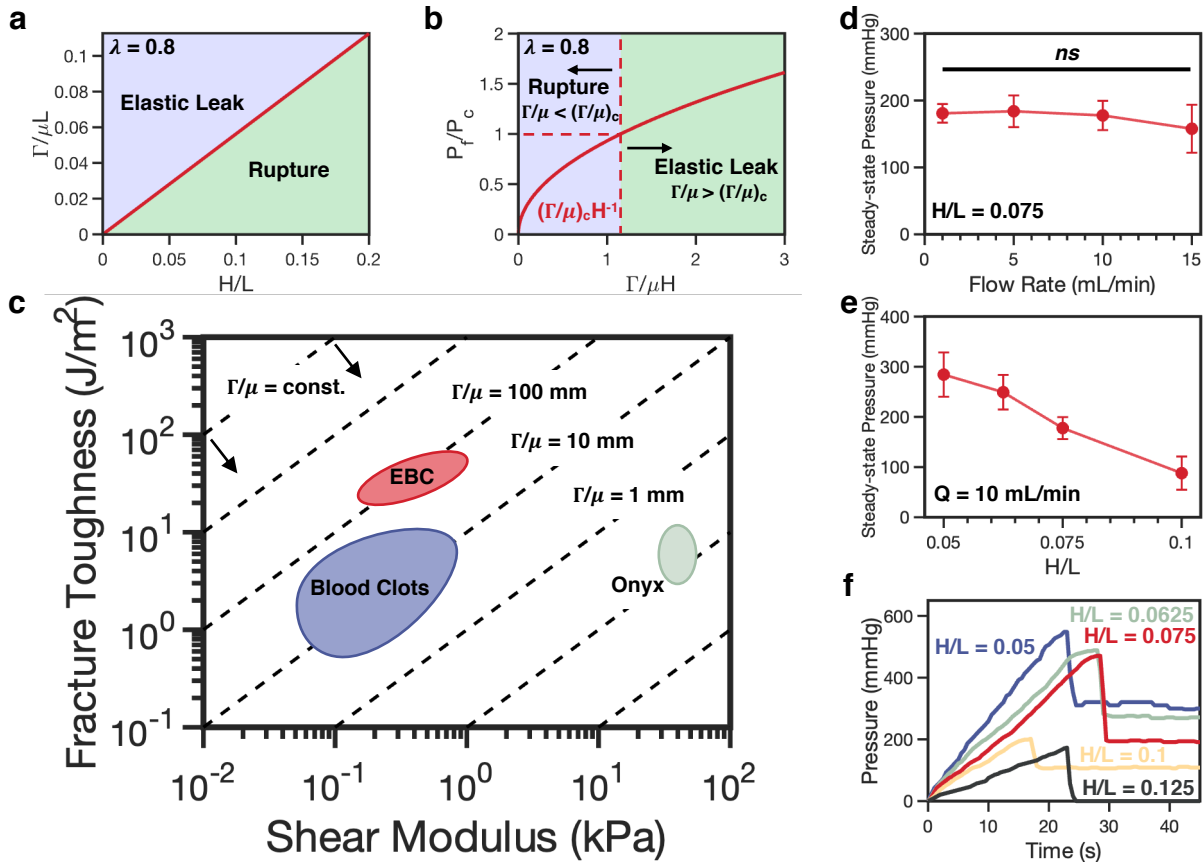


Figure 4.7 Material properties ensure elastic leak for reliable embolization

(a) Phase diagram of the failure modes for embolization in the $\Gamma/\mu L$ - H/L plane. Precompression of the embolic material is fixed at $\lambda = 0.8$. (b) Plot of the failure criteria (P_f/P_c) as a function of $\Gamma/\mu H$. Precompression is fixed at $\lambda = 0.8$. (c) Ashby plot showing the fracture toughness (Γ) and shear modulus (μ) of various embolic materials. Dashed lines indicate where Γ/μ is constant; lines closer to the upper-left corner indicate a larger value of Γ/μ . The data from this study for NBCs was combined with previously reported data from (138). (d) Steady-state leaking pressure (p_s) as a function of the injection flow rate. The non-dimensionalized geometric parameter (H/L) is fixed at 0.075. (e) Steady-state leaking pressure (p_s) as a function of the non-dimensionalized geometric parameter (H/L). The injection flow rate (Q) is fixed at 10 mL/min. (f) Pressure-time curves of EBC in vitro embolization at various geometric parameters. For $H/L = 0.0125$, there is no steady-state leaking pressure, indicating elastic leak did not occur. Values in (d) and (e), represent the mean \pm SD for $n = 3$ independent experiments. P values were determined by one-way analysis of variance (ANOVA) with Tukey post hoc comparisons—not significant (ns), $P > 0.05$.

The in vitro occlusion experiments were repeated while varying the injection rate and the geometric parameters. Here we report the steady-state leaking pressure (p_s) and not the leak-initiation pressure (p_i), as the critical elastic leak pressure (P_c) predicts steady-state leaking from

equation 2.1; $p_s = P_c$. From Figure 4.7d, we observe p_s is insensitive to changes in the injection rate, agreeing with the theoretical model and experimental observations from Liu et. al. (131, 133). In particular, we expect p_s to depend only on the material and geometric parameters of the system. Indeed, by varying the geometric parameter H/L we observe a change in p_s (Fig. 4.7e). By changing the diameter of the PDMS tube, while fixing the seal length, we observe that increasing H/L reduces p_s , while decreasing H/L increases p_s . At a value of $H/L = 0.125$, no steady-state leaking is observed (the pressure drops to zero) indicating elastic leak did not occur (Fig. 4.7f).

4.4 Biocompatibility and Biodegradation

4.4.1 Cytocompatibility and Cell Proliferation

We conducted in vitro tests to evaluate the safety and efficacy of EBCs for in vivo use. Cytotoxicity of EBCs was evaluated by culturing immortalized human vocal fold fibroblasts (hVFFs) with EBC extract media for 24 hours (Fig. 4.8a). Fibroblasts were used as a model system to measure cytocompatibility. Cells cultured in DMEM were used as the positive control and cells cultured in Onyx extract media were used as a comparison. Tests were repeated for all samples with and without the addition of fetal bovine serum (FBS), to evaluate a material's ability to support cell proliferation. A live/dead assay showed high cell viability ($> 97\%$) for all samples, with the exception of Onyx, which had much lower cell viability—26.7% without FBS and 31.8% with FBS (Fig. 4.8b). The low cell viability result from Onyx can be explained from the use of DMSO, a cytotoxic organic solvent, which is dissipated into its surroundings after the injection of the material. Complications, such as vasospasm and systemic toxicity, have been associated with the use of DMSO in Onyx (158). Conversely, EBCs demonstrate the ability to substantially promote cell proliferation even when FBS supplement is absent in the media. Results without FBS show a significant increase in cell density after 24 hours when cells are cultured in EBC extract, compared with the control (Fig. 4.8c). The regenerative capacity of EBCs illustrates its potential as a bioactive material that can improve healing outcomes when used in embolization procedures. To demonstrate the hemocompatibility of EBCs, assays were conducted in accordance with the ISO 10993-4 protocol to assess their hemolytic potential. EBCs exhibited relatively low hemolysis (3.62%), comparable to NBCs (2.38%) and clinically used metallic coils (2.06%) (Fig. S5). A hemolysis rate below 5% is considered permissible for blood-contacting materials (159); the hemolysis induced by a gelatin slurry was significantly higher (6.83%).

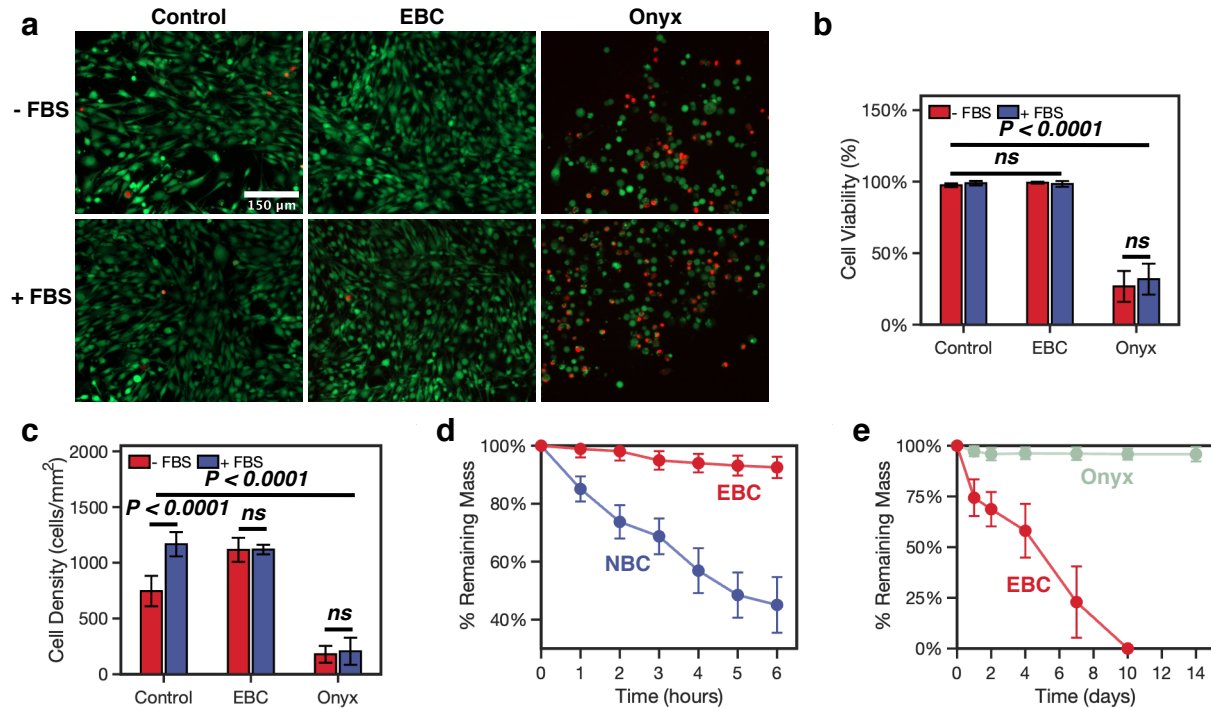


Figure 4.8 Biocompatibility and in vitro degradation of Engineered Blood Clots

(a) Representative images of hVFFs cultured with extract medium of either EBC or Onyx, both with and without the supplement of FBS in the medium. Living cells were stained in green; dead cells were stained in red. Cells cultured in DMEM were used as the control. (b) Cell viability after 24 hours, calculated as the as the percentage of live cells to total cells in the sample. (c) Cell proliferation after 24 hours, calculated as the as the cell density in the sample. (d) In vitro degradation of EBC and NBC incubated in bovine plasma supplemented with tPA. Degradation is calculated as the percentage of wet-mass remaining compared to the initial wet-mass. (e) In vitro degradation of EBC and Onyx incubated in PBS supplemented with hyaluronidase. Values in (b), (c), (d), and (e) represent the mean \pm SD. $n = 10$ for cytotoxicity experiments in (b) and (c); $n = 5$ for degradation experiments in (d) and (e). P values were determined by one-way analysis of variance (ANOVA) with Tukey post hoc comparisons—not significant (ns), $P > 0.05$.

4.4.2 In Vitro Biodegradation

Material degradation is a crucial aspect of temporary embolization as it ensures normal blood flow can be restored once the underlying issue has been addressed. The use of autologous blood clots for embolization was associated with particularly fast degradation and subsequent recanalization. An in vitro degradation assay was performed to measure the effect of fibrinolysis on EBCs, compared to NBCs. Materials were incubated in bovine plasma supplemented with tPA, which activates the fibrinolytic system, degrading NBCs and the associated fibrin network. EBCs, however, are resistant to fibrinolysis, showing minimal degradation after 6 hours, while NBCs

show significant clot lysis (Fig. 4.8d and S6)—only ~40% of the mass remains after 6 hours. Further, EBCs can maintain structural integrity even after degradation of the fibrin network and complete RBC lysis, strictly through HA crosslinked through proteins tethered to the cell's cytoskeleton (Fig. S7). However, EBCs are biodegradable through an enzymatic process. Hyaluronidase, which is present within human plasma (147), mediates the degradation of the HA component of EBCs. EBCs fully degrade within 10 days when incubated in PBS supplemented with hyaluronidase, compared to Onyx, which remains even after 14 days (Fig. 4.8e); Onyx is not biodegradable and results in a permanent embolization.

4.5 In Vivo Embolization

4.5.1 Rat Abdominal Artery Embolization

To assess the safety and efficacy of EBCs as an embolic material, an in vivo experiment was conducted wherein the abdominal artery of a rat was embolized using EBC before testing in a larger porcine model. The abdominal artery was selected due to its large size compared to the other rat vasculature. The study aimed to test the feasibility of injecting EBCs into an artery under physiological conditions, its mechanical stability post-injection, and its retention at the injection site without causing non-target embolization. 100 μ L of EBC_{DBCO} containing 1% wt/v HA-DBCO was injected distally into the abdominal artery of rats (Fig. 4.9a). EBCs were easily injectable through 1-mL syringes with a 30G needle. Following injection, the hindlimbs of the rats exhibited a gradual darkening and a noticeable decrease in temperature. Within 10 minutes after injection the colour of the rats' hindlimbs were visibly darker (Fig. 4.9b). This indicates an interruption of hindlimb perfusion signifying successful embolization and occlusion of the artery. Following the procedure, the animals were euthanized. Radiopacity of EBCs and absence of non-target distal migration or fragmentation was confirmed through post-procedure microCT imaging (Mediso nanoScan PET/CT). Hyperdense spots were visible near the proximal side of the injection, while an absence of hyperdense spots near the distal side indicates a stable occlusion without fragmentation or distal migration after embolization with EBCs (Fig. 4.9c). This result is further illustrated by the 3D reconstructions of the microCT images which show that the EBC remains at the injection site (Fig. 4.9d).

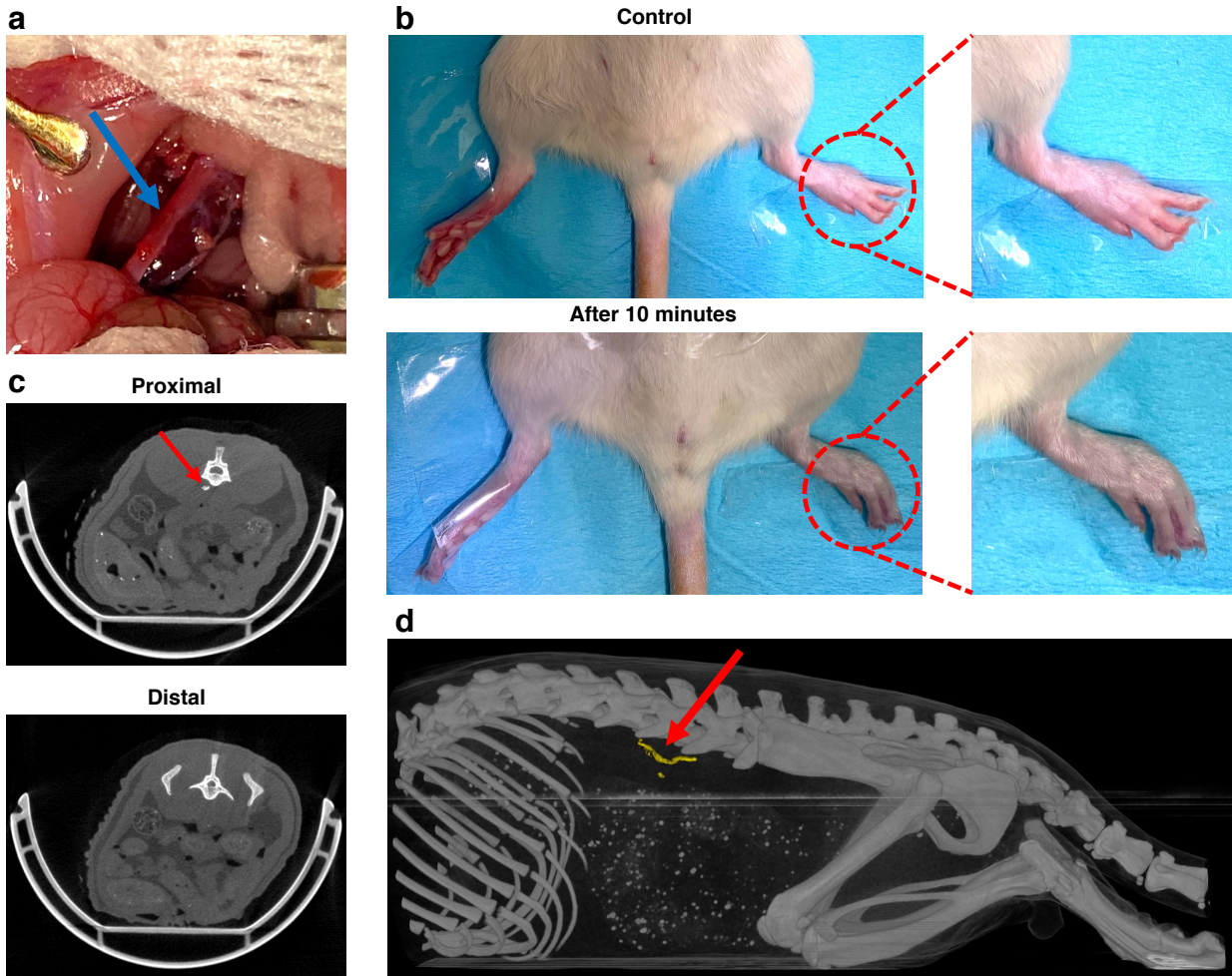


Figure 4.9 In vivo embolization of rat abdominal artery

(a) Image of the rat abdominal artery after injection of EBC with a 30G needle. The arrow indicates the approximate location of the injection. (b) Image of the rat hindlimbs before and 10 minutes after embolization. Discolouration after embolization indicates reduced hindlimb perfusion and successful embolization. (c) In vivo post-surgery μ CT images. Hyperdense spots were visible proximally (red arrow), while no hyperdense spots were found distally to the embolization, indicating EBC is stable within the abdominal artery post-embolization. (d) 3D reconstruction of μ CT images. The red arrow indicates the radiopaque biomaterial, which was artificially coloured yellow.

4.5.2 Porcine Embolization Model

To demonstrate the feasibility and efficacy of EBCs for future clinical use we employed a porcine embolization model. Specifically, six distinct arterial sections were targeted for embolization: the stomach, liver (left and right lobes), spleen, and left and right kidneys (inferior pole). EBC_{DBCO} containing a total polymer content of 1% wt/v HA-DBCO was used as the embolic material. Two

days prior to the procedure blood was collected from the pigs; EBCs were formed using the autologous blood components of each animal. Before the procedure the pigs were anesthetized and intubated; the femoral artery was catheterized under US guidance using a 4Fr Cobra catheter. The catheter was then advanced to the common hepatic artery. A supraseductive catheterization of the gastroepiploic artery was then performed using a 2.8Fr Progreat microcatheter (Teurmo Interventional Systems) and a baseline digital subtraction angiography (DSA) was obtained (Fig. 4.10a). Contrast backflow into the gastroduodenal and the superior pancreaticoduodenal artery was observed. After injection of EBC, DSA acquisition demonstrated an immediate and complete embolization of the right gastroepiploic artery—beginning from approximately 15 mm from the gastroduodenal bifurcation (Fig. 4.10b). Opacification of the superior pancreaticoduodenal and the gastroduodenal arteries was identical to the DSA acquired before embolization suggesting no non-targeted embolization of these segments. The microcatheter was then advanced into the right lateral hepatic artery and a baseline DSA was acquired (Fig. 4.10e). The right lateral hepatic artery was visible; some backflow of contrast in the left hepatic artery was observed. The right lateral hepatic artery was embolized using EBC; DSA demonstrated a complete embolization of the right lateral hepatic artery (Fig. 4.10f). The microcatheter was then advanced into the splenic artery; a baseline DSA was acquired (Fig. 4.10i). Following injection of EBC, the splenic artery was completely embolized (Fig. 4.10j). The left lateral hepatic artery and the lower polar arteries of both the left and right kidneys were also embolized following the same procedure (Fig. S8). Following the procedure, the animals were allowed to recover from anesthesia and survived for 7 days before euthanasia. Prior to euthanasia, animals were reanesthetized for angiography. At the 7-day post-embolization mark, all the embolized arteries exhibited either partial or complete recanalization (Fig. 4.10c, g, and k). This recanalization suggests that EBC is suitable for temporary vascular occlusion applications, rather than providing a long-term or permanent solution. Following euthanasia, the targeted tissues were analyzed for signs of occlusion. The necropsy revealed necrosis of the targeted organs compatible with ischemia due to occlusion of the embolized arteries (Fig. 4.10h and l). Remnants of the EBC was found in the gastroepiploic artery, compatible with the partial recanalization observed from the 7-day post-embolization DSA (Fig. 4.10d). The appearance of the EBC was translucent, rather than opaque suggesting an intact HA gel and lysis of the RBC crosslinkers.

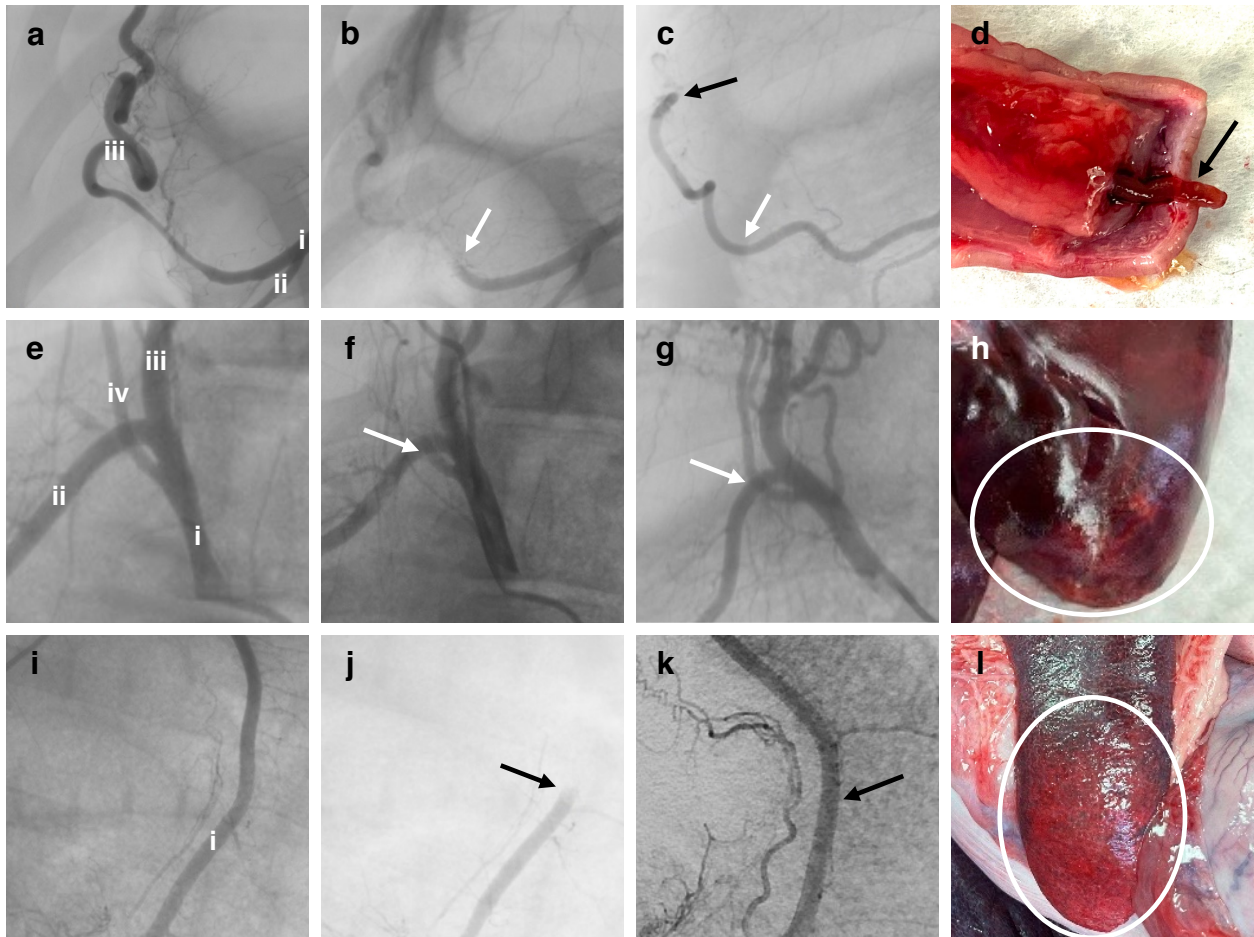


Figure 4.10 Preliminary porcine embolization indicates feasibility for temporary applications

(a) Baseline DSA of the right gastroepiploic artery. (i) gastroduodenal artery; (ii) superior pancreaticoduodenal artery; (iii) gastroepiploic artery. **(b)** Post-embolization DSA; contrast injection revealed lack of opacification of the gastroepiploic artery, indicating successful embolization. **(c)** 7-day post-embolization DSA, the white arrow indicates the original beginning of the embolized segment, the black arrow shows the partial recanalization of the artery after 7 days. **(d)** Image revealing EBC which remains in the gastroepiploic artery (black arrow) 7 days after embolization. **(e)** Baseline DSA of the right lateral hepatic artery. (i) hepatic artery; (ii) gastroduodenal artery; (iii) left hepatic artery; (iv) right lateral hepatic artery. **(f)** Post-embolization DSA showing successful embolization. The white arrow indicates the beginning of the embolized segment. **(g)** 7-day post-embolization DSA showing recanalization of the artery. **(h)** Image of the liver showing localized pale discoloration of approximately 8 cm at the caudal aspect of the right lateral lobe (white circle), compatible with ischemia of the right lateral hepatic artery. **(i)** Baseline DSA of the splenic artery. (i) splenic artery. **(j)** Post-embolization DSA showing successful embolization. The black arrow indicates the beginning of the embolized segment. **(k)** 7-day post-embolization DSA showing recanalization of the artery. **(l)** Image of the caudal portion of the spleen showing a pale coloration over approximately 5 cm (white circle), compatible with ischemia of the splenic artery.

5 Discussion

Chapter 5 provides a comprehensive analysis and interpretation of the experimental results presented in the previous chapter. This section will provide an in-depth exploration of the findings, drawing connections to gain a clearer understanding of the implications and significance of the research. The discussion will cover various aspects, including the design and optimization of EBCs for embolization purposes; the mechanics of embolization and how this relates to the mechanical properties of embolic materials; the biocompatibility of EBCs; and the results of in vivo experiments. This discussion will critically analyze the data and provide insights into the clinical applications, limitations, and future directions of this research.

5.1 Design and Optimization of EBCs

The design and optimization of EBCs is a crucial aspect of this research, with the aim of developing a safe and effective material for endovascular embolization. One of the main objectives of this study was to optimize the EBC material system based on clinical needs using in vitro models that characterize embolic performance. Through extensive experimentation and analysis of different EBC formulations, we identified the optimal formulation of EBCs which can provide reliable occlusion, while also allowing for tunability of the physical properties based on procedural needs. In this work, EBCs were formed using HA functionalized with either DBCO or Tz groups and RBCs modified with the corresponding click motif, Az or TCO. This strategy, in its most basic form, is highly versatile and applicable to a wide range of polymer linkers and cells. HA was chosen due to its large hydrodynamic size—required to provide adequate linkage between cells—and due to its biocompatible and biodegradable properties necessary to provide successful temporary embolization. Future iterations could use other long-chain polymers such as chitosan, alginate, or poly(vinyl) alcohol. Using polymers with different degradation profiles from HA can provide a more permanent occlusion, if desired. Further, the use of RBCs may be substituted for various other cell types, such as fibroblasts or stem cells, among others, to tailor the use for specific applications or to further improve healing outcomes.

We explored the use of two separate bioorthogonal reactions, with vastly different gelation kinetics, to form EBCs: the SPAAC reaction between DBCO-Az and the IEDDA reaction between

Tz-TCO. The DBCO-Az reaction is much more applicable to use for embolization due to its slower reaction rate. The reaction between Tz and TCO is very fast and makes the initial injection difficult. Even using the DBCO-Az reaction, the injectability of EBCs is time-dependent. This highlights one of the limitations of using an in situ chemical reaction as the gelation mechanism. However, the gelation times of EBCs are well within the typical injection time windows of other liquid embolic systems (160-162). Quantities of the Tz-TCO ligation pair may be incorporated within the EBC if a smaller depth of penetration and a more robust initial occlusion are desired. Different formulations of EBCs can be used depending on the application or if larger catheters are used, allowing for easier injection (163).

The iodine-based, radiopaque molecule iodixanol was added to EBCs to improve its radiopacity. Iodixanol was incorporated within EBCs through the addition of Visipaque 320, a radiocontrast agent which is non-ionic and isosmotic to blood. Visipaque is commonly used in clinical settings with indications for multiple intra-arterial and intravenous procedures. The incorporation of 30% wt/v iodixanol did not significantly affect the rheological properties of EBCs, suggesting a stable interaction between iodixanol and RBCs within EBCs. Further increasing the concentration of iodixanol alters the physical properties of EBCs, leading to a material with a significantly reduced G' . Previous studies, however, indicate that 30% wt/v iodixanol will demonstrate sufficient intensity to allow for adequate visibility (148). Iodixanol has previously been incorporated within hydrogel-based embolic materials (68, 70). These studies show iodixanol is rapidly released from the gel, with gels losing 56% of their radiopacity within 4 hours after injection (68). This temporary radiopacity is ideal for clinical use, as it mitigates long-term imaging artifacts, allowing for clearer imaging in future interventions or monitoring (68). Release of iodixanol from EBCs, and subsequent time-dependant loss of radiopacity, should be explored in future studies.

5.2 Mechanics of Embolization

The efficacy of the embolization procedures hinges on the selection and design of the embolic agent. One important consideration, that is often overlooked, is the mechanical properties of the material—which plays a crucial role in its performance as an embolic agent. The theoretical failure models of elastomeric seals, as discussed above, highlights the importance of fracture toughness. Tough materials are crack-insensitive, while materials with low toughness are prone to fracture. In the context of embolization, this implies that embolic agents—particularly liquid/gel embolic

agents—should be tough and soft, rather than brittle and stiff, to resist fragmentation of the material. Should an embolic agent have inadequate toughness, it could potentially fracture within the occluded vessel. The unique structure of EBCs, with RBCs being the main structural component, affords them with superior mechanical properties. RBCs are both highly elastic and strong, allowing them to deform up to approximately 250% of their initial length (164). These quantities, combined with the dual-network structure from HA and the fibrin network, make EBCs highly tough and soft ($\Gamma/\mu \approx 63$ mm). In terms of embolization, this means EBCs are highly resistant to fragmentation, non-target complications, and more likely to fail by elastic leak. In this attribute, EBCs outperformed the other tested embolic materials—namely NBCs ($\Gamma/\mu \approx 9$ mm) and Onyx ($\Gamma/\mu \approx 0.16$ mm). Fragmentation of various embolic agents, such as Onyx, n-BCA, and PVA has been observed in clinical practice, and is associated with severe complications (151, 152, 165-167). When an embolic agent fragments, there's a risk that the smaller pieces will travel to unintended areas, leading to non-target embolization. This can result in ischemia (reduced blood flow) or infarction (tissue death) of tissues supplied by the unintentionally blocked vessels. Fragmentation can also result in an inefficient occlusion, where if the embolic agent fragments excessively or unpredictably, it may not effectively block the target vessel, necessitating additional intervention or resulting in suboptimal treatment outcomes. Here our model intends to use solid mechanics to capture the mechanical failure of an embolic material, however, under physiological conditions the situation is much more complex. In this model we do not consider biological effects. However, our model demonstrates EBCs form a robust initial occlusion.

Adhesion also plays a significant role in the effectiveness and safety of embolization. In the context of embolization, adhesion refers to the ability of the embolic agent to stick or adhere to the vessel walls and to stay in place once deployed. While the theoretical models discussed do not account for adhesion, it follows that adhesion to the endovascular layer can enhance the embolization pressure, making the embolic agent more difficult to displace. EBCs are somewhat adhesive towards to endovascular layer, ascribed to the fibrin network, which can form covalent bonds with collagen present in the endovascular layer (144). While adhesion is generally beneficial for embolization, it is worth noting that too much adhesion, especially regarding liquid agents, can lead to adherence to the delivery catheter, making their removal challenging and risking vessel injury. Our results show that EBCs are non-adhesive to materials used in catheters, meaning they can be easily and safely delivered without the risk of complications.

5.3 Biocompatibility and Biodegradation

In vitro biocompatibility tests were used to evaluate the safety and efficacy of EBCs as an embolic material, as well as to evaluate the interaction between EBCs and the biological environment. The results of these experiments indicate that EBCs exhibit a high degree of biocompatibility. This is in accordance with one of the design principles of EBCs. With biocompatibility in mind, EBCs were designed to possess the advantages of autologous blood clots but can be easily used in a clinical setting. EBCs demonstrate the ability to promote cell proliferation an essential property to improve soft tissue healing outcomes (*168*). Similar to autologous blood clots, EBCs contain many growth factors and cytokines, affording it with similar regenerative properties (*169*). This contrasts with other commonly used embolic agents, such as Onyx or n-BCA, which are associated with cytotoxicity and can hinder tissue healing. These findings are highly promising and supports the use of EBCs as a promising new embolic agent with unique advantages over the current standard treatments. Here we used hVFFs as a model system to study the cytocompatibility of EBCs. Future studies should investigate the interaction of EBCs with HUVEC, as they are the first line of contact when the EBC enters the vessel lumen—in this case we would expect similar results.

Material degradation is another crucial aspect of temporary embolization that was considered. Biodegradation is an essential characteristic for temporary embolic agents as it ensures that the induced occlusions are non-permanent, and that normal blood flow can eventually be restored once the underlying issue has been addressed. Degradation of temporary embolic agents is highly variable depending on the particular agent used (*170*). Gelfoam, a commonly used temporary embolic agent, typically degrades within 2–3 weeks but can last up to 4 months (*34*). Longer degradation of Gelfoam reduces its potential for restoring vascular continuity and has resulted in unintended permanent occlusions (*36*). The use of autologous blood clots for embolization was associated with fast degradation and subsequent recanalization (*171*). Occlusion from autologous blood clot embolization typically lasts for 8–24 hours (*170*). EBCs demonstrate prolonged degradation, in vitro, compared to NBCs. While the degradation process of NBCs is relatively fast due to fibrinolysis, the degradation of the HA component of EBCs acts as a rate limiting step, slowing down the degradation process. Further, the degradation process of EBCs is highly biocompatible. When introduced into the bloodstream, HA undergoes degradation primarily mediated by enzymatic actions, notably by hyaluronidases, which cleave the glycosidic bonds

between its disaccharide units (147, 172). Moreover, the degradation products of EBCs are highly biocompatible, easily excreted, and all typically present within the bloodstream (172, 173).

5.4 In Vivo Embolization

Preliminary in vivo experiments in rat and porcine models suggest EBCs are suitable for use as a temporary embolic agent. In the rat abdominal embolization model, occlusion of the artery was successfully achieved and subsequently confirmed through microCT imaging, paving the way for the more intricate pig model study. During these experiments it was noted that EBCs are easily injectable through clinical microcatheters and the click clotting process allows for a sufficient injection time window. Once injected, EBCs immediately and successfully embolize the target artery, forming a tough occlusion. EBC_{DBCO} can penetrate and occlude subsegmental branches, while incorporating other biorthogonal reactions—such as Tz-TCO ligation—can improve the initial mechanical properties of the gel, if a more robust initial occlusion is desired.

The pig embolization model revealed partial or full recanalization of the target arteries at the 7-day mark, indicating degradation of the material. Remnants of the EBC recovered during the necropsy were translucent in appearance—rather than opaque as is seen after the initial formation. This translucent appearance indicates lysis of the RBCs, leaving the HA framework intact. This suggests that the HA component is the rate-limited step when it comes to the material degradation, a fact which was implied from our in vitro results. These observations, combined with our in vitro results, indicate that the degradation period of EBCs lies within that of autologous blood clots and Gelfoam—with degradation occurring over the 7-day period. Further studies are required to assess the in vivo degradation profile of EBCs and confirm its efficacy as a temporary embolic agent. Future research could also focus on tailoring the degradation rate or improving its long-term stability to cater to a broader spectrum of clinical needs.

The main complication that was observed during the in vivo studies relates to the radiopacity of the material. EBCs exhibited poor visibility on fluoroscopic imaging. This was an important setback as it impacted the ability of the interventionist to properly assess whether the occlusion was completed. To address this, future efforts will focus on enhancing the radiopacity of the EBCs, possibly by incorporating higher concentrations of radiopaque agents or exploring alternative compounds that provide better contrast under fluoroscopy, ensuring more precise and confident assessments by the interventionist during procedures.

6 Conclusion

6.1 Summary

This thesis aimed to develop a novel biomaterial for temporary endovascular embolization procedures that combines excellent biocompatibility with superior mechanical properties. Here we designed and validated *Engineered Blood Clots* as a temporary embolic agent. Taking a systematic approach, the design and optimization of EBCs was successfully carried out based on clinical needs using in vitro models. By characterizing various EBC formulations, we identified the optimal material system that offers reliable occlusion and tunability of physical properties. In vitro findings were further validated through both rat and porcine in vivo models, confirming the successful use of EBCs for temporary applications. Moreover, the study of the mechanical properties of EBCs provided valuable insights regarding the mechanics of embolization—a previously unexplored topic. The understanding of the role of mechanics provides guidelines on developing a safe and effective embolic material. It will also help clinicians and researchers better understand the failure of embolic materials in vivo and why such complications occur. In conclusion, this research has provided a foundation for further research and potential clinical trials to investigate the potential of EBCs in the treatment of diseases requiring temporary embolization.

6.2 Future Directions

Insights from this thesis have resulted in a variety of directions for both fundamental research and clinical development. Firstly, further optimization of EBCs is necessary to further enhance their use as embolic agents. In particular, the visibility of EBCs under fluoroscopic imaging needs to be improved if EBCs are to be used successfully in a clinical setting. Future iterations could incorporate small amounts of tantalum powder to increase the visibility, while not significantly impacting the material's physical properties. Optimization of the EBC system can also involve refining the synthesis process of EBCs, allowing for faster modification and prolonged storage of the modified RBCs. Ideally, EBCs can be used as a point-of-care embolic material using autologous cells which are modified on site, or which have been stored in a blood bank. The current modification process takes several hours, limiting its use in point-of-care settings. Future research can focus on simplifying this modification process or exploring the stability of modified-RBCs

suitable for blood bank storage. One concern of using blood from patients who would undergo embolization is that they may have some type of disease which would impact the quality of blood. The use of blood from blood bank storage to manufacture EBCs ensures that the blood is derived from a healthy source, offering a potential solution to this issue. Here we demonstrate the feasibility of EBCs as an embolic agent for temporary embolization procedures, however, further developments are needed when considering the translational requirements of embolic materials. Factors such as, shelf life, sterilization, off-the-shelf readiness, and cost should be addressed in future experiments. Additionally, future directions of this work should involve further in vivo experiments to assess the safety and efficacy of EBCs in clinical scenarios. Future experiments should use clinically relevant in vivo models in which a temporary occlusion is desired. By performing these experiments, researchers can gather valuable data on the performance of EBCs in situations that closely resemble real-world applications. In particular, the in vivo degradation of EBCs needs to be further explored to confirm their efficacy as temporary embolic agents. Furthermore, in vitro experiments and theoretical modelling should be explored regarding the mechanics of embolization, with these principles being applied to other embolic agents.

Appendix A–Supplementary Information

Materials and Methods

Unmodified RBC Confocal Imaging

Confocal imaging of unmodified RBCs was performed as a negative control, in order to confirm successful modification of RBCs. Bovine whole blood (Lampire Biological Laboratories, 7200804) was first centrifuged (1000g, 5 min) to obtain unmodified RBCs. The separated RBCs were then thoroughly washed three times with cold PBS (9:1 PBS to RBC ratio) and centrifuged to remove the supernatant. Following washing, RBCs were incubated with a Cy5 DBCO fluorescent probe (Click Chemistry Tools, A130) at a concentration of 10 µg/mL for 1 hour at 37°C. Following incubation, the RBCs were thoroughly washed with PBS three times to remove any unreacted fluorescent probe. The cells were then diluted in PBS at a 100:1 PBS to RBC ratio and imaged using a confocal laser scanning microscope (Zeiss, LSM710).

Hemolysis

Hemolysis tests were performed with EBCs and NBCs according to the ISO 10993-4 protocol (159). 1 mL of each material was injected into a centrifuge tube and fully gelled. EBCs and NBCs were washed thoroughly with PBS to remove any uncrosslinked RBCs. RBCs were obtained from bovine whole blood by centrifugation at 1000g for 5 minutes. Separated RBCs were diluted in PBS at a ratio of 1:50. 9 mL of diluted RBCs were added to each tube and subsequently incubated at 37°C for 1 hour under gentle agitation (100 rpm). 9mL of RBCs diluted at a 1:50 ratio in PBS or DI water were used as the negative and positive controls respectively. Embolic coils (Cook Medical, G47416) and a gelatin sponge slurry (SURGIFOAM Absorbable Gelatin Sponge, Ethicon) were also tested for comparison. Following incubation, the tubes were centrifuged (1000g, 5 min), and the absorbance of the supernatant at 540 nm (AU_{sample}) was measured using a microplate reader (Synergy HTX Multimode Reader). Percent hemolysis was calculated according to the following equation:

$$\% \text{ Hemolysis} = \frac{AU_{sample} - AU_{negative}}{AU_{positive} - AU_{negative}} \cdot 100\%$$

$AU_{positive}$ and $AU_{negative}$ are the absorbance of the positive and negative controls, respectively. Hemolysis was also assessed to determine if RBC rupture occurs after injection through clinically used 2.4Fr microcatheters (Teleflex, 5305). Percent hemolysis was measured using an adaptation of the ISO 10993-4 protocol. 1 mL of EBCs containing 25% v/v modified RBCs was injected into 15-mL centrifuge tubes filled with 9 mL of cold PBS. The tubes were subsequently centrifuged (1000g, 5 min), and the absorbance of the supernatant at 540 nm was measured by using a microplate reader. 0.25 mL of washed RBCs added to 9 mL of PBS or DI water were used as the negative and positive controls respectively. 0.25 mL of isolated RBCs diluted with 0.75 mL of PBS and injected through a 2.4Fr microcatheter was tested as a comparison. Percent hemolysis was calculated according to the same equation as previously stated.

Fibrinolysis Spectrophotometric Assay

Fibrinolysis of EBCs and NBCs was measured using a spectrophotometric assay according to the principle that as blood clots degrade they will release RBCs into the supernatant. The absorbance of the supernatant at 540 nm can be measured to determine the extent of clot degradation. First, samples were thoroughly in PBS to remove unreacted and excess RBCs. Plasma was obtained by centrifugation of bovine whole blood at 1000g for 5 minutes. 10 μ g/mL of tPA (Sigma-Aldrich, T0831) was added to the plasma (146). EBCs were formed using 1 mL of modified whole blood, while NBCs were formed with 1 mL of native whole blood. The samples were sealed and incubated in the supplemented plasma at 37°C under gentle agitation (100 rpm). At pre-determined time intervals, the supernatant was removed, and its absorbance at 540 nm was measured using a microplate reader.

EBC Cell Lysis

RBCs were lysed in order to show the structural stability of EBCs after the lysis of the cell crosslinkers. EBCs were formed in a 96-well plate. After gelation, EBCs were removed and incubated in DI water at 37°C to lyse the RBCs. After 24 hours, the samples were washed, and the material physical properties were noted.

Results

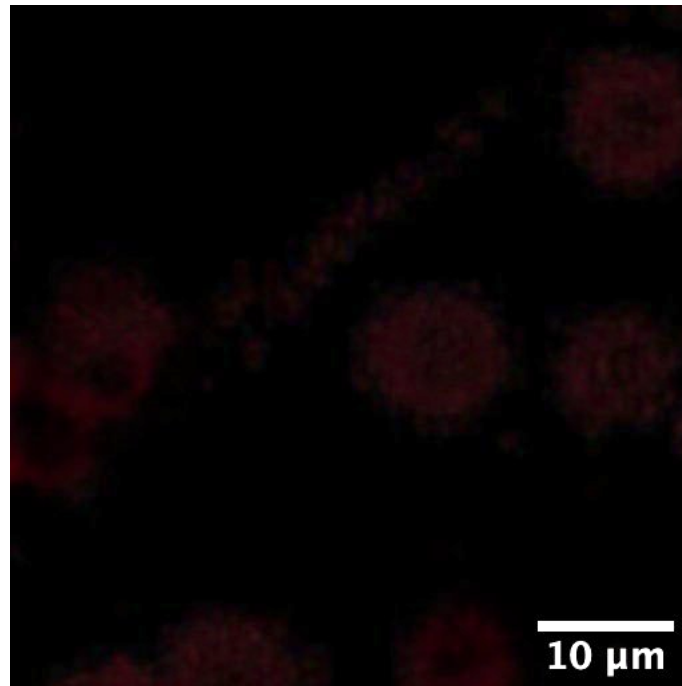


Figure S1 Confocal images of unmodified red blood cells

Unmodified RBCs incubated with a DBCO conjugated fluorescent probe (Cy5-DBCO) emit negligible fluorescent signal. Small fluorescent signal is possibly due to non-specific absorption.

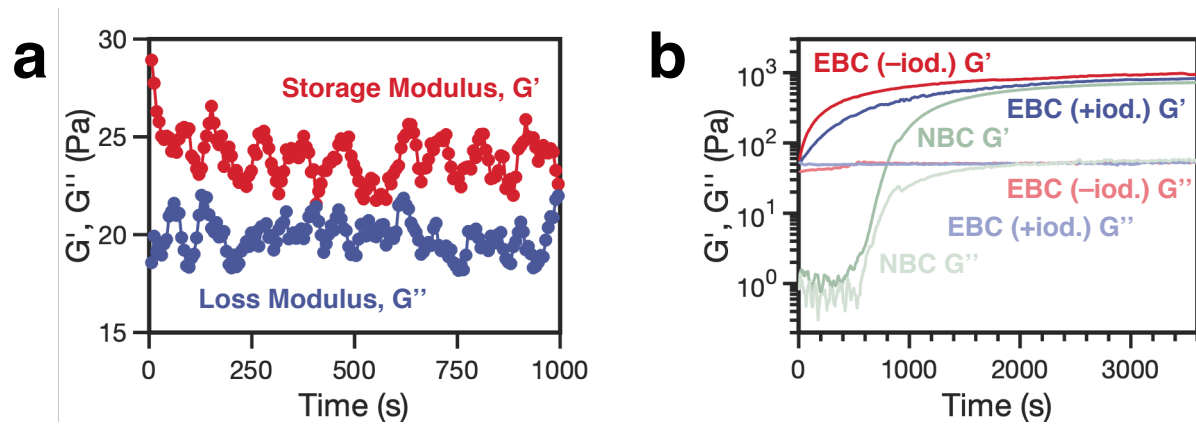


Figure S2 Rheological analysis of Engineered Blood Clots

(a) Time sweep of unmodified RBCs mixed with 1% wt/v HA-DBCO, showing lack of gelation. **(b)** Time sweep showing the gelation kinetics of EBCs incorporated with and without 30% wt/v iodixanol (iod.), compared with the coagulation kinetics of a native blood clot (NBC).

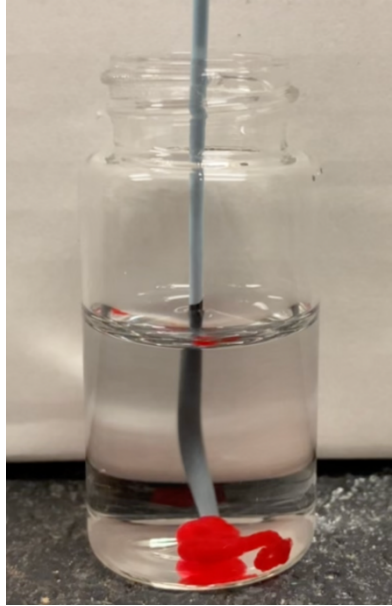


Figure S3 Injection of Engineered Blood Clot through 5Fr catheter

(a) Injection by hand of EBC containing 1% wt/v HA-DBCO through a 5Fr catheter (Cook Medical, G13794) into a PBS reservoir.

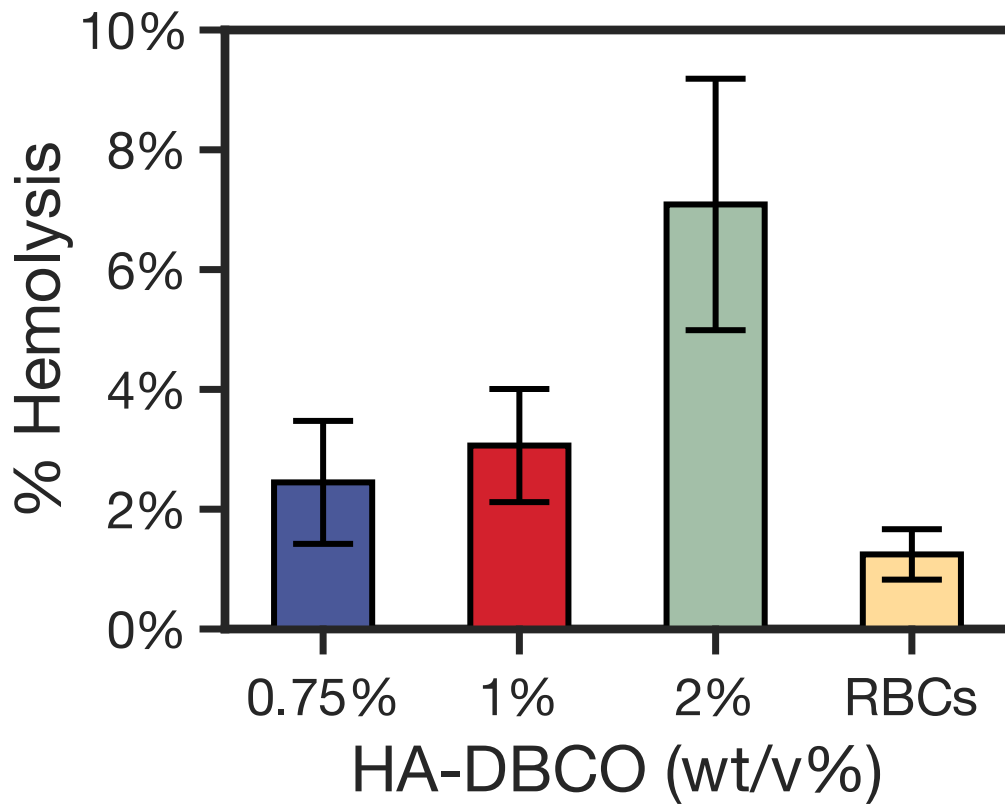


Figure S4 Percent hemolysis of RBCs after injection

Rupture of RBCs after injection of EBCs of varying polymer concentrations through a 2.4Fr microcatheter. Injection of isolated red blood cells (RBCs) was tested for comparison. Values represent the mean \pm SD (n = 3).

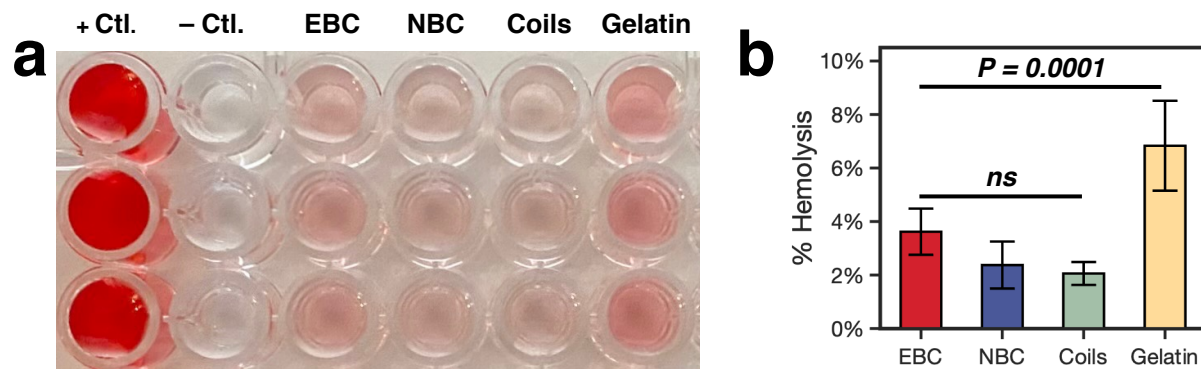


Figure S5 Hemocompatibility of Engineered Blood Clots

(a) 96-well plate hemolysis assay of RBCs in contact with EBCs, NBCs, clinically used metallic coils (Cook Medical, G47416) and a gelatin sponge slurry. Positive control is RBCs diluted in DI water, while negative control is RBCs diluted in PBS. (b) Hemolysis assay results. Values represent the mean \pm SD ($n = 3$). P values were determined by one-way analysis of variance (ANOVA) with Tukey post hoc comparisons—not significant (ns), $P > 0.05$.

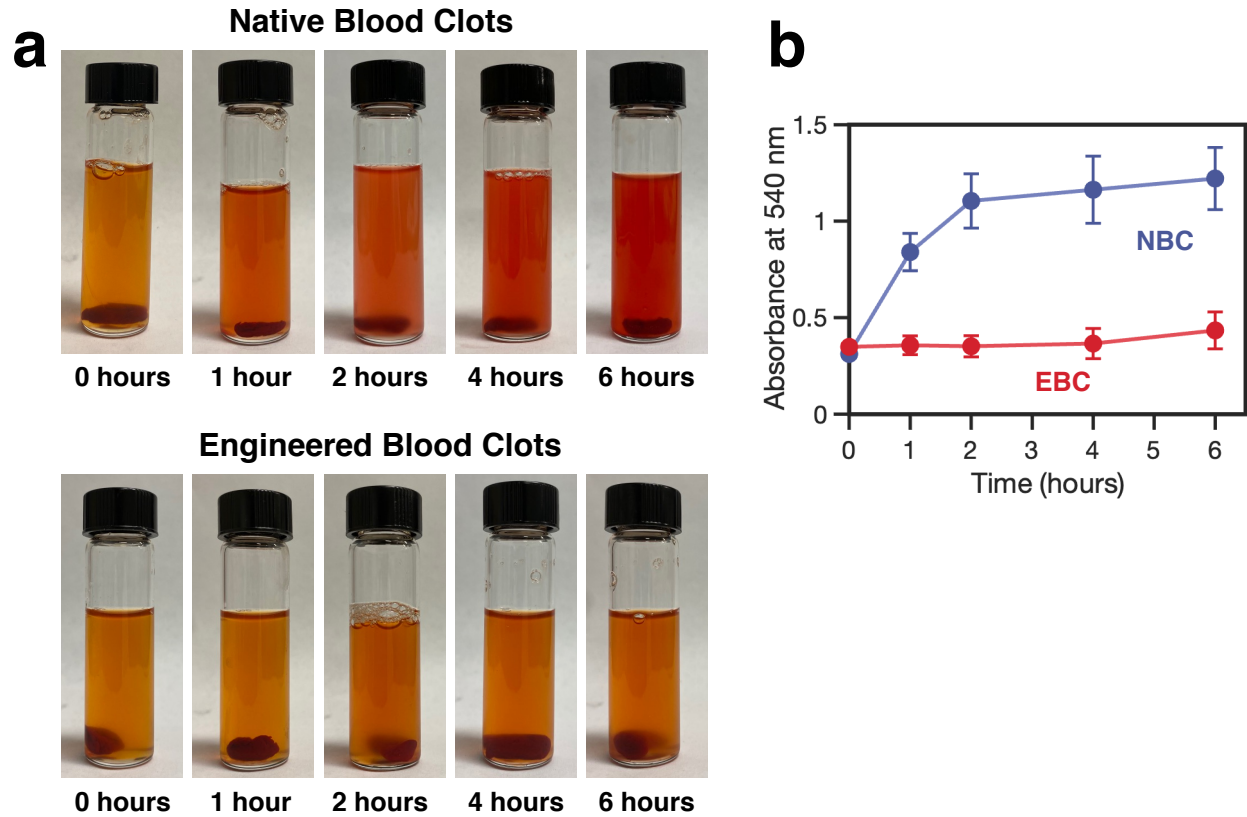


Figure S6 Blood clot fibrinolysis spectrophotometric assay

(a) Images of NBCs and EBCs incubated in bovine plasma supplemented with tPA at various timepoints.
(b) Absorbance values of the supernatant at 540 nm was used as a measure of clot degradation. Values represent the mean \pm SD (n = 3).

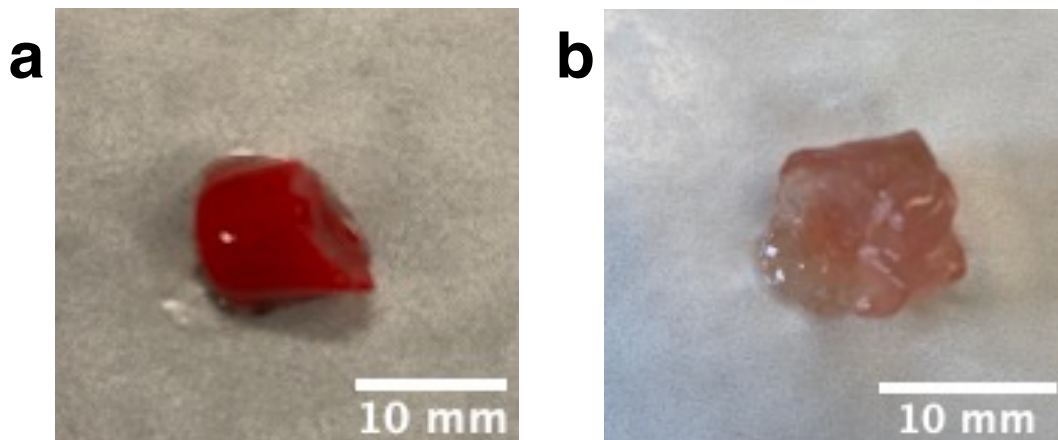


Figure S7 Structure of Engineered Blood Clot after cell lysis

(a) Image of a pristine EBC sample immediately following gelation. **(b)** Image of a EBC sample after incubation in DI water to lyse RBC crosslinkers. EBC maintains its structural stability even though the loss of its red color and its translucent appearance indicate the lysis of RBCs.

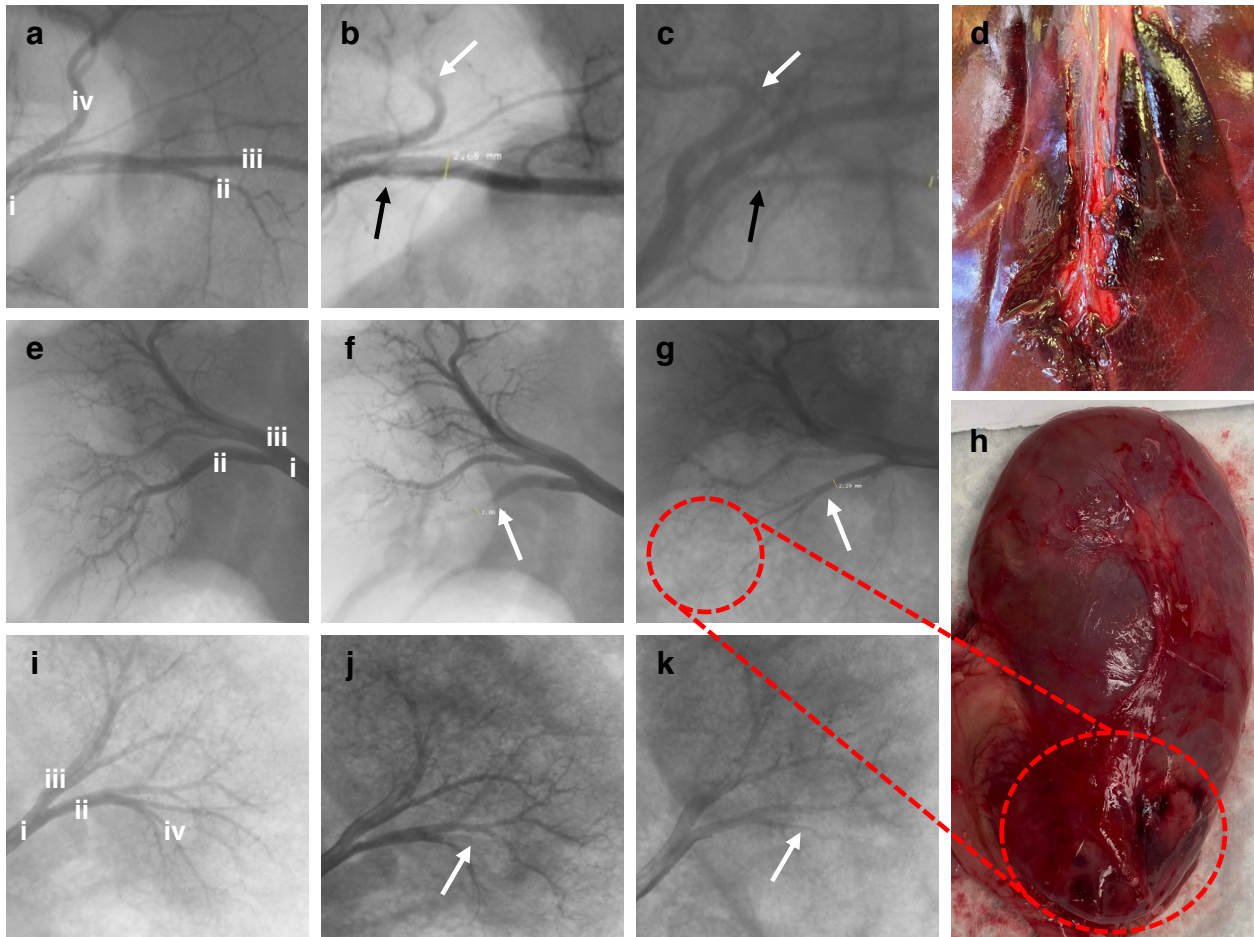


Figure S8 Porcine embolization model

(a) Baseline DSA of the left lateral hepatic artery. (i) left median hepatic artery; (ii) left lateral hepatic artery; (iii) segment III segmental artery; (iv) segment IV segmental artery. **(b)** Post-embolization DSA; contrast injection revealed lack of opacification of the left lateral hepatic artery (white arrow), indicating successful embolization. Black arrow indicates embolization of the segment IV segmental artery. **(c)** 7-day post-embolization DSA. **(d)** A portion of the segmental hepatic arteries of the left lateral lobe. The vessels did not contain blood and the perivascular tissue was pale, pink and softer than adjacent tissues, suggesting complete necrosis of this region. **(e)** Baseline DSA of the right renal artery. (i) right renal artery; (ii) lower polar artery; (iii) upper polar artery. **(f)** Post-embolization DSA showing successful embolization of the lower polar artery (white arrow) and reduced opacification of the inferior lobe of the kidney. **(g)** 7-day post-embolization DSA showing partial recanalization of the artery. **(h)** Image of the right kidney showing dark necrotic region (red circle), corresponding to the lack of opacification in the inferior lobe of the right kidney. **(i)** Baseline DSA of the left renal artery. (i) left renal artery; (ii) lower polar artery; (iii) upper polar artery; (iv) posterior branch of the lower polar artery. **(j)** Post-embolization DSA showing successful embolization of the posterior branch of the lower polar artery (white arrow) and reduced opacification of the inferior lobe of the kidney. **(k)** 7-day post-embolization DSA showing partial recanalization of the artery.

References

1. J. Hu *et al.*, Advances in Biomaterials and Technologies for Vascular Embolization. *Adv Mater* **31**, e1901071 (2019).
2. J. E. Lopera, Embolization in trauma: principles and techniques. *Semin Intervent Radiol* **27**, 14-28 (2010).
3. J. L. Doppman, G. Di Chiro, A. Ommaya, Obliteration of spinal-cord arteriovenous malformation by percutaneous embolisation. *Lancet* **1**, 477 (1968).
4. T. H. Newton, J. E. Adams, Angiographic demonstration and nonsurgical embolization of spinal cord angioma. *Radiology* **91**, 873-876 passim (1968).
5. J. Rösch, C. T. Dotter, M. J. Brown, Selective arterial embolization. A new method for control of acute gastrointestinal bleeding. *Radiology* **102**, 303-306 (1972).
6. R. A. Sheth *et al.*, Endovascular Embolization by Transcatheter Delivery of Particles: Past, Present, and Future. *J Funct Biomater* **8**, (2017).
7. S. Vaidya, K. R. Tozer, J. Chen, An overview of embolic agents. *Semin Intervent Radiol* **25**, 204-215 (2008).
8. N. Janjua, A. Alkawi, M. F. Suri, A. I. Qureshi, Impact of arterial reocclusion and distal fragmentation during thrombolysis among patients with acute ischemic stroke. *AJNR Am J Neuroradiol* **29**, 253-258 (2008).
9. F. Kunstlinger, F. Brunelle, P. Chaumont, D. Doyon, Vascular occlusive agents. *AJR Am J Roentgenol* **136**, 151-156 (1981).
10. C. Gianturco, J. H. Anderson, S. Wallace, Mechanical devices for arterial occlusion. *Am J Roentgenol Radium Ther Nucl Med* **124**, 428-435 (1975).
11. M. Guimaraes, M. Wooster, Onyx (Ethylene-vinyl Alcohol Copolymer) in Peripheral Applications. *Semin Intervent Radiol* **28**, 350-356 (2011).
12. S. K. Hilal, J. W. Michelsen, Therapeutic percutaneous embolization for extra-axial vascular lesions of the head, neck, and spine. *J Neurosurg* **43**, 275-287 (1975).
13. F. J. Miller, Jr., R. S. Rankin, J. B. Gliedman, Experimental internal iliac artery embolization: evaluation of low viscosity silicone rubber, isobutyl 2-cyanoacrylate, and carbon microspheres. *Radiology* **129**, 51-58 (1978).
14. B. Jiang, M. Paff, G. P. Colby, A. L. Coon, L. M. Lin, Cerebral aneurysm treatment: modern neurovascular techniques. *Stroke Vasc Neurol* **1**, 93-100 (2016).
15. I. Manyonda *et al.*, Uterine-Artery Embolization or Myomectomy for Uterine Fibroids. *N Engl J Med* **383**, 440-451 (2020).
16. H. West, J. O. Jin, Transarterial Chemoembolization. *JAMA Oncology* **1**, 1178-1178 (2015).
17. E. J. Duffis *et al.*, Head, neck, and brain tumor embolization guidelines. *J Neurointerv Surg* **4**, 251-255 (2012).
18. I. Robertson, in *Transcatheter Embolization and Therapy*, D. Kessel, C. Ray, Eds. (Springer London, London, 2009), pp. 3-13.
19. F. E. Boas, D. Fleischmann, CT artifacts: Causes and reduction techniques. *Imaging in Medicine* **4**, 229-240 (2012).
20. S. Young, N. Rostambeigi, J. Golzarian, The Common but Complicated Tool: Review of Embolic Materials for the Interventional Radiologist. *Semin Intervent Radiol* **38**, 535-541 (2021).

21. K. H. Barth, J. D. Strandberg, S. L. Kaufman, R. I. White, Jr., Chronic vascular reactions to steel coil occlusion devices. *AJR Am J Roentgenol* **131**, 455-458 (1978).
22. T. Liebig *et al.*, Fibered electrolytically detachable platinum coils used for the endovascular treatment of intracranial aneurysms. Initial experiences and mid-term results in 474 aneurysms. *Interv Neuroradiol* **10**, 5-26 (2004).
23. G. Girdhar, M. Read, J. Sohn, C. Shah, S. Shrivastava, In-vitro thrombogenicity assessment of polymer filament modified and native platinum embolic coils. *J Neurol Sci* **339**, 97-101 (2014).
24. Y. Murayama *et al.*, Bioabsorbable polymeric material coils for embolization of intracranial aneurysms: a preliminary experimental study. *J Neurosurg* **94**, 454-463 (2001).
25. D. Fiorella, F. C. Albuquerque, C. G. McDougall, Durability of aneurysm embolization with matrix detachable coils. *Neurosurgery* **58**, 51-59; discussion 51-59 (2006).
26. Y. Niimi, J. Song, M. Madrid, A. Berenstein, Endosaccular treatment of intracranial aneurysms using matrix coils: early experience and midterm follow-up. *Stroke* **37**, 1028-1032 (2006).
27. D. J. Rivet *et al.*, Single-institution experience with matrix coils in the treatment of intracranial aneurysms: comparison with same-center outcomes with the use of platinum coils. *AJNR Am J Neuroradiol* **28**, 1736-1742 (2007).
28. C. A. Taschner, X. Leclerc, H. Rachdi, A. M. Barros, J. P. Pruvo, Matrix detachable coils for the endovascular treatment of intracranial aneurysms: analysis of early angiographic and clinical outcomes. *Stroke* **36**, 2176-2180 (2005).
29. Y. Murayama *et al.*, Initial clinical experience with matrix detachable coils for the treatment of intracranial aneurysms. *J Neurosurg* **105**, 192-199 (2006).
30. A. Sadato, M. Hayakawa, K. Adachi, I. Nakahara, Y. Hirose, Large Residual Volume, Not Low Packing Density, Is the Most Influential Risk Factor for Recanalization after Coil Embolization of Cerebral Aneurysms. *PLoS One* **11**, e0155062 (2016).
31. B. R. Bendok *et al.*, The Hydrogel Endovascular Aneurysm Treatment Trial (HEAT): A Randomized Controlled Trial of the Second-Generation Hydrogel Coil. *Neurosurgery* **86**, 615-624 (2020).
32. T. J. Speakman, Internal Occlusion of a Carotid-Cavernous Fistula. *J Neurosurg* **21**, 303-305 (1964).
33. M. Brinckman, in *Transcatheter Embolization and Therapy*, D. Kessel, C. Ray, Eds. (Springer London, London, 2009), pp. 41-50.
34. H. T. Abada, J. Golzarian, Gelatine sponge particles: handling characteristics for endovascular use. *Tech Vasc Interv Radiol* **10**, 257-260 (2007).
35. A. Al-Thunyan *et al.*, Buttock necrosis and paraplegia after bilateral internal iliac artery embolization for postpartum hemorrhage. *Obstet Gynecol* **120**, 468-470 (2012).
36. J. Golzarian, G. P. Siskin, M. Sharafuddin, H. Mimura, D. M. Coldwell, in *Vascular Embolotherapy: A Comprehensive Approach Volume 1 General Principles, Chest, Abdomen, and Great Vessels*, J. Golzarian, S. Sun, M. J. Sharafuddin, Eds. (Springer Berlin Heidelberg, Berlin, Heidelberg, 2006), pp. 15-33.
37. J. D. Lindquist, R. L. Vogelzang, Pelvic Artery Embolization for Treatment of Postpartum Hemorrhage. *Semin Intervent Radiol* **35**, 41-47 (2018).
38. J. P. Pelage *et al.*, Uterine artery embolization in sheep: comparison of acute effects with polyvinyl alcohol particles and calibrated microspheres. *Radiology* **224**, 436-445 (2002).
39. S. C. Goodwin, J. B. Spies, Uterine fibroid embolization. *N Engl J Med* **361**, 690-697 (2009).

40. M. Bendszus *et al.*, Efficacy of trisacryl gelatin microspheres versus polyvinyl alcohol particles in the preoperative embolization of meningiomas. *AJNR Am J Neuroradiol* **21**, 255-261 (2000).
41. M. A. Lazzaro *et al.*, Endovascular embolization of head and neck tumors. *Front Neurol* **2**, 64 (2011).
42. G. J. Dubel, S. H. Ahn, G. M. Soares, Contemporary endovascular embolotherapy for meningioma. *Semin Intervent Radiol* **30**, 263-277 (2013).
43. G. P. Siskin *et al.*, Embolic agents used for uterine fibroid embolization. *AJR Am J Roentgenol* **175**, 767-773 (2000).
44. E. Liapi, K. H. Lee, C. C. Georgiades, K. Hong, J. F. Geschwind, Drug-eluting particles for interventional pharmacology. *Tech Vasc Interv Radiol* **10**, 261-269 (2007).
45. D. F. Carli, M. Sluzewski, G. N. Beute, W. J. van Rooij, Complications of particle embolization of meningiomas: frequency, risk factors, and outcome. *AJNR Am J Neuroradiol* **31**, 152-154 (2010).
46. C. W. Kerber, Flow-controlled therapeutic embolization: a physiologic and safe technique. *AJR Am J Roentgenol* **134**, 557-561 (1980).
47. B. Bakar *et al.*, Evaluation of the toxicity of onyx compared with n-butyl 2-cyanoacrylate in the subarachnoid space of a rabbit model: an experimental research. *Neuroradiology* **52**, 125-134 (2010).
48. J. C. Chaloupka, F. Viñuela, H. V. Vinters, J. Robert, Technical feasibility and histopathologic studies of ethylene vinyl copolymer (EVAL) using a swine endovascular embolization model. *AJNR Am J Neuroradiol* **15**, 1107-1115 (1994).
49. A. J. Molyneux, S. Cekirge, I. Saatci, G. Gál, Cerebral Aneurysm Multicenter European Onyx (CAMEO) trial: results of a prospective observational study in 20 European centers. *AJNR Am J Neuroradiol* **25**, 39-51 (2004).
50. H. S. Cekirge *et al.*, Late angiographic and clinical follow-up results of 100 consecutive aneurysms treated with Onyx reconstruction: largest single-center experience. *Neuroradiology* **48**, 113-126 (2006).
51. R. J. Rosen, S. Contractor, The use of cyanoacrylate adhesives in the management of congenital vascular malformations. *Semin Intervent Radiol* **21**, 59-66 (2004).
52. P. O. Comby *et al.*, Endovascular Use of Cyanoacrylate-Lipiodol Mixture for Peripheral Embolization: Properties, Techniques, Pitfalls, and Applications. *J Clin Med* **10**, (2021).
53. M. F. Brothers, J. C. Kaufmann, A. J. Fox, J. P. Deveikis, n-Butyl 2-cyanoacrylate--substitute for IBCA in interventional neuroradiology: histopathologic and polymerization time studies. *AJNR Am J Neuroradiol* **10**, 777-786 (1989).
54. D. F. Vollherbst, R. Chapot, M. Bendszus, M. A. Möhlenbruch, Glue, Onyx, Squid or PHIL? Liquid Embolic Agents for the Embolization of Cerebral Arteriovenous Malformations and Dural Arteriovenous Fistulas. *Clin Neuroradiol* **32**, 25-38 (2022).
55. M. M. Rana, M. P. Melancon, Emerging Polymer Materials in Trackable Endovascular Embolization and Cell Delivery: From Hype to Hope. *Biomimetics (Basel)* **7**, (2022).
56. M. L. Martin, B. L. Dolmatch, P. D. Fry, L. S. Machan, Treatment of type II endoleaks with Onyx. *J Vasc Interv Radiol* **12**, 629-632 (2001).
57. R. Jahan *et al.*, Embolization of arteriovenous malformations with Onyx: clinicopathological experience in 23 patients. *Neurosurgery* **48**, 984-995; discussion 995-987 (2001).
58. W. Yakes, R. Baker, Cardiopulmonary collapse: sequelae of ethanol embolotherapy. *Radiology* **189**, 145 (1993).

59. T. A. Becker, D. R. Kipke, T. Brandon, Calcium alginate gel: a biocompatible and mechanically stable polymer for endovascular embolization. *J Biomed Mater Res* **54**, 76-86 (2001).
60. G. I. Olivas, G. V. Barbosa-Cánovas, Alginate–calcium films: Water vapor permeability and mechanical properties as affected by plasticizer and relative humidity. *LWT - Food Science and Technology* **41**, 359-366 (2008).
61. G. D. Nicodemus, S. J. Bryant, Cell encapsulation in biodegradable hydrogels for tissue engineering applications. *Tissue Eng Part B Rev* **14**, 149-165 (2008).
62. S. O. Blacklow *et al.*, Bioinspired mechanically active adhesive dressings to accelerate wound closure. *Sci Adv* **5**, eaaw3963 (2019).
63. M. Dai *et al.*, Chitosan-alginate sponge: preparation and application in curcumin delivery for dermal wound healing in rat. *J Biomed Biotechnol* **2009**, 595126 (2009).
64. T. A. Becker, M. C. Preul, W. D. Bichard, D. R. Kipke, C. G. McDougall, Preliminary investigation of calcium alginate gel as a biocompatible material for endovascular aneurysm embolization in vivo. *Neurosurgery* **60**, 1119-1127; discussion 1127-1118 (2007).
65. Y. Dobashi *et al.*, Dynamically tunable intravascular catheter delivery of hydrogels for endovascular embolization. *MRS Advances* **6**, 66-71 (2021).
66. Y. Dobashi *et al.*, Photomodulated Extrusion as a Localized Endovascular Hydrogel Deposition Method. *Adv Healthc Mater* **12**, e2202632 (2023).
67. J. C. Ku *et al.*, Photosensitive Hydrogel-Based Embolic Agent Treatment of Wide-Necked Aneurysms: Preliminary Animal Results. *Gels* **8**, (2022).
68. J.-M. Coutu, A. Fatimi, S. Berrahmoune, G. Soulez, S. Lerouge, A new radiopaque embolizing agent for the treatment of endoleaks after endovascular repair: Influence of contrast agent on chitosan thermogel properties. *Journal of Biomedical Materials Research Part B: Applied Biomaterials* **101B**, 153-161 (2013).
69. A. Chenite, M. Buschmann, D. Wang, C. Chaput, N. Kandani, Rheological characterisation of thermogelling chitosan/glycerol-phosphate solutions. *Carbohydrate Polymers* **46**, 39-47 (2001).
70. A. Fatimi, F. Zehtabi, S. Lerouge, Optimization and characterization of injectable chitosan-iodixanol-based hydrogels for the embolization of blood vessels. *Journal of Biomedical Materials Research Part B: Applied Biomaterials* **104**, 1551-1562 (2016).
71. Y. Wang *et al.*, In vivo assessment of chitosan/ β -glycerophosphate as a new liquid embolic agent. *Interv Neuroradiol* **17**, 87-92 (2011).
72. X. Ning *et al.*, Experimental study of temperature-sensitive chitosan/ β -glycerophosphate embolic material in embolizing the basicranial rete mirabile in swines. *Exp Ther Med* **10**, 316-322 (2015).
73. J. S. Lym *et al.*, Sulfamethazine-based pH-sensitive hydrogels with potential application for transcatheter arterial chemoembolization therapy. *Acta Biomaterialia* **41**, 253-263 (2016).
74. Q. V. Nguyen *et al.*, A novel sulfamethazine-based pH-sensitive copolymer for injectable radiopaque embolic hydrogels with potential application in hepatocellular carcinoma therapy. *Polymer Chemistry* **7**, 5805-5818 (2016).
75. Q. V. Nguyen *et al.*, pH-Sensitive sulfamethazine-based hydrogels as potential embolic agents for transcatheter vascular embolization. *Journal of Materials Chemistry B* **4**, 6524-6533 (2016).
76. R. K. Avery *et al.*, An injectable shear-thinning biomaterial for endovascular embolization. *Sci Transl Med* **8**, 365ra156 (2016).

77. A. K. Gaharwar *et al.*, Shear-thinning nanocomposite hydrogels for the treatment of hemorrhage. *ACS Nano* **8**, 9833-9842 (2014).
78. C. M. Riley, R. McLemore, M. C. Preul, B. L. Vernon, Gelling process differences in reverse emulsion, in situ gelling polymeric materials for intracranial aneurysm embolization, formulated with injectable contrast agents. *Journal of Biomedical Materials Research Part B: Applied Biomaterials* **96B**, 47-56 (2011).
79. C. R. Brennecka, M. C. Preul, W. D. Bichard, B. L. Vernon, In vivo experimental aneurysm embolization in a swine model with a liquid-to-solid gelling polymer system: initial biocompatibility and delivery strategy analysis. *World Neurosurg* **78**, 469-480 (2012).
80. C. R. Brennecka, M. C. Preul, T. A. Becker, B. L. Vernon, In vivo embolization of lateral wall aneurysms in canines using the liquid-to-solid gelling PPODA-QT polymer system: 6-month pilot study. *J Neurosurg* **119**, 228-238 (2013).
81. B. H. Lee *et al.*, In vitro and in vivo demonstration of physically and chemically in situ gelling NIPAAm-based copolymer system. *J Biomater Sci Polym Ed* **24**, 1575-1588 (2013).
82. O. Poupard *et al.*, In vitro Implementation of Photopolymerizable Hydrogels as a Potential Treatment of Intracranial Aneurysms. *Front Bioeng Biotechnol* **8**, 261 (2020).
83. A. Fatimi *et al.*, A new injectable radiopaque chitosan-based sclerosing embolizing hydrogel for endovascular therapies. *Acta Biomater* **8**, 2712-2721 (2012).
84. X. Shi, H. Gao, F. Dai, X. Feng, W. Liu, A thermoresponsive supramolecular copolymer hydrogel for the embolization of kidney arteries. *Biomater Sci* **4**, 1673-1681 (2016).
85. Q. Wang *et al.*, Precision Embolism: Biocompatible Temperature-Sensitive Hydrogels as Novel Embolic Materials for Both Mainstream and Peripheral Vessels. *Advanced Functional Materials* **31**, 2011170 (2021).
86. H. Yang *et al.*, Injectable PEG/polyester thermogel: A new liquid embolization agent for temporary vascular interventional therapy. *Mater Sci Eng C Mater Biol Appl* **102**, 606-615 (2019).
87. A. Poursaid *et al.*, In situ gelling silk-elastinlike protein polymer for transarterial chemoembolization. *Biomaterials* **57**, 142-152 (2015).
88. F. Zhou *et al.*, Novel Hydrogel Material as a Potential Embolic Agent in Embolization Treatments. *Sci Rep* **6**, 32145 (2016).
89. R. Xie *et al.*, Injectable Hydrogel Capable of In Situ Covalent Crosslinking for Permanent Embolization. *ACS Appl Mater Interfaces* **13**, 56988-56999 (2021).
90. S. Ganguli, R. Lareau, T. Jarrett, M. C. Soulen, A Water-Based Liquid Embolic: Evaluation of its Safety and Efficacy in a Rabbit Kidney Model. *J Vasc Interv Radiol* **32**, 813-818 (2021).
91. R. J. Stewart, M. Sima, J. Karz, J. P. Jones, Material characterization of GPX((R)): A versatile in situ solidifying embolic platform technology. *Front Bioeng Biotechnol* **11**, 1095148 (2023).
92. J. P. Jones, M. Sima, R. G. O'Hara, R. J. Stewart, Water-Borne Endovascular Embolics Inspired by the Undersea Adhesive of Marine Sandcastle Worms. *Adv Healthc Mater* **5**, 795-801 (2016).
93. M. Liu *et al.*, Solvent Exchange Induced In Situ Formed Hydrogel as Liquid Embolic Agents. *Advanced Functional Materials*, (2023).
94. Z. Jin *et al.*, Gluing blood into gel by electrostatic interaction using a water-soluble polymer as an embolic agent. *Proc Natl Acad Sci U S A* **119**, e2206685119 (2022).

95. A. J. R. Amaral, G. Pasparakis, Cell membrane engineering with synthetic materials: Applications in cell spheroids, cellular glues and microtissue formation. *Acta Biomaterialia* **90**, 21-36 (2019).
96. S. R. Caliari, J. A. Burdick, A practical guide to hydrogels for cell culture. *Nature Methods* **13**, 405-414 (2016).
97. H. Zhan, H. de Jong, D. W. P. M. Löwik, Comparison of Bioorthogonally Cross-Linked Hydrogels for in Situ Cell Encapsulation. *ACS Applied Bio Materials* **2**, 2862-2871 (2019).
98. C. Echaliier, L. Valot, J. Martinez, A. Mehdi, G. Subra, Chemical cross-linking methods for cell encapsulation in hydrogels. *Materials Today Communications* **20**, 100536 (2019).
99. J. L. Drury, D. J. Mooney, Hydrogels for tissue engineering: scaffold design variables and applications. *Biomaterials* **24**, 4337-4351 (2003).
100. A. Ovsianikov, A. Khademhosseini, V. Mironov, The Synergy of Scaffold-Based and Scaffold-Free Tissue Engineering Strategies. *Trends in Biotechnology* **36**, 348-357 (2018).
101. M. Hospodiuk, M. Dey, D. Sosnoski, I. T. Ozbolat, The bioink: A comprehensive review on bioprintable materials. *Biotechnology Advances* **35**, 217-239 (2017).
102. J. Zhang, S. Yun, Y. Du, A. Zannettino, H. Zhang, Hydrogel-based preparation of cell aggregates for biomedical applications. *Applied Materials Today* **20**, 100747 (2020).
103. H. Koo *et al.*, Bioorthogonal Click Chemistry-Based Synthetic Cell Glue. *Small* **11**, 6458-6466 (2015).
104. Z. J. Gartner, C. R. Bertozzi, Programmed assembly of 3-dimensional microtissues with defined cellular connectivity. *Proc Natl Acad Sci U S A* **106**, 4606-4610 (2009).
105. D. Rogozhnikov, P. J. O'Brien, S. Elahipanah, M. N. Yousaf, Scaffold Free Bio-orthogonal Assembly of 3-Dimensional Cardiac Tissue via Cell Surface Engineering. *Sci Rep* **6**, 39806 (2016).
106. W. Luo *et al.*, A Dual Receptor and Reporter for Multi-Modal Cell Surface Engineering. *ACS Chem Biol* **10**, 2219-2226 (2015).
107. M. D. Krebs *et al.*, Formation of ordered cellular structures in suspension via label-free negative magnetophoresis. *Nano Lett* **9**, 1812-1817 (2009).
108. B. S. Schon, G. J. Hooper, T. B. F. Woodfield, Modular Tissue Assembly Strategies for Biofabrication of Engineered Cartilage. *Annals of Biomedical Engineering* **45**, 100-114 (2017).
109. B. Lee *et al.*, Challenges and Solutions for Commercial Scale Manufacturing of Allogeneic Pluripotent Stem Cell Products. *Bioengineering (Basel)* **7**, (2020).
110. K. Y. Lee, H. J. Kong, R. G. Larson, D. J. Mooney, Hydrogel Formation via Cell Crosslinking. *Advanced Materials* **15**, 1828-1832 (2003).
111. Z. Piao, J. K. Park, B. Jeong, Cytogel: A Cell-Crosslinked Thermogel. *ACS Applied Materials & Interfaces* **15**, 17688-17695 (2023).
112. M. Ito, T. Taguchi, Enhanced insulin secretion of physically crosslinked pancreatic beta-cells by using a poly(ethylene glycol) derivative with oleyl groups. *Acta Biomater* **5**, 2945-2952 (2009).
113. V. Javvaji, M. B. Dowling, H. Oh, I. M. White, S. R. Raghavan, Reversible gelation of cells using self-assembling hydrophobically-modified biopolymers: towards self-assembly of tissue. *Biomaterials Science* **2**, 1016-1023 (2014).
114. A. J. R. Amaral, G. Pasparakis, Macromolecular cell surface engineering for accelerated and reversible cellular aggregation. *Chemical Communications* **51**, 17556-17559 (2015).

115. E. M. Sletten, C. R. Bertozzi, Bioorthogonal Chemistry: Fishing for Selectivity in a Sea of Functionality. *Angewandte Chemie International Edition* **48**, 6974-6998 (2009).
116. D. J. Vocadlo, H. C. Hang, E. J. Kim, J. A. Hanover, C. R. Bertozzi, A chemical approach for identifying O-GlcNAc-modified proteins in cells. *Proc Natl Acad Sci U S A* **100**, 9116-9121 (2003).
117. R. Huisgen, 1,3-Dipolar Cycloadditions. *Proceedings of the Chemical Society*, 357-396 (1961).
118. R. J. Griffin, The medicinal chemistry of the azido group. *Prog Med Chem* **31**, 121-232 (1994).
119. N. J. Agard, J. A. Prescher, C. R. Bertozzi, A Strain-Promoted [3 + 2] Azide–Alkyne Cycloaddition for Covalent Modification of Biomolecules in Living Systems. *Journal of the American Chemical Society* **126**, 15046-15047 (2004).
120. V. V. Rostovtsev, L. G. Green, V. V. Fokin, K. B. Sharpless, A stepwise huisgen cycloaddition process: copper(I)-catalyzed regioselective "ligation" of azides and terminal alkynes. *Angew Chem Int Ed Engl* **41**, 2596-2599 (2002).
121. C. W. Tornøe, C. Christensen, M. Meldal, Peptidotriazoles on solid phase: [1,2,3]-triazoles by regiospecific copper(i)-catalyzed 1,3-dipolar cycloadditions of terminal alkynes to azides. *J Org Chem* **67**, 3057-3064 (2002).
122. X. Ning, J. Guo, M. A. Wolfert, G. J. Boons, Visualizing metabolically labeled glycoconjugates of living cells by copper-free and fast huisgen cycloadditions. *Angew Chem Int Ed Engl* **47**, 2253-2255 (2008).
123. M. F. Debets *et al.*, Aza-dibenzocyclooctynes for fast and efficient enzyme PEGylation via copper-free (3+2) cycloaddition. *Chemical Communications* **46**, 97-99 (2010).
124. M. F. Debets, J. C. M. van Hest, F. P. J. T. Rutjes, Bioorthogonal labelling of biomolecules: new functional handles and ligation methods. *Organic & Biomolecular Chemistry* **11**, 6439-6455 (2013).
125. M. L. Blackman, M. Royzen, J. M. Fox, Tetrazine Ligation: Fast Bioconjugation Based on Inverse-Electron-Demand Diels–Alder Reactivity. *Journal of the American Chemical Society* **130**, 13518-13519 (2008).
126. M. R. Karver, R. Weissleder, S. A. Hilderbrand, Synthesis and Evaluation of a Series of 1,2,4,5-Tetrazines for Bioorthogonal Conjugation. *Bioconjugate Chemistry* **22**, 2263-2270 (2011).
127. V. Tutwiler *et al.*, Rupture of blood clots: Mechanics and pathophysiology. *Sci Adv* **6**, eabc0496 (2020).
128. S. Xu *et al.*, Model predictions of deformation, embolization and permeability of partially obstructive blood clots under variable shear flow. *J R Soc Interface* **14**, (2017).
129. T. V. Colace, R. W. Muthard, S. L. Diamond, Thrombus growth and embolism on tissue factor-bearing collagen surfaces under flow: role of thrombin with and without fibrin. *Arterioscler Thromb Vasc Biol* **32**, 1466-1476 (2012).
130. N. Tobin, M. Li, G. Hiller, A. Azimi, K. B. Manning, Clot embolization studies and computational framework for embolization in a canonical tube model. *Scientific Reports* **13**, 14682 (2023).
131. Q. Liu, Z. Wang, Y. Lou, Z. Suo, Elastic leak of a seal. *Extreme Mechanics Letters* **1**, 54-61 (2014).
132. Z. Wang, C. Chen, Q. Liu, Y. Lou, Z. Suo, Extrusion, slide, and rupture of an elastomeric seal. *Journal of the Mechanics and Physics of Solids* **99**, 289-303 (2017).

133. B. Chen, C. Chen, Y. Lou, Z. Suo, Strain-stiffening seal. *Soft Matter* **18**, 2992-3003 (2022).
134. M. D. Kerr *et al.*, Immune-responsive biodegradable scaffolds for enhancing neutrophil regeneration. *Bioengineering & Translational Medicine* **8**, e10309 (2023).
135. K. Barker *et al.*, Biodegradable DNA-enabled poly(ethylene glycol) hydrogels prepared by copper-free click chemistry. *J Biomater Sci Polym Ed* **27**, 22-39 (2016).
136. H. Choi, M. Kwon, H. E. Choi, S. K. Hahn, K. S. Kim, Non-Invasive Topical Drug-Delivery System Using Hyaluronate Nanogels Crosslinked via Click Chemistry. *Materials (Basel)* **14**, (2021).
137. I. Youm, V. Agrahari, J. B. Murowchick, B. B. Youan, Uptake and cytotoxicity of docetaxel-loaded hyaluronic acid-grafted oily core nanocapsules in MDA-MB 231 cancer cells. *Pharm Res* **31**, 2439-2452 (2014).
138. S. Liu, G. Bao, Z. Ma, C. J. Kastrup, J. Li, Fracture mechanics of blood clots: Measurements of toughness and critical length scales. *Extreme Mechanics Letters* **48**, 101444 (2021).
139. O. Poupart *et al.*, Pulsatile Flow-Induced Fatigue-Resistant Photopolymerizable Hydrogels for the Treatment of Intracranial Aneurysms. *Front Bioeng Biotechnol* **8**, 619858 (2020).
140. P. E. Andersen, A. D. Kjeldsen, Embolization of pulmonary AVMs of feeding arteries less than 3 mm: reports of two cases and an 8-year follow-up without embolization. *Acta Radiol Short Rep* **1**, (2012).
141. C. Mendez, E. Gete, Volume staging for arteriovenous malformation SRS treatment using VMAT. *J Appl Clin Med Phys* **23**, e13815 (2022).
142. A. M. Netlyukh *et al.*, Invasive intracranial arterial pressure monitoring during endovascular cerebral aneurysms embolization for cerebral perfusion evaluation. *Acta Neurochir Suppl* **120**, 177-181 (2015).
143. L. Zarrinkoob *et al.*, Blood flow distribution in cerebral arteries. *J Cereb Blood Flow Metab* **35**, 648-654 (2015).
144. D. B. Camasão, D. Mantovani, The mechanical characterization of blood vessels and their substitutes in the continuous quest for physiological-relevant performances. A critical review. *Materials Today Bio* **10**, 100106 (2021).
145. G. Bao *et al.*, Liquid-infused microstructured bioadhesives halt non-compressible hemorrhage. *Nat Commun* **13**, 5035 (2022).
146. S. Wang *et al.*, Accelerating thrombolysis using a precision and clot-penetrating drug delivery strategy by nanoparticle-shelled microbubbles. *Sci Adv* **6**, eaaz8204 (2020).
147. R. Stern, M. J. Jedrzejewski, Hyaluronidases: their genomics, structures, and mechanisms of action. *Chem Rev* **106**, 818-839 (2006).
148. Z. Zhang *et al.*, Treatment of Ruptured and Nonruptured Aneurysms Using a Semisolid Iodinated Embolic Agent. *Adv Mater* **34**, e2108266 (2022).
149. W. Rungseewijitprapa, R. Bodmeier, Injectability of biodegradable in situ forming microparticle systems (ISM). *European Journal of Pharmaceutical Sciences* **36**, 524-531 (2009).
150. D. C. Madoff *et al.*, Transhepatic ipsilateral right portal vein embolization extended to segment IV: improving hypertrophy and resection outcomes with spherical particles and coils. *J Vasc Interv Radiol* **16**, 215-225 (2005).
151. C. Keegan *et al.*, Onyx™ Cast Fragmentation After Embolization of Endoleaks. *J Endovasc Ther* **29**, 266-274 (2022).
152. H. Hill, J. F. B. Chick, A. Hage, R. N. Srinivasa, N-butyl cyanoacrylate embolotherapy: techniques, complications, and management. *Diagn Interv Radiol* **24**, 98-103 (2018).

153. A. I. Qureshi *et al.*, Occurrence and Management Strategies for Catheter Entrapment with Onyx Liquid Embolization. *J Vasc Interv Neurol* **8**, 37-41 (2015).
154. K. Y. Chan *et al.*, Adhesion of Blood Clots Can Be Enhanced When Copolymerized with a Macromer That Is Crosslinked by Coagulation Factor XIIIa. *Biomacromolecules* **17**, 2248-2252 (2016).
155. K. Neubauer, B. Zieger, Endothelial cells and coagulation. *Cell Tissue Res* **387**, 391-398 (2022).
156. D. D. Wagner, P. S. Frenette, The vessel wall and its interactions. *Blood* **111**, 5271-5281 (2008).
157. R. I. Litvinov, J. W. Weisel, Blood clot contraction: Mechanisms, pathophysiology, and disease. *Res Pract Thromb Haemost* **7**, 100023 (2023).
158. M. Saeed Kilani *et al.*, Ethylene vinyl alcohol copolymer (Onyx®) in peripheral interventional radiology: Indications, advantages and limitations. *Diagnostic and Interventional Imaging* **96**, 319-326 (2015).
159. J. Hu *et al.*, Silk Embolic Material for Catheter-Directed Endovascular Drug Delivery. *Advanced Materials* **34**, 2106865 (2022).
160. E. J. Gandras, T. Jarrett, R. Lareau, Evaluation of a Hydrogel Liquid Embolic Agent in a Porcine Mesenteric Hemorrhage Model. *J Vasc Interv Radiol* **33**, 653-659 (2022).
161. R. Siekmann, Basics and Principles in the Application of Onyx LD Liquid Embolic System in the Endovascular Treatment of Cerebral Arteriovenous Malformations. *Interv Neuroradiol* **11**, 131-140 (2005).
162. R. McLemore, M. C. Preul, B. L. Vernon, Controlling delivery properties of a waterborne, in-situ-forming biomaterial. *Journal of Biomedical Materials Research Part B: Applied Biomaterials* **79B**, 398-410 (2006).
163. T. A. Becker, D. R. Kipke, Flow properties of liquid calcium alginate polymer injected through medical microcatheters for endovascular embolization. *Journal of Biomedical Materials Research* **61**, 533-540 (2002).
164. N. Mohandas, P. G. Gallagher, Red cell membrane: past, present, and future. *Blood* **112**, 3939-3948 (2008).
165. L. M. Eysenbach *et al.*, Migration of n-BCA glue as a complication of venous malformation treatment in children. *Radiol Case Rep* **16**, 3526-3533 (2021).
166. F. L. Ho, R. Chapot, Removal of distal fragments of liquid embolic agents during arteriovenous malformation embolization using the TIGERTRIEVER 13: a technical report. *J Neurointerv Surg* **12**, 794-797 (2020).
167. W. Luo, T. Hu, Y. Mao, Q. Yu, Fragmentation of microspheres after bronchial artery injection: a case report and review of the literature. *J Med Case Rep* **15**, 522 (2021).
168. N. X. Landén, D. Li, M. Ståhle, Transition from inflammation to proliferation: a critical step during wound healing. *Cell Mol Life Sci* **73**, 3861-3885 (2016).
169. D. M. Richter *et al.*, Autologous blood clots: a natural biomaterial for wound healing. *Frontiers in Materials* **10**, (2023).
170. R. E. Forster *et al.*, Characterisation of physico-mechanical properties and degradation potential of calcium alginate beads for use in embolisation. *J Mater Sci Mater Med* **21**, 2243-2251 (2010).
171. I. Altun *et al.*, Blood-Derived Biomaterial for Catheter-Directed Arterial Embolization. *Adv Mater* **32**, e2005603 (2020).

172. J. R. Fraser, T. C. Laurent, A. Engström-Laurent, U. G. Laurent, Elimination of hyaluronic acid from the blood stream in the human. *Clin Exp Pharmacol Physiol* **11**, 17-25 (1984).
173. D. C. West, I. N. Hampson, F. Arnold, S. Kumar, Angiogenesis induced by degradation products of hyaluronic acid. *Science* **228**, 1324-1326 (1985).

ⁱ Created with biorender.com

ⁱⁱ Images of vascular diseases are used with the proper licenses from shutterstock

ⁱⁱⁱ Reproduced with permission from <https://www.stryker.com/>

^{iv} Reproduced with permission from <https://www.terumo.com/>

^v Images of gelatin-based embolic, shear-thinning embolic agent, and Onyx embolic system are reproduced from: <https://www.merit.com/>; <https://mydevicemd.com/>; and <https://www.bostonscientific.com/>, respectively.